NTNU

Norwegian University of
Science and Technology

One-pot Conversion of Cellulose to Ethylene Glycol using CNT Supported Tungsten Catalysts

Petter Kaalstad

Chemical Engineering
Submission date: July 2017
Supervisor: De Chen, IKP

Norwegian University of Science and Technology
Department of Chemical Engineering

NTNU
Norges teknisk-naturvitenskapelige universitet
Fakultet for naturvitenskap og teknologi
Institutt for kjemisk prosessteknologi

MASTER THESIS

One-pot Conversion of Cellulose to Ethylene Glycol using CNT Supported Tungsten Catalysts

By

Petter Kaalstad

Norwegian University of Science and Technology
Department of Chemical Engineering
Catalysis Research Group

Submission date: July 2017
Supervisor: De Chen, IKP
Co-supervisor: Haakon Rui, IKP

Preface

This Master Thesis is the result of work done in the Catalysis Group in the Department of Chemical Engineering at NTNU in the spring of 2017. The risk assessment performed for all experimental work done throughout this study can be seen in NTNU's digital risk assessment system under the following ID number: 13523.

I want to express sincere gratitude to my supervisor, Professor De Chen, for his guidance and support during my work on this project. Sincere gratitude is also directed to my co-supervisor, PhD student Haakon Rui, for his tremendous amount of help and guidance throughout the project. In addition, I want to thank PhD student Cornelis Gerardus van der Wijst for his assistance with using the analytical equipment.

I also want to thank my fellow student colleagues in the Catalysis Group for providing moral support throughout the project. Among them, I especially want to thank Björn Baumgarten for his assistance and relevant discussions regarding the biomass conversion processes.

I declare that this is an independent work according to the exam regulations of the Norwegian University of Science and Technology (NTNU).

Name Date

Abstract

The one-pot catalytic conversion of cellulose to ethylene glycol (EG) is a promising approach for biomass utilization. The catalysts developed for this process have to be bifunctional, catalysing both retro-aldol condensation and hydrogenation. In this study, various tungsten-based catalysts (mostly WO_3/CNT and W_2C/CNT) were tested for their retro-aldol condensation activity alone and with the addition of copper (Cu) to examine the promotion effect of Cu on the hydrogenation activity. The nominal loading of each catalyst was typically 10 wt% W and 10 wt% Cu, which were tested at 245 °C and 60 bar H_2 for 90/180 minutes in a batch reactor with cellulose as the feedstock. From these results it was evident that copper did exhibit a promotional effect on the hydrogenation activity, but the hydrogenation of copper was very low with a maximum EG and 1,2-PG yield of 7.7% and 3.5%, respectively, after 180 minutes with W_2C-Cu/CNT. The low yields were a result of the insufficient hydrogenation activity of copper, resulting in a large amount of unsaturated by-products.

The WO_3/CNT and W_2C/CNT catalysts were also tested in combination with Cu_xO/CNT and Ru/CNT in order to assess the hydrogenation ability of Cu and Ru. When tested in combination with Cu_xO/CNT (Cu/W ratio = 1.0) the EG and 1,2-PG yield was higher than without the presence of Cu, but the EG yield was lower than the tungsten-copper catalysts. The Cu/W ratio was therefore too low to allow for sufficient hydrogenation. When tested in combination with Ru/CNT (Ru/W = 0.1), the hydrogenation activity was significantly increased, producing a maximum of 30.5% EG and 12.3% 1,2-PG with 10 wt% WO_3/CNT + Ru/CNT. The W_2C/CNT + Ru/CNT resulted in lower EG and 1,2-PG yields and higher glycerol, sorbitol, and mannitol yields due to the combined hydrogenation by both W_2C and Ru. The Ru/W ratio is therefore too high with W_2C/CNT, but may be increased with WO_3/CNT. The use of WO_3/CNT with both copper and ruthenium resulted in less side products being formed, and in the case of Ru, inhibited the HMF degradation pathway entirely. This shows promising uses for WO_3 as a catalyst as the EG selectivity and yield may be greatly enhanced.

Table of Contents

List of Tables

List of Figures

1. Introduction

The search for alternative fuels has gained a lot of interest in recent years due to diminishing fossil resources and increased environmental concerns. The growth of the global economy is currently greatly dependent on fossil energy, causing significant depletion of these resources as well as environmental deterioration [1]. The world has therefore been faced with the great challenges of sustainable development, resulting in a recent pivot towards various forms of clean and renewable energy resources [2]. One potential renewable energy source is the utilization of biomass, which has a complex structure of C:H:O:N similar to fossil resources except in a different ratio. The knowledge and technology developed from the fossil fuel industry over the years may therefore be transferred and utilized for biomass processing, but new product lines need to be developed [3]. Several different processes have been suggested and studied for the conversion of biomass to chemicals and fuels, such as pyrolysis, gasification, and hydrolysis. These processes result in numerous intermediate products, such as synthesis gas, bio-oil, and sugars, which again may be utilized further to produce fuels and chemical products, potentially replacing fossil based products [4].

There are many positive aspects of biomass utilization, however, the “food for fuel” debate imposes a dilemma for biomass production, as growing biomass for the sole purpose of fuel and chemical production will compete with food production from starch or corn [5]. One solution to this problem is the use of non-edible lignocellulosic biomass, such as wood and wood residues, non-wood energy crops, and agricultural waste. Lignocellulosic biomass is one of the most abundant renewable biomass feedstocks on earth, with an estimated global production of 170 billion tons/year [6]. Lignocellulose is a complex fibrous material consisting of approximately 40–50% cellulose, 25–30% hemicellulose, and 15–30% lignin [7]. However, the complex structure of lignocellulose, shown in Figure 1.1, makes it difficult to produce a high yield and selectivity of target fuels and chemicals. One way to simplify the conversion process is to separate the carbohydrate fraction (hemicellulose and cellulose) from lignin based on their different reactivity, isolating the carbohydrate fractions from the phenolic compounds in lignin. In addition, the most difficult and energy-consuming step of lignocellulose conversion is the decomposition and degradation of cellulose [8]. Cellulose has therefore been used as a model compound for lignocellulose in many recent studies as it is the most robust and abundant component of lignocellulose.

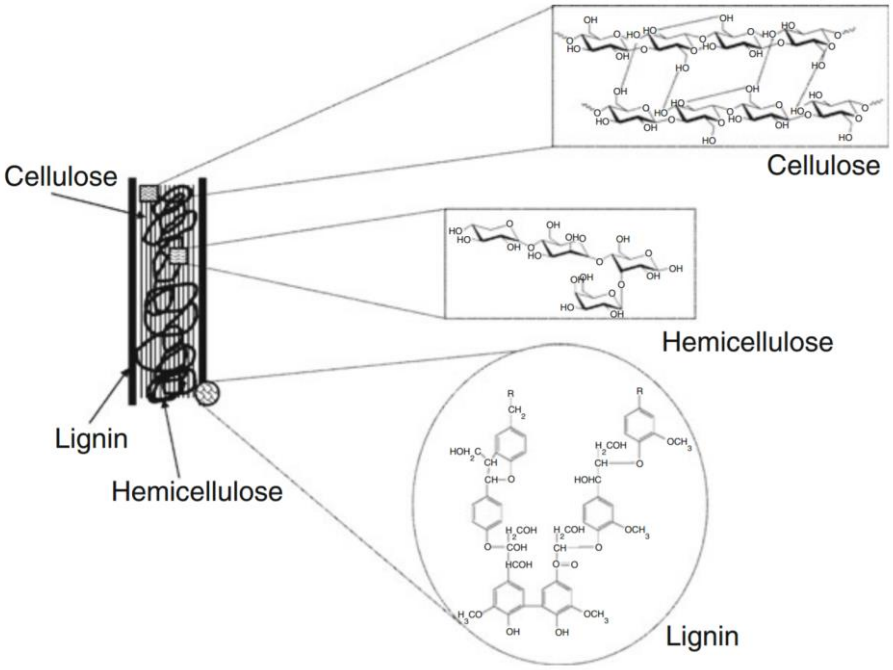

Figure 1.1: Structure of lignocellulose, including cellulose, hemicellulose, and lignin [9]

The conversion of cellulose into fuels and chemicals has been regarded as one of the most promising approaches to sustainable energy production thus far [10]. Cellulose is a polymer consisting of D-glucose monomers linked together by β-1,4-glycosidic bonds, resulting in a highly crystalline structure that is difficult to hydrolyze. [6]. The conversion of cellulose can be divided into two general steps: (1) the selective hydrolysis of cellulose into glucose and (2) further conversion of glucose into fuels and chemicals. Previously, the hydrolysis of cellulose has been done using mineral acids, base, enzymes, or supercritical water, but these processes suffer from problems such as product separation, corrosion hazards, and enzyme control [10]. The ideal method for cellulose conversion into fuels or chemicals would be a one-pot single-step catalytic process. The main challenge of developing a one-pot process for cellulose conversion is the development of a suitable catalyst that can promote several reactions such as cellulose hydrolysis and subsequent hydrogenolysis and/or hydrogenation [10].

A wide variety of products can be produced from the conversion of cellulose. However, cellulose has a much higher O/C ratio than fuels, meaning excess oxygen has to be removed when cellulose is converted into fuels, which would occur at the expense of C or H. The production of fuels from cellulose therefore has a low efficiency from the viewpoint of atom economy [11]. On the other hand, converting cellulose into oxygenates such as polyols would

result in a much higher atom economy as the oxygen-functional groups present in cellulose would still be present in the desired products [12]. Polyols, such as ethylene glycol (EG), propylene glycol (1,2-PG), sorbitol, mannitol, and glycerol are important chemical used in a variety of industries, such as monomers in the plastic industry, intermediates in the pharmaceutical industry, and additives in the food industry [13]. Among these polyols, EG has the largest market with a consumption exceeding 20 million metric tons per year (2011) for the synthesis of antifreezes and polymers, especially polyethylene terephthalate (PET) bottles and fibers [14]. However, EG is currently being produced from ethylene derived from petroleum via multiple steps of cracking, epoxidation, and hydration [13]. The biomass route for EG production presents noticeable advantages of a one-pot process and a renewable feedstock compared to the non-renewable multi-step petroleum process.

The one-pot conversion of cellulose to EG has recently been investigated in numerous studies, but it has not yet reached the industrial scale. The objective of this study is to expand on the research related to the catalytic conversion of cellulose to EG by using tungsten-based catalysts supported on carbon nanotubes (CNT). The tungsten-based catalysts (WO_3, W_2C, and W_2C-WC) were tested by themselves and with the addition of copper to examine the promotion effect of copper (Cu). WO_3 and W_2C were also tested in combination with Cu_xO/CNT and Ru/CNT in order to assess the hydrogenation ability of copper and ruthenium. The effect of tungsten loading was also examined by using 10 and 50 wt% WO_3 and W_2C in combination with Ru/CNT while maintaining a constant Ru/W ratio. A very dilute amount of sulfuric acid (H_2SO_4) was also used to examine if the EG yield could be further increased with the addition H_2SO_4. This report will discuss the theoretical basis, experimental setup, and reaction results for these catalytic systems.

2. Literature Review

This section focuses on reviewing the literature surrounding the catalysts and methods used in this study. The role of various catalysts on the production of EG from cellulose is discussed, as well as the reaction conditions. The potential use of these catalysts for the conversion of lignocellulose and the stability of different catalytic systems is also examined. Finally, different catalytic supports and catalyst synthesis methods are discussed.

2.1 One-Pot Catalytic Conversion of Cellulose

One-step catalytic processes for the conversion of cellulose to polyols have recently become a focal point for a lot of research. The combination of acid-catalyzed cellulose hydrolysis with *in situ* hydrolytic hydrogenation or hydrogenolysis in the same reactor results in a synergistic effect since the unstable intermediates derived from cello-oligosaccharides and sugars are quickly removed. Therefore, the combination of cellulose hydrolysis with glucose hydrogenation over a supported metal catalyst or glucose hydrogenolysis over a tungsten-based catalyst in one reactor results in hexitols (sorbitol and mannitol) or 1,2-alkanediols (EG and 1,2-PG), respectively, as the main products [15].

Fukuoka et al. were among the first to demonstrate the one-pot catalytic transformation of cellulose. In this study, supported Pt and Ru catalysts were used in water to produce hexitols such as sorbitol and mannitol, from cellulose. They proposed a reaction scheme involving the hydrolysis of cellulose to glucose followed by the subsequent reduction of glucose to hexitols [16]. The highest reported yield was 31% (25% sorbitol and 6% mannitol) with a Pt/Al_2O_3 heterogeneous catalyst, at 423 K and 5 MPa H_2 for 24 hours. The activity and selectivity of certain catalysts towards polyols was also studied, and it was found that both the type of metal and support material were of great influence in the selectivity of certain reaction products [16].

2.1.1 Ruthenium-Based Catalysts

Several other studies have been conducted based on the one-pot cellulose conversion process. Among them, Luo et al. created a Ru/C catalyst, changing the support material to carbon as well as elevating the reaction temperature, resulting in an increased cellulose conversion and hexitol yield. The highest yield reported was 39.3% hexitols with 4 wt% Ru/C in water at 518 K and 6 MPa H_2 for 30 minutes [17]. Supported noble metals, including Ru, act as hydrogenation catalysts resulting in polyols as the main product. Ruthenium metal

particles supported on various carbides and oxides have been shown to be the most efficient among noble metals in achieving selective conversion of carbonyl groups into alcohols [18]. Lee et al. performed high-throughput screening of monometallic catalysts and determined that Ru is the most active metal for the hydrogenation of non-furanic carbonyl groups in aqueous phase reactions [19].

Several experiments have also been conducted on the solvent effect on hydrogenation activity of Ru, and it was determined that the reaction rate of Ru catalysts was significantly enhanced in water [20]. Wan et al. performed detailed kinetic investigation of various solvents over a Ru/C catalyst and determined that the highest hydrogenation activity occurred in protic solvents, with water giving the maximum rate enhancement [21]. This is because H^+ ions are reversibly formed in high temperature water, which are capable of catalysing cellulose hydrolysis without the presence of a catalyst [5]. The ruthenium catalyst is then responsible for the successive hydrogenation reaction of the hydrolysate sugars to polyols [17]. However, the ruthenium sites do not act solely for the hydrogenation of sugar, but also promote cellulose hydrolysis via heterolytic dissociation of H_2 [16], in which the acidic sites originate from acidic groups on the surface of the support or from water itself [17].

2.1.2 Tungsten-Based Catalysts

Although Ru/C is an effective hydrogenation catalyst, tungsten-based catalysts are required for the hydrogenolysis of glucose. Tungsten-based catalysts cause C-C single bond cleavage, resulting in 1,2-alkanediols as the major product rather than hexitols [22]. Earlier studies used base catalysts, such as CaO, to function as the hydrogenolysis agent. However, base catalyst may cause the isomerization of glucose to fructose, resulting in glycerol rather than EG as the major product [23]. Tungsten-based catalysts are therefore the most effective catalyst to promote hydrogenolysis of cellulose for EG production [13]. This is due to the bifunctional role of tungsten in both cellulose hydrolysis and C-C cleavage [24]. The active species for C-C cleavage is water soluble H_xWO_3, in which the α-OH group adjacent to the carbonyl group on sugars undergoes C-C bond cleavage. There is then a complex rearrangement of the C-C bonds in the sugars to form the corresponding EG or 1,2-PG [15]. Additionally, a difference was noted between different tungsten based catalyst, in which the catalyst with a single active phase, W_2C, was slightly more active and selective towards EG than a catalyst with both W_2C and WC as active phases [10].

EG and 1,2-PG are formed from their corresponding precursors of glucose and fructose, respectively. However, in most cases more EG than 1,2-PG is formed due to the higher selectivity of glucose during cellulose hydrolysis [15]. In addition to acting as hydrogenolysis catalysts, tungsten carbide catalysts behave similarly to noble metal catalysts for hydrogenation. The unique properties of tungsten carbides were attributed to the insertion of carbon atoms into the lattice of the parental metals, causing a contraction of the d-band and leading to a d-electron density similar to noble metals [25]. Zheng et al. reported that tungsten catalysts were more efficient than noble metal catalysts, achieving 100% cellulose conversion in aqueous solution for 30 minutes at 518 K and 6 MPa H_2 [26]. This was also confirmed by Ji et al. as Pt and Ni on activated carbon (AC) exhibited a moderate conversion of cellulose and a low EG yield, while the tungsten carbide on AC lead to almost complete conversion of cellulose and a much higher EG yield [10].

One disadvantage of using solid W_2C catalysts is that they undergo oxidation under hydrothermal conditions. A series of temperature-controlled phase-transfer W catalyst, such as WO_3 and tungsten acid (H_2WO_4), have therefore also been developed. WO_3 and H_2WO_4 can be dissolved in hot water and go through a phase transformation to tungsten bronze (H_xWO_3) in the presence of H_2 [27]. H_xWO_3 is a highly active homogenous catalyst capable of promoting cellulose hydrolysis and selective C-C cleavage of cellulose to glycolaldehyde, which can then by hydrogenated over Ru/AC for the production of diols [15]. Tai et al. reported an EG yield of 54.4% using H_2WO_4-Ru/AC after 30 minutes at 518 K and 6 MPa H_2, even after being reused 20 times [27]. Additionally, H_xWO_3 can be precipitated out of solution easily in cold water and recovered by filtration, simplifying catalyst recovery [15]. Another study by Zhang et al. used phosphotungstenic acid (PTA), rather than tungsten acid, as a homogenous catalyst with Ru/AC and achieved an EG yield of 53.1% after 50 minutes at 523 K and 6 MPa H_2 [28].

2.1.3 Promotion Effect of Transition Metals

Previous studies performed by Ji et al. showed that the EG yield from tungsten carbide catalysts was significantly improved when promoted by a small amount of nickel (Ni). They tested the effect of Ni on 30 wt% W_2C/AC at 518 K and 6 MPa H_2 for 30 minutes. The EG yield without nickel was reported to be 27.4%, and when a small amount of Ni (0.5 wt%) was added the yield increased to 39.4%. When the nickel loading was increased to 2 wt%, the EG yield increased even further to 61.0%, but a further increase of nickel loading resulted in a decrease in EG yield [22]. However, Ji et al. performed another study investigating the effect

of preparation methods, and were able to achieve an EG yield of 73% with 10%Ni-30%W_2C/AC when Ni was loaded by post-impregnation rather than by co-impregnation [29]. This may be because the introduction of Ni by post-impregnation, rather than co-impregnation, resulted in re-dispersion of the W component, resulting in a significantly higher dispersion of active sites [29].

The Ni-W_2C/AC catalyst showed remarkable selectivity towards EG when compared to other catalysts, such as Pt/Al_2O_3 and Ru/C [10]. The promotion effect of Ni on W_2C results from the close contact of Ni with the support, resulting in electron transfer from Ni to the W species. This results in a synergistic effect on the activating adsorption of H_2 and the reduction of W, accelerating the selective C-C and C-O bond cleavage in the intermediate sugars [30]. Ji et al. also performed surface science studies of EG on WC and Ni- W_2C in order to understand the modification effect of Ni on W_2C. It was determined that the bonding configuration of EG on W_2C was significantly modified by Ni, in which the Ni on W_2C reduced the decomposition of EG due to weaker bonding between EG and Ni-W_2C compared to W_2C [10].

Following this development Zheng et al. tested several monometallic group 8, 9, and 10 metal [M(8,9,10)] catalysts, such as Pd/AC, Pt/AC, Ru/AC, Ni/AC, and Ir/AC, and discovered that these catalysts were incapable of degrading cellulose as efficiently as W/AC [26]. They then developed a series of bimetallic catalysts (Pd-W, Pt-W, Ru-W, Ni-W, and Ir-W) by co-loading them on the same support, which resulted in significantly higher cellulose conversion. The cellulose conversion of these bimetallic catalysts was comparable to the tungsten carbide catalyst performance, and resulted in EG yields in the range of 50%-76% [26]. Zheng et al. also presented experimental evidence that the tungsten species played a role in the hydrogenolysis of sugars into C_2 and other unsaturated compounds, while the M(8,9,10) metals were responsible for the hydrogenation of the unsaturated compounds to polyols such as EG. This was demonstrated by physically mixing the W/AC and Ni/AC catalysts, which resulted in a good EG yield of 46.6%, suggesting that the conversion process involves several cascading reactions on different functional sites of the catalyst [26].

The promotional effects of transition metals is due to their excellent hydrogenation activity, which can compensate for the insufficient ability of WC_x/AC [13]. The presence of transition metals also prevents tungsten carbide from undergoing oxidation by spill-over of dissociated hydrogen [31]. However, the promotion effect of transition metals is only significant when the hydrogenation of WC_x is insufficient. This was demonstrated by Zhang et

al. when using a mesoporous carbon (MC) as the support, resulting in an EG yield of 73%, without a transition metal. The promotional effect of transition metals was negligible in this case as the yield only increased to 75% [32]. The effect of MC as a support may be attributed to the better dispersion and accessibility of WC_x due to the 3D mesoporous structure, as well as the transportation of molecules within the structure, resulting in enhanced hydrogenation activity for the unsaturated intermediates [13]. In addition, MC showed preferential adsorption for glycosidic bonds in cellulose, resulting in enhanced catalytic activity for cellulose hydrolysis [33].

2.1.4 Activity and Selectivity of Various Tungsten-Based Catalysts

The conversion of cellulose is nearly complete over all tungsten-based catalysts at typical reaction conditions of 518 K and 6 MPa H_2 for a minimum of 30 minutes, indicating high activity for cellulose degradation. However, the EG yield varies greatly depending on the catalyst employed, reflecting the great differences in EG selectivity [13]. Tungsten carbide is in itself a multifunctional catalyst, meaning it is capable of cellulose hydrolysis and subsequent hydrogenolysis of sugars without promotion of a transition metal. The acid sites can arise both from hot water and from surface tungsten oxides [17], while the hydrogenation sites arise from the platinum-like electronic properties of tungsten carbides [34]. This multifunctional property of tungsten-carbide results in moderate EG yields (~30%) without the presence of a transition metal [10]. In addition to EG and other polyols, a large fraction of unsaturated compounds and a trace amount of gases (CH_4, C_2H_6, CO_2, CO, etc.) are formed, reducing EG selectivity [13]. However, the addition of a transition metal results in an increase in EG yield by 10-40% depending on the transition metal, as well as reducing the amount of unsaturated by-products and intermediates, thereby increasing the selectivity towards EG [13].

Another group of effective tungsten-based catalysts consist of tungsten oxide and tungsten species (W, WO_3, H_2WO_4, PTA, etc.) and a transition metal [13]. These catalysts are different from WC_x because they are only active for C-C bond cleavage and inactive for the subsequent hydrogenation. They must therefore be used in combination with a hydrogenation catalyst in order to produce EG as they do not exhibit the same multifunctional properties [35]. Cellulose conversion was still complete without the presence of transition metals, but no polyols were produced [13], meaning transition metals are mandatory for these catalysts whereas they are promotional for tungsten carbide catalysts. The EG yield is largely dependent on the relative amount of each component, meaning the different functions of each component

need to cooperate with one another in the cascade reaction of cellulose to EG. Wang et al. determined that the maximum EG yield was obtained at ratios of Ni/W = 1.0 and Ru/W = 0.1 [13]. When comparing Ni and Ru catalysts, Ni is a better option than Ru for high EG yield, as Ru catalyzes the further degradation of EG into gases such as CH_4 and CO_2 [27], while Ni does not [13].

2.1.5 Promotion Effect of Sulfuric Acid

Some studies have also been done using H_2SO_4 as an additive. This is because H_2SO_4 is a widely used acid catalyst to promote cellulose hydrolysis, which is the rate-determining step in cellulose transformation reactions [36]. The hydrolysis reaction is kinetically slower than the subsequent reactions when using a weak acid catalyst such as H_2WO_4, which limits the C-C cleavage, resulting in a low yield of glycolaldehyde [37], and therefore also EG if a hydrogenation catalyst is also used. Xu et al. performed a study investigating the effect of extremely dilute H_2SO_4 on the cellulose conversion to ethylene glycol and discovered that the yield was increased from 32.6% to 52.6% when H_2SO_4 was added at a H_2SO_4/H_2WO_4 ratio of 0.03 with Ru/C after 30 minutes at 245 °C and 6 MPa H_2 [38]. They also determined that the promotional effect became negligible at a H_2SO_4/H_2WO_4 ratio greater than 0.04, and was actually reversed to exhibiting an inhibiting effect. Too much H_2SO_4 resulted in side reactions, such as dehydration and condensation, of glucose into HMF and humins [38]. In order to determine whether or not H_2SO_4 promotes the C-C cleavage, Xu et al. used cellulose and cellobiose as a feedstock and determined that the glycolaldehyde yield remained almost unchanged with or without the addition of H_2SO_4, showing further evidence that it only promoted the hydrolysis step [38].

2.1.6 The Effect of Reaction Conditions

The EG yield from cellulose is greatly affected by H_2 pressure, reaction temperature, and reaction time. Ji et al. conducted a second study on the optimisation of EG yield by varying these three parameters. With regard to H_2 pressure, they determined that the highest EG yield was obtained at 6 MPa, as the yield increased from 5 MPa but remained nearly unchanged when increased to 7 MPa [10]. The optimum temperature was determined to be 518 K, as temperatures above and below this point resulted in lower EG yields. This suggests that EG formation is not a thermally stable process due to further decomposition of EG at higher reaction temperatures [10]. When studying the effect of reaction time it was determined that

the EG yield was initially highest after 30 minutes, and then exhibits an unusual decline in yield after 60 minutes. However, after this unusual drop in yield, the EG yield continued to increase at prolonged times. The 1,2 PG yield was also reported to increase with the reaction time, but did not experience the same drop as EG, meaning that further optimising the reaction time can lead to high yields of both EG and 1,2-PG [10].

In addition to temperature, pressure, and time, a study by Xiao et al. examined the effects of cellulose concentration on conversion and product yield using a CuCr catalyst at 518 K and 6 MPa H2 for 5 hours [5]. They reported that complete cellulose conversion was obtained up to a cellulose concentration of 15 wt% in water. However, the yield of 1,2-PG increased initially and passed a maximum of 36.3% at 10 wt% cellulose, and then gradually decreased to 11.1% at 15 wt% cellulose. The same trend was seen for EG yield as well as the total yield, reaching a maximum at 10 wt % cellulose (7.6% EG and 72.5% total) [5]. This is because initially the catalysts have enough available active sites for hydrogenolysis, but as the cellulose concentration is increased, the concentration of water-soluble saccharides becomes so large that they cover the active sites, suppressing the desorption of products, resulting in a lower yield of polyols [5].

2.1.7 The Role of High-Temperature Water

Another important factor for cellulose conversion is the role of subcritical water. Water is a polar solvent at ambient temperature, but as it is heated its density decreases. This is caused by increased thermal movement of the water molecules, leading to weaker hydrogen bonds between water molecules [39]. Additionally, the polarity of water decreases as the temperature increases, but the polarity of single water molecules remains unchanged. This means that if a polar compound is present in the water, it will attack the water molecules nearby. A high multi-valent cation will therfore interact with the oxygen atom in water, resulting in the elimination of a proton (H^+), thereby behaving as a strong acid. Consequently, if a hydrogen atom from water interacts with an organic molecule, such as cellulose, it will react and enhance cellulose hydrolysis [40].

The temperature also plays a major role in the hydrothermal conversion of cellulose, which occurs at a temperature of 200-370 °C and a pressure of 40-200 bar to maintain water in its liquid state [41]. This temperature range can be explained by the ion product of water, which is defined as the product of the concentration of acidic and basic forms of water [40]. The

impact of temperature on the ion product (K_w) can be seen in Figure 2.1, illustrating a large ion product between 200 °C and 370 °C and a maximum around 250 °C. This means that water will produce protons at elevated temperatures, which will in turn promote cellulose hydrolysis without the presence of a catalyst.

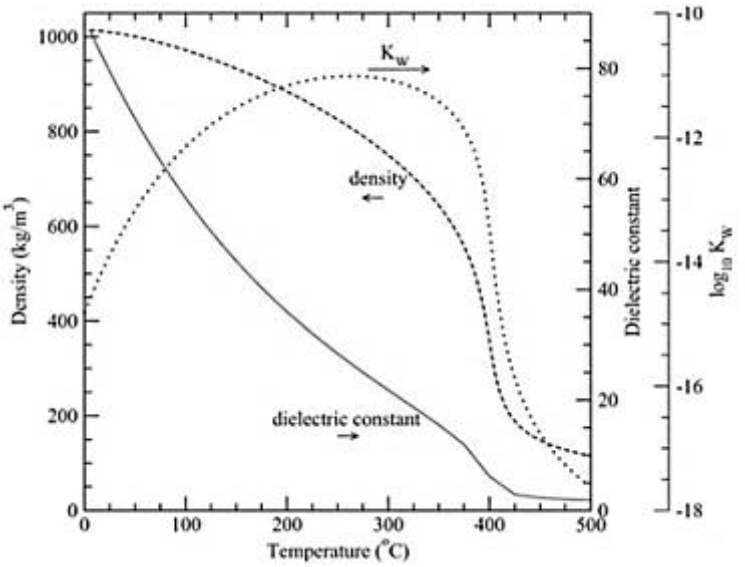

Figure 2.1: Effect of temperature on the ion product (K_w) of water [40]

2.1.8 Summary - One-Pot Catalytic Conversion of Cellulose

There have been numerous reports on the one-pot conversion of cellulose to ethylene glycol. The majority of reports use ruthenium-based catalysts, tungsten-based catalysts, and/or transition metal catalysts in some combination or alone due to their specific activities on cellulose conversion mentioned in the previous sections. From these reports it is clear that W is the key component for C-C bond cleavage, while Ru and M(8,9,10) metals are responsible for the subsequent hydrogenation reactions of unsaturated intermediates. Some of the most recent results for the one-pot conversion of cellulose to ethylene glycol are shown in Table 2.1, including those that have already been mentioned.

Table 2.1: Recent results of one-pot conversion of cellulose to EG and 1,2-PG

Entry	Catalyst	Reaction Conditions (T, P, t)	EG Yield (%)	1,2-PG Yield (%)	Ref.
1	Pt/AC	245 °C, 6 MPa, 0.5 h	8.2	5.9	[10]
2	Ni/AC	245 °C, 6 MPa, 0.5 h	5.2	3.1	[10]
3	30%W_2C/AC	245 °C, 6 MPa, 0.5 h	27.9	5.6	[22]
4	2%Ni-30%W_2C/AC	245 °C, 6 MPa, 0.5 h	61.0	7.6	[22]
5	10%Ni-30%W_2C/AC	245 °C, 6 MPa, 0.5 h	73.0	8.5	[29]
6	WC_x/AC	245 °C, 6 MPa, 0.5 h	47.5	3.6	[32]
7	WC_x/MC	245 °C, 6 MPa, 0.5 h	72.9	5.1	[32]
8	2%Ni-WC_x/AC	245 °C, 6 MPa, 0.5 h	61.7	3.4	[32]
9	2%Ni-WC_x/MC	245 °C, 6 MPa, 0.5 h	74.4	4.5	[32]
10	Ni/W/SiO_2-Al_2O_3	245 °C, 6 MPa, 2 h	24.0	5.5	[42]
11	5%Ni-25%W/SBA-15	245 °C, 6 MPa, 0.5 h	75.4	3.2	[35]
12	1.2%Ru/MC + H_2WO_4	245 °C, 6 MPa, 0.5 h	58.5	3.5	[27]
13	1%Ru/C + H_2WO_4	245 °C, 6 MPa, 0.5 h	32.6	5.6	[38]
14	1%Ru/C + H_2WO_4 + H_2SO_4	245 °C, 6 MPa, 0.5 h	52.6	4.4	[38]
15	Raney Ni + H_2WO_4	245 °C, 6 MPa, 0.5 h	65.4	3.3	[43]
16	5%Ru/AC + PTA	250 °C, 6 MPa, 0.83 h	53.1	5.5	[28]
17	3%Ru/AC	205 °C, 6 MPa, 0.5 h	7.5[a]	3.3[a]	[44]
18	3%Ru/AC + W_2C	205 °C, 6 MPa, 0.5 h	50.8[a]	11.4[a]	[44]
19	3%Ru/AC + WO_3	205 °C, 6 MPa, 0.5 h	51.5[a]	6.7[a]	[44]

[a] Selectivity

From these results it is evident that noble metals and transition metals do not exhibit adequate C-C cleavage, resulting in low EG and 1,2-PG yields (Table 1, Entry 1-2), but higher hexitol yields. When W_2C/AC is used as the catalyst, the EG yield is significantly improved due to the multifunctional nature of tungsten carbide, allowing for C-C cleavage and subsequent hydrogenation (Table 1, Entry 3). The EG yield can be further increased by the promotion effect of Ni on tungsten carbide (Table 1, Entry 4-5). The type of support also plays a role in EG yield, and it is evident that using MC as the support for tungsten carbide results in higher yields than AC (Table 1, Entry 6-9). In addition, using SiO_2-Al_2O_3 as the support resulted in lower yields than AC and MC (Table 1, Entry 10) while SBA-15 exhibited the highest EG yield currently reported (Table 1, Entry 11).

The use of Ru/C with H_2WO_4 also results in relatively high EG yields, as the H_2WO_4 causes C-C cleavage and the Ru/C causes subsequent hydrogenation (Table 1, Entry 12-13). The EG yield from this system could be increased even further with the addition of extremely dilute sulfuric acid (Table 1, Entry 14). Raney Ni was also tested in combination with tungsten

acid, which resulted in even higher EG yields than Ru/C (Table 1, Entry 15). Another tungsten containing acid known as phosphotungstic acid (PTA) was also tested in combination with Ru/C, which resulted in similar EG yields to using H_2WO_4 (Table 1, Entry 16). In addition to combining Ru/C with a homogenous catalyst, it can also be combined with solid tungsten catalysts, resulting in a relatively high EG selectivity in combination, but very low selectivity if only Ru/C is used (Table 1, Entry 17-19) for the same reason that Ni and Pt are insufficient for EG formation by themselves.

2.2 Reaction Mechanism

The process of converting cellulose to EG involves a series of sequential steps. First, the cellulose undergoes hydrolysis to form oligosaccharides and glucose due to the catalytic reaction caused by protons in high-temperature water [17]. The oligosaccharides and glucose then undergo further catalytic degradation to glycolaldehyde by C-C cleavage in the presence of tungsten species. The C-C cleavage occurs selectively at the position between the α-β carbons [26]. The degradation of glucose-based oligosaccharides therefore results in glycolaldehyde (C_2) due to the terminal aldehyde group present. On the other hand, if glucose isomerizes to fructose, fructose will be degraded to C_3 molecules [45]. The hydrogenation of unsaturated C_2 and C_3 intermediates then occurs to produce EG and 1,2-PG respectively [26]. The series of subsequent reactions from cellulose to various polyols is shown in Figure 2.2.

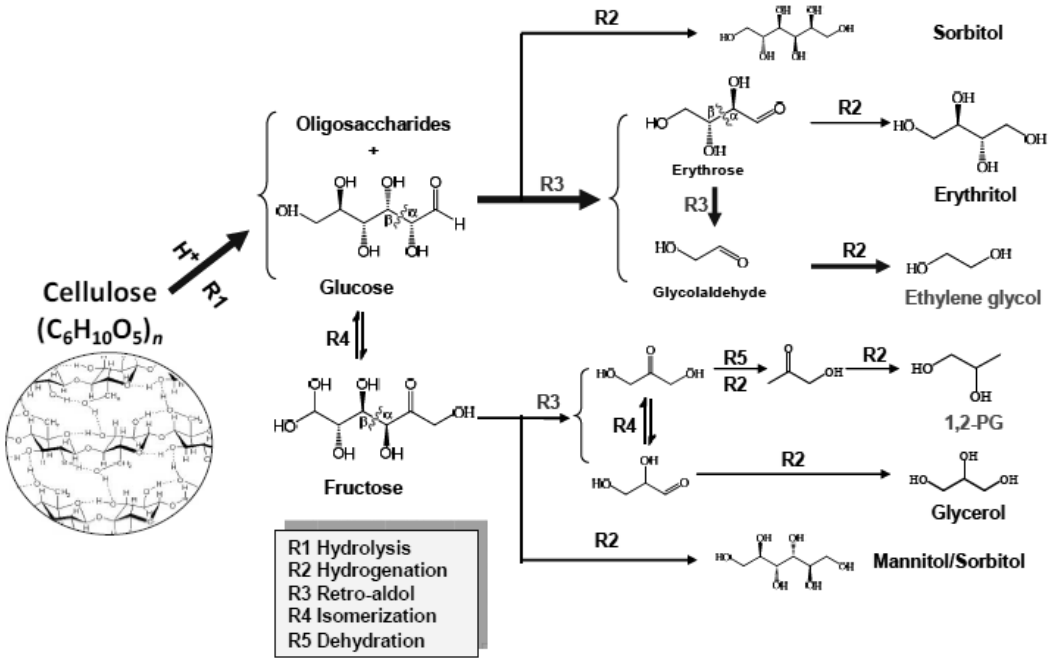

Figure 2.2: Reaction mechanism of cellulose conversion to polyols over tungsten-based catalysts [26]

2.2.1 Active Species and Methods for C-C Cleavage

In order to determine the active species for C-C cleavage, Liu et al. examined the phase-change of various tungsten species (W, W_2C, WO_3, and WO_2) using Raman spectroscopy and surface-sensitive XPS before and after the reaction. They discovered that the surface of the catalyst after the reaction was always dominated by WO_3, regardless of the initial tungsten species [44]. The authors therefore suggested WO_3 was the active species for C-C cleavage. However, these studies were performed ex situ, so another study was performed by Wang et al., and it was discovered that the WO_3 recovered after the reaction showed the typical XRD pattern of tungsten bronze (H_xWO_3). This result suggests that the various tungsten species are transformed into tungsten bronze by H_2 during the reaction [13]. In addition, dissolved tungsten bronze was found in low concentrations (20-200 ppm) after each reaction and was active in the conversion of cellulose to EG when it was combined with a hydrogenation catalyst such as Ni or Ru [13].

Upon this discovery, Wang et al. concluded that dissolved H_xWO_3 is the catalytically active species for C-C cleavage, proceeding through a homogeneous pathway [13]. This conclusion is rational considering that solid catalysts have difficulty accessing the β-1,4-glygosidic bonds in cellulose as well as the C-C bonds in sugars due to steric hindrance. This problem is overcome by a homogeneous catalyst, which results in the high cellulose conversion and EG formation [13]. An important note is that the solubility of various tungsten species is much larger in hot water than that determined after the reaction due to the temperature-controlled phase transfer of H_xWO_3 [27]. This means that the tungsten species are transformed into H_xWO_3 (at least partially) as the solubility increases with water temperature. After the reaction, the dissolved H_xWO_3 is precipitated out of solution and transformed into H_2WO_4 upon cooling, and finally into WO_3 with exposure to air over time [13]. This provides an attractive opportunity to combine the high efficiency of a homogeneous catalyst with the easy recovery of a heterogeneous catalyst. The reaction mechanism proposed by Wang et al. is shown in Figure 2.3.

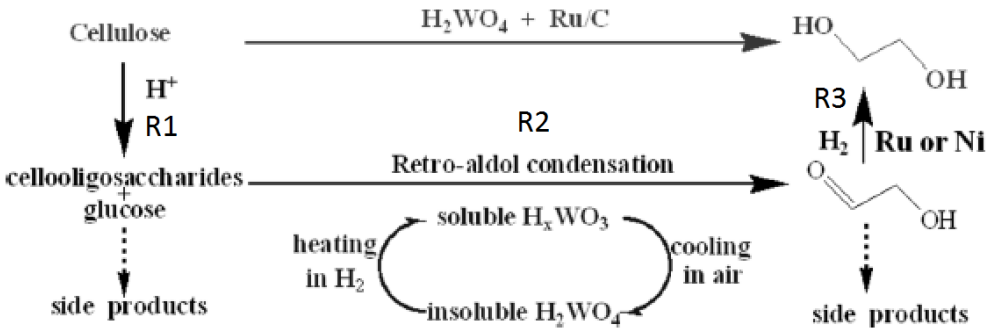

Figure 2.3: Reaction pathway for cellulose conversion to EG over tungsten-based catalysts (Adapted from [13])

There are numerous reports that have conclusively documented that the C-C cleavage of sugars or oligosaccharides follows the retro-aldol pathway in supercritical water [46, 47]. Under typical reaction conditions of 518 K and 6 MPa H_2 for 30 minutes, the water is not in a supercritical state. Wang et al. therefore studied the glycolaldehyde yield from cellulose over tungsten species without the presence of a hydrogenation catalyst. The authors found that under these reaction conditions glycolaldehyde was found in a yield of 5-7 wt%, which is rather low due to the instability of glycolaldehyde under these conditions. However, this yield is still 4-6 times higher than without any catalyst, and its presence as an intermediate to EG suggests that the C-C cleavage catalysed by H_xWO_3 also follows retro-aldol condensation [13]. In addition, a comparative study using glucose and fructose as the feedstock showed that EG and 1,2-PG are formed from the respective sugars with a Ni-W_2C/AC catalyst [45]. This is due to the different positions of the carbonyl group in the glucose and fructose isomers, which further suggests that C-C cleavage occurs via retro-aldol condensation.

2.2.2 Reaction Pathway Kinetics

The reaction pathway shown proposed by Wang et al. in Figure 3 follows the same sequential reaction pathway proposed by Zheng et al. in Figure 2, but with tungsten bronze as the active species for retro-aldol condensation. The first step is the hydrolysis of cellulose into oligosaccharides and sugars through the catalytic reaction of a proton released from both high-temperature water and dissolved H_xWO_3 (R1). These sugar intermediates undergo retro-aldol condensation through the homogeneous catalysis of H_xWO_3, forming glycolaldehyde as the key intermediate (R2). Glycolaldehyde is then rapidly hydrogenated to EG through the heterogeneous catalysis of a transition metal such as Ni or Ru (R3). However, there are also numerous side reactions that arise from metastable intermediate sugars and glycolaldehyde

present in the reaction [13]. In order to limit these side reactions for a high selectivity towards EG, the concentrations of intermediates must be kept low by ensuring the rates of the three consecutive reactions follow the following relationship: R1 < R2 < R3 [13].

Wang et al. performed kinetic studies on the conversion of cellulose using a H_2WO_4 + Ru/C dual catalyst and determined that cellobiose underwent two parallel reactions. One was the hydrolysis of cellobiose and the other was retro-aldol condensation to glycoaldehyde and glucosyl-erythrose in equimolar ratios [13]. The activation energies of cellobiose and retro-aldol condensation at high temperatures were 90 and 161 kJ/mol respectively, satisfying the relationship R1 < R2 due to the higher activation energy of retro-aldol condensation [13]. This is also consistent with what has been observed when the reaction occurs in supercritical water [48]. Since cellobiose undergoes hydrolysis much more easily than cellulose, R1 << R2 in the case of cellulose hydrolysis [13]. In addition, the rate of glycolaldehyde hydrogenation (R3) is 1-2 orders of magnitude higher than R1 and R2 due to the significantly lower activation energy of 42.9 kJ/mol [13]. The combination of tungsten species for retro-aldol condensation, an optimum mixture of tungsten species and transition metals for hydrogenation, and a high reaction temperature therefore favor the kinetics toward EG formation as R1 << R2 << R3.

2.2.3 Alternate Reaction Pathways

Although the kinetics are favoured for EG formation with these catalytic systems, EG and 1,2-PG are not the only possible products, as shown in Figure 2.4. As previously mentioned, EG is formed from glucose produced from cellulose hydrolysis by retro-aldol condensation (2) followed by hydrogenation (3). Alternatively, glucose isomerization to fructose may occur, in which fructose may also undergo retro-aldol condensation and hydrogenation to form 1,2-PG, glycerol, and EG. However, glycerol is in equilibrium with glyceraldehyde, indicating that the reversible reaction of glycerol can result in full conversion to 1,2-PG and EG. In addition, both the fructose and glucose pathways may result in hydrogenation before retro-aldol condensation, favouring the production of mannitol and sorbitol. However, these reactions are also in equilibrium and reversible. Another possibility is the dehydration of fructose, resulting in 5-hydroxymethylfurfural (HMF), which can undergo further reactions to form 2,5-dihydroxymethylfuran (2,5-DHF), tetrahydro-2,5-furandimethanol (THFDM), 1,2,6-hexanetriol, 1,2-hexanediol, and 1,6-hexanediol. In addition, the erythrose produced from glucose may undergo a secondary reaction pathway other than EG formation, forming erythritol and 1,2-butanediol.

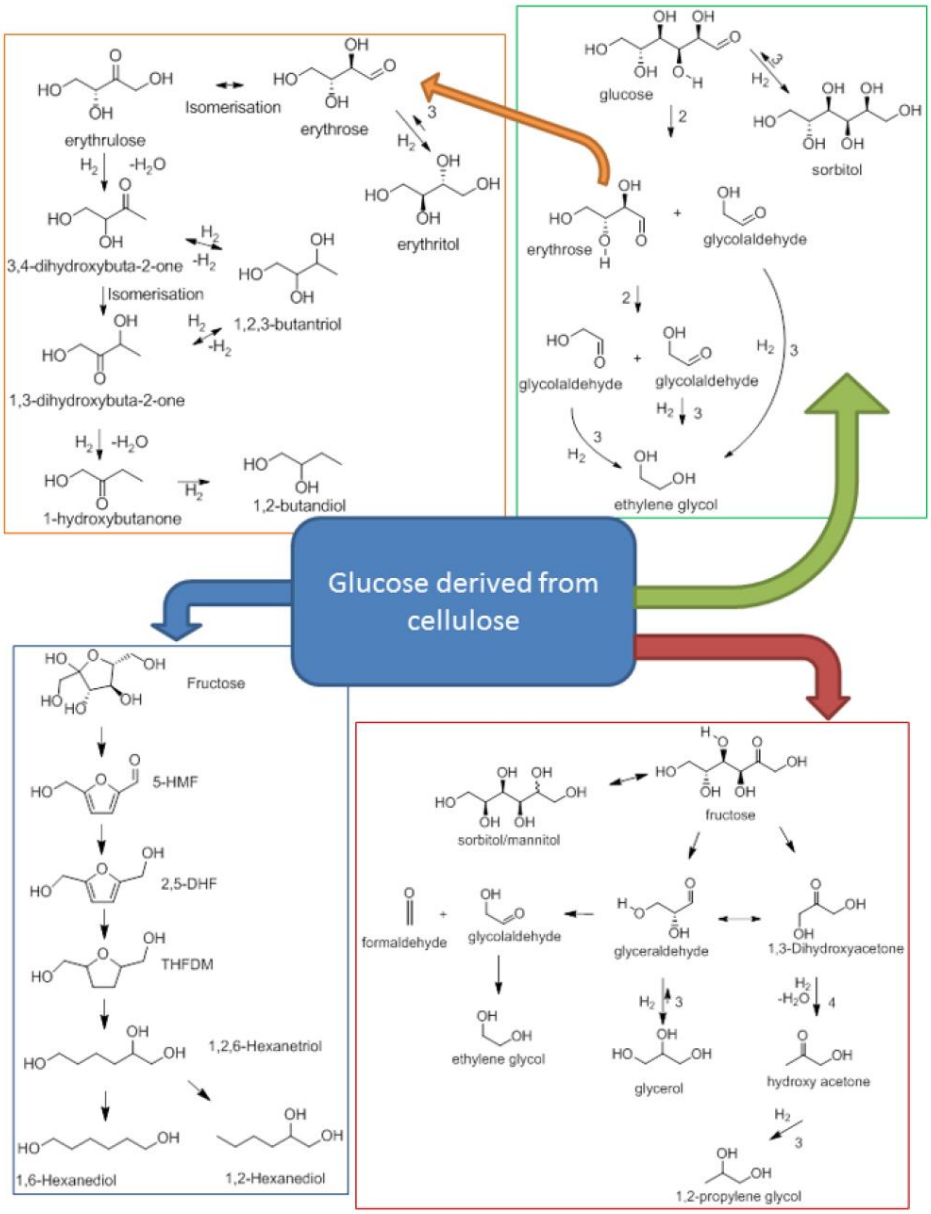

Figure 2.4: Reaction network of the catalytic conversion of cellulose [49]

Although this reaction network shows a consecutive sequence for HMF degradation pathway, another study by Yao et al. proposes a non-consecutive pathway. Yao et al. used HMF as a feedstock to form 1,2,6-hexantriol and proposed that THFDM is a side product rather than an intermediate in the HMF pathway as proposed by van der Wijst [50]. They reported that in all cases, the pathway begins with the hydrogenation of the aldehyde group on HMF, producing 2,5-DHF. The formation of THFDM or 1,2,6-hexanetriol depended on the orientation of adsorption onto the catalyst, as 2,5-DHF may be completely hydrogenated to form THFDM, or ring opened by cleavage of the C-O bond, then hydrogenated to form 1,2,6-hexantriol [50] . This proposed reaction pathway is shown in Figure 2.5.

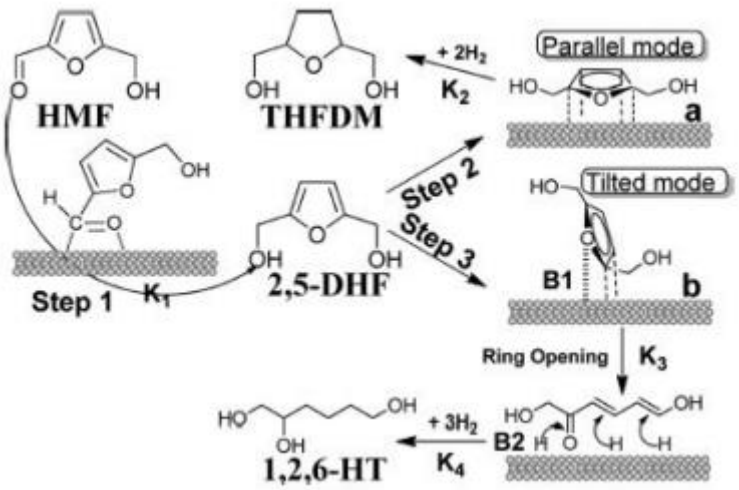

Figure 2.5 Reaction pathway for HMF degradation [50]

2.3 Direct Conversion of Lignocellulose

Although the work of this paper, along with a large amount of other research, focuses on the conversion of cellulose as a model compound for biomass, it would be more profitable from an industrial point of view to use raw lignocellulose as the feedstock. However, the challenge of using lignocellulose as a feedstock is being able to degrade the three main components of lignocellulose simultaneously. Li et al. demonstrated a one-pot hydrocracking process for the conversion of various lignocellulosic materials using 4%Ni-30%W_2C/AC and determined that the carbohydrate fractions (cellulose and hemicellulose) could be cracked into diols while the lignin fraction could be cracked into monomeric phenols, converting all three fractions simultaneously [51].

The EG yield from cellulose was reported to be 61% at reaction conditions of 518 K and 6 MPa H_2 for 30 minutes from their earlier work, while the EG yield from birch was reported to be 51.4% at reaction conditions of 508 K and 6 MPa H_2 for 4 hours. [51]. These results are fairly comparable considering that no pre-treatment was done to the biomass before the reaction. Another interesting result is that the 1,2-PG yield from birch wood (14.2%) is nearly twice as high as that obtained from cellulose alone (7.6%). They proposed that the higher 1,2-PG yield from birch wood is due to the fact that birch wood contains 19.3 wt% hemicellulose, which is a C_5 sugar polymer that is different from the structure of cellulose [51]. The proposed reaction pathway from cellulose and hemicellulose to diols is shown in Figure 2.5.

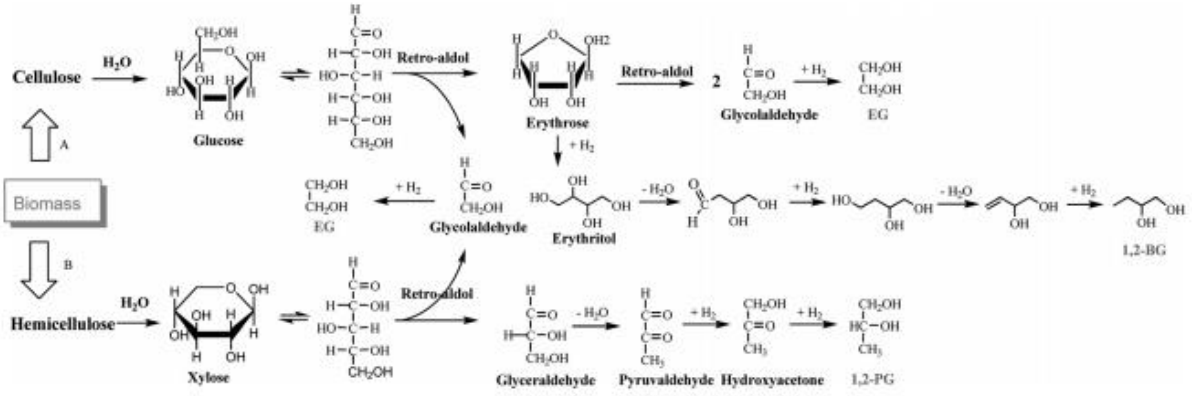

Figure 2.6: Reaction pathway of diol formation from cellulose and hemicellulose [51]

Li et al. also noted a mono-phenol yield of 36.9% from birch wood using the same catalyst and reaction conditions. The four main monophenols produced were syringylpropane, guaiacylpropane, syringylpropanol, and guaiacypropanol, which are all derived from lignin [51], as shown in Figure 2.7. The authors also showed that the mono-phenol yield from lignin could be increased if the reaction was performed with small-molecule alcohol as the solvent. When methanol was used as the solvent the mono-phenol yield increased to 42.2%, and when EG was used as the solvent the yield increased even further to 46.5% [51]. This is most likely due to the increased solubility of the lignin present in birch in both methanol and EG [52]. In addition, small-molecule alcohols increase the solubility of hydrogen [53], which may assist in the hydrogenolysis of phenolic ether linkages [51]. These results suggest that the Ni- W_2C/AC is effective for lignin degradation, but it may not exhibit the same synergistic effect as that seen for EG formation.

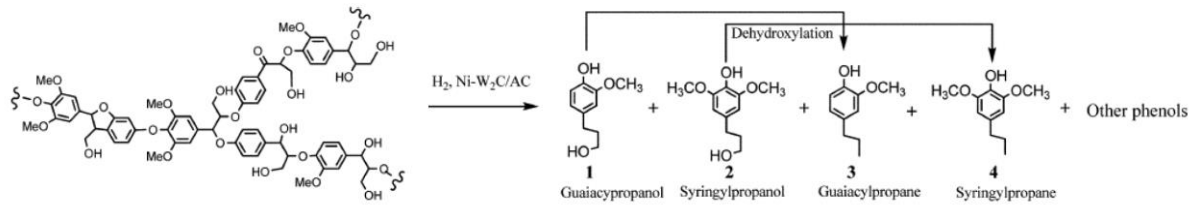

Figure 2.7: Degradation of lignin into mono-phenols using Ni-W2C/CNT

Although Li et al. did not specifically test the synergistic effect between Ni and W_2C for lignin degradation from birch wood, they did test it between noble metals and W_2C by using Pd, Pt, Ir, and Ru both as monometallic and bimetallic catalysts with W_2C. The bimetallic catalysts resulted in higher EG yields than the monometallic catalysts as expected from other

research, but they did not show any superiority over monometallic catalysts for the conversion of lignin components [51]. The mono-phenol yields over the monometallic catalysts were 40.9%, 44.1%, and 55.1% for Ir/AC, Pt/AC, and Pd/AC respectively. The corresponding noble-metal modified W_2C bimetallic catalysts resulted in lower yields of 30.6%, 26.7%, and 28.4% respectively, indicating that there is no synergistic between W_2C and noble metals for lignin degradation [51]. Another interesting discovery was that the behaviour of Ru was very different from the other noble metal catalysts when using birch wood. Only trace amounts of diols and mono-phenols were formed with the Ru-W_2C/AC catalyst, but the gas products attributed to 72.08 wt% of the total carbon in the feedstock, with methane being the main product (59.9% yield). The results were very similar when using a monometallic Ru/AC catalyst, indicating that the main products from birch wood were gases when using Ru [51].

Li et al. also examined the conversion of other lignocellulosic biomass (pine, poplar, basswood, ashtree, xylosma, beech, and yate) using the same procedure in order to investigate the product distribution and conversion efficiency of different biomass feedstocks. They found that both the product distribution and conversion efficiency were affected by the feedstock, in which the lignin content was the key factor for inhibiting diol formation [51]. Biomass feedstocks with lignin content below 20% resulted in EG yields of approximately 50% and a total diol yield greater than 70%, while a lignin content of approximately 25% resulted in approximately 35% and 60% yields respectively. Biomass with lignin content above 30% resulted in the poorest results, with the lowest EG yield being 16.3% and the total diol yield being 30.6% [51]. The distribution and total yield of mono-phenols also varied greatly with varying biomass feedstocks due to the different lignin structures of various lignocellulosic biomass [51].

2.4 Catalyst Stability and Reusability

Another important factor when considering the catalytic conversion of lignocellulose is the ability to recycle the catalyst after metal-catalysed liquid-phase reactions, although it will not be examined in this study. Ji et al. examined the recyclability of the Ni-W_2C/AC catalyst and reported that the EG yield decreased when re-used for a second run, but remained nearly constant when used again for a third run [10]. They therefore concluded that leaching of the metal catalyst was negligible and not the main cause for yield loss after recycling. However, after performing XRD on the used catalyst after each run they noticed that the active W_2C phase was slightly oxidized, which may be the cause of decreased EG yield after recycling

[10]. Li et al. also examined the recyclability of their Ni-W_2C/AC catalyst, which showed promising reusability for the conversion of the carbohydrate fraction of lignocellulose as the EG and total diol yields only decreased slightly after being re-used four times. However, the total mono-phenol yield decreased considerably in the fourth run, while remaining relatively stable for the first three [51]. They also performed XRD on the used catalysts and reported similar results to Ji et al., as the partial oxidation of W_2C occurred during the reaction. In their results some leaching of Ni and W was also reported, which in combination with oxidation of the active phase, could lead to loss in activity [51]. In addition, tar formation was noticed after the third and fourth runs, which may have mixed with the catalyst and formed aggregates on the surface, inhibiting the catalytic reaction [51].

Zhang et al. also examined the recyclability of their 3D mesoporous carbon (MC) support for tungsten carbide catalysts. They reported that their support greatly facilitated the transport of reactant and product molecules, as well as providing better dispersion of tungsten carbide [32]. The better dispersion and accessibility of active sites using a MC support significantly increased the catalytic performance of the tungsten carbide catalyst compared to activated carbon (AC). Activated carbon is a microporous material, which often gives rise to low dispersion and poor active site accessibility [32]. However, they also reported that partial oxidation of tungsten carbide had occurred on the recovered catalyst, and the EG yield decreased. They therefore attempted to regenerate the tungsten carbide phase by reduction in hydrogen flow, which resulted in the EG yield being partly recovered [32]. This further suggests that the loss of activity and selectivity is due to the surface oxidation of the tungsten carbide species. Although the new MC support also resulted in EG yield loss, it was not as significant as the yield loss reported by Li et al. using an AC support [51]. This may be due to leaching of W not being the main cause of EG yield loss for the MC support, but it was for the AC support, as AC resulted in more than half of the W being lost after four runs [32]. This suggests that MC has a better stability than AC when used as the support for tungsten carbide catalysts.

In an attempt to mitigate the stability issues of the Ni-W_2C/AC catalyst, Tai et al. developed a catalyst system using H_2WO_4 in combination with 1.2% Ru/C. This catalytic system is more robust than solid tungsten carbide catalysts and capable of handling the hydrothermal reaction conditions [27]. In a similar manner that solid tungsten species form H_xWO_3 in hot water and acts as a homogenous catalyst, the H_2WO_4 acts as a homogenous

catalyst for cellulose hydrolysis and C-C cleavage. This catalyst system exhibited excellent recyclability as it could be used more 20 times without a notable decrease in EG yield [27]. Wang et al. expanded this study to 34 runs using the same catalyst system, producing an average EG yield above 50% in more than 30 runs [13]. This may be attributed to the high resistance of noble metals to oxidation and dissolution under hydrothermal conditions [13]. There was no sintering or leaching of Ru after 30 repetitive runs [27], which is not the case for Ni and W [10, 51]. The results of these reusability tests using three different tungsten-based catalyst systems are summarized in Figure 2.6.

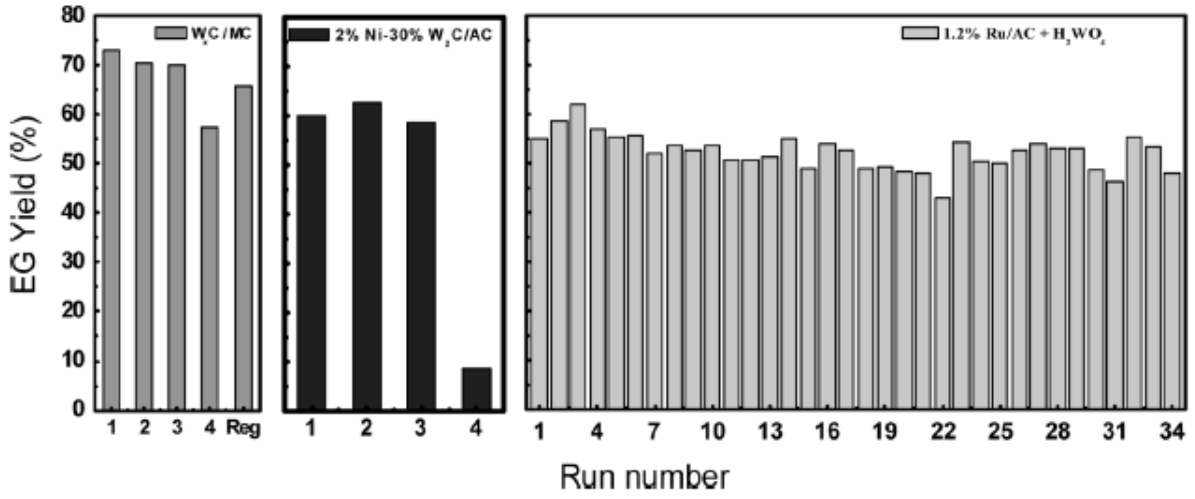

Figure 2.8: Reusability of various tungsten-based catalyst systems [13]

2.5 Catalyst Support and Synthesis

Numerous catalysts have been developed and tested for the conversion of cellulose or lignocellulose to polyols, and both the choice of support material and active metal play an important role. In the case of conversion of cellulose to EG, hot compressed water is used as the reaction medium, meaning the catalyst must be resistant to hydrothermal attack [13]. The structural stability of the support is therefore essential to the reaction, and many commercially available metal oxide supports, such as silica and alumina, suffer from deterioration and collapse under hydrothermal reaction conditions [13]. For example, although the Ni-W/SBA-15 has shown the highest EG yield reported so far (75.4%) it cannot be reused because the mesoporous structure of the support experiences complete collapse after just one run [35]. Commercially available carbon supports are therefore preferred, as carbon has excellent stability under hydrothermal conditions, high resistance to basic and acidic attack, and it is inert toward chelating with other chemicals [13]. Numerous carbon materials, such as activated

carbon (AC) [22], mesoporous carbon (MC) [32], carbon nanotubes (CNT) [54], and carbon nanofibers (CNF) [55] have been successfully used as supports for cellulose conversion.

2.5.1 Carbon Supports

Activated carbon has been widely used due to the advantage of high surface area and well-developed porosity [56]. However, during reactions using hydrogen, methanation may occur, resulting in noticeable side-reactions at high temperature [56]. In addition, the microporous structure of AC results in mass transfer limitations during the reaction [57]. On the other hand, CNTs and CNFs have a mesoporous open structure, in contrast to the microporous structure of AC, which affects the catalytic activity as well as the catalyst preparation method [13]. Zhang et al. reported higher EG yields for their mesoporous support compared to microporous supports with regard to tungsten carbide catalysts, which may be due to better dispersion of tungsten carbide [32]. Ji et al. reported that the EG yield was significantly lower when alumina was used as the support, rather than activated carbon, for W_2C. They noted the presence of a large fraction of unidentified unsaturated products, which are assumed to result from the insufficient hydrogenation activity of WC_x/Al_2O_3 [22]. This further suggests that the type of support greatly influences the catalytic activity of tungsten carbide. They attributed this difference to the different active phases of tungsten carbide formed on the different supports. It was found that W_2C formed on activated carbon, while WC formed on alumina, suggesting that the W_2C had a higher intrinsic activity than WC [22].

2.5.2 Carbon Nanotubes as Support

Carbon nanomaterials, such as CNF or CNT, have shown promising applications as catalyst supports. Both types consist of carbon atoms arranged into planes, in which CNFs can be arranged into a platelet, ribbon, or fishbone structure while CNTs are arranged into an axial tube with a hollow cavity [57]. Unique characteristics such as mesoporous structure, high surface area (80-200 m^2/g), high mechanical strength and electric conductivity, and high resistance to strong acids and bases distinguish CNTs and CNFs from AC [57]. However, impurities and remaining grow catalysts from the production of CNTs have been shown to affect the catalyst activity and selectivity [58], so pre-treatment of CNT in acid is required. The textural properties of CNFs and CNTs are advantageous for liquid-phase reactions requiring minimal mass transfer limitations. This makes them suitable for the conversion of biomass as

CNTs and CNFs facilitate the mass transfer of large organic molecules due to the open mesoporous structure [57].

2.5.3 Catalyst Synthesis

Catalyst synthesis to obtain the desired catalyst involves a series of steps, including loading the support with a metal precursor followed by drying and heat-treating the precursor to obtain the desired compound on the support. There are several methods for precursor loading, but in this case a solid support is used so liquid-solid methods are the most appropriate. One such method is a deposition technique referred to as impregnation, which involves contacting the solid support with a solution containing the desired deposition compounds [59]. This method can be performed in a variety of ways, including dry or pore volume impregnation, incipient wetness impregnation, co-impregnation, successive impregnation and precipitation-deposition. Co-impregnation refers to loading two or more active components in a single step where as successive impregnation refers to loading two or more active components sequentially with drying and heat treating taking place between each impregnation [59]. Several processes take place during the loading process regardless of the impregnation method, and the resulting product depends on the nature of the solid support and the liquid containing the active components as well as the process conditions [59].

According to literature, it seems that incipient wetness is the preferred method for loading carbon supports with tungsten with regard to cellulose conversion to polyols [22, 35, 51]. This is a form of pore volume impregnation, which works well for the deposition of species that interact weakly with the support. The volume of precursor solution added to the support is identical to the volume of the pores in the support, which is empirically determined beforehand by using water to find the volume at which the surface becomes wetted [59]. However, it has been shown that incipient wetness impregnation of CNTs did not show promising results despite using two different tungsten precursors [60]. This may be because after CNTs are pre-treated with acid, the surface becomes negatively charged. Since the tungsten precursor forms an anionic solution in water, the charges of the support and precursor solution will repel and cause poor distribution [60]. One possible method to overcome this problem is to use a sol-gel loading method. One example of a sol-gel method is the Pechini method, which involves the formation of a three-dimensional polymer resin of a metal complex [61]. The Pechini method is dependent on the in situ polymerization between citric acid and ethylene glycol, along with the chosen metal precursor, which leads to the formation of a metal citrate complex solution

[61], as seen in Figure 2.7. This solution can be used for impregnation of the support material, which results in a better distribution on the support due to the distribution of metal ions within the metal citrate complex.

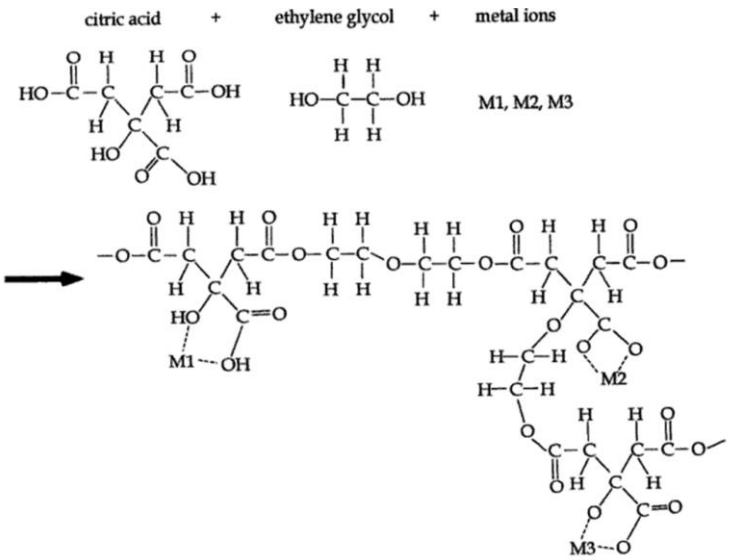

Figure 2.9: Metal citrate complex formed using Pechini method [62]

Once the precursor has been loaded onto the support, the support is dried and then calcined. Calcination is done in order to transform the precursor into the desired metal component. When using the Pechini method for loading, calcination initiates pyrolysis of the organic species resulting in the desired metal oxide [61]. In this study, ammonia metatungstate (AMT) was chosen as the precursor due to its high solubility in water [63]. The calcination temperature influences the final product formed from the precursor, as lower temperatures will result in tungsten oxide while higher temperatures will result in tungsten carbide [63]. Thermal decomposition of AMT to WO_3 in inert atmosphere is one possible calcination process to create WO_3/CNT, resulting in the formation of hexagonal WO_3 in the temperature range 380-500 °C and monoclinic WO_3 in the temperature range 500-600 °C [64].

The WO_3 can then be treated further by reduction with H_2 or H_2/carbon to create tungsten metal (W). A reduction temperature above 650 °C produces α-W while temperatures below 575 °C produces β-W when H_2 is used [65]. The reduction reaction of WO_3 has been reported to be virtually identical regardless of using H_2 alone or in combination with carbon up to 675 °C. The reduction of WO_3 with carbon only occurs at a temperature above 900 °C via the formation of CO [66]. In order to produce tungsten carbide from tungsten metal, a carbon source is needed. Using a gas mixture of methane (CH_4) and H_2 is one method, which results

in the formation of W_2C and WC depending on the carbon content and reaction temperature [67]. Gao et al. proposed that the phase of tungsten metal has an effect on the tungsten carbide formation, with α-W resulting in WC and β-W resulting in W_2C. The reduction and carburization can also be done in a single step by carbothermal hydrogen reduction (CHR). The tungsten precursor is heated to an elevated temperature and a carburization gas mixture, such as CH_4/ H_2, is introduced acting as the reducing and carburizing agents [67]. The CHR reaction can often be described by the following sequenced reaction: $WO_3 \rightarrow WO_2 \rightarrow W \rightarrow W_2C \rightarrow WC$ [66].

3. Experimental

This section focuses on the experimental methods used for this study. The catalyst preparation and catalytic characterization methods are discussed. The reaction parameters for testing each catalyst are also mentioned, along with the analysis of the reaction products.

3.1 Catalyst Preparation

The experimental method used to prepare various tungsten-based catalysts supported on CNT involved using the Pechini method and incipient wetness impregnation for loading followed by calcination and carburization to obtain the final catalyst. The chronological order of the method is shown in Figure 3.1 and will be discussed further in the following sections. The carburization in CH_4/H_2 was only done if tungsten carbide was desired, so the order of carburization and copper impregnation depended on whether Cu was to be loaded onto WO_3 or WC_x. There was no further calcination after loading the Cu precursor as the reduction and passivation step involved heating in inert gas before the desired temperature for reduction was reached, which resulted in burning off the precursor prior to reduction. The reduction and passivation step was only done when Cu was loaded onto the support as the tungsten species did not require further reduction.

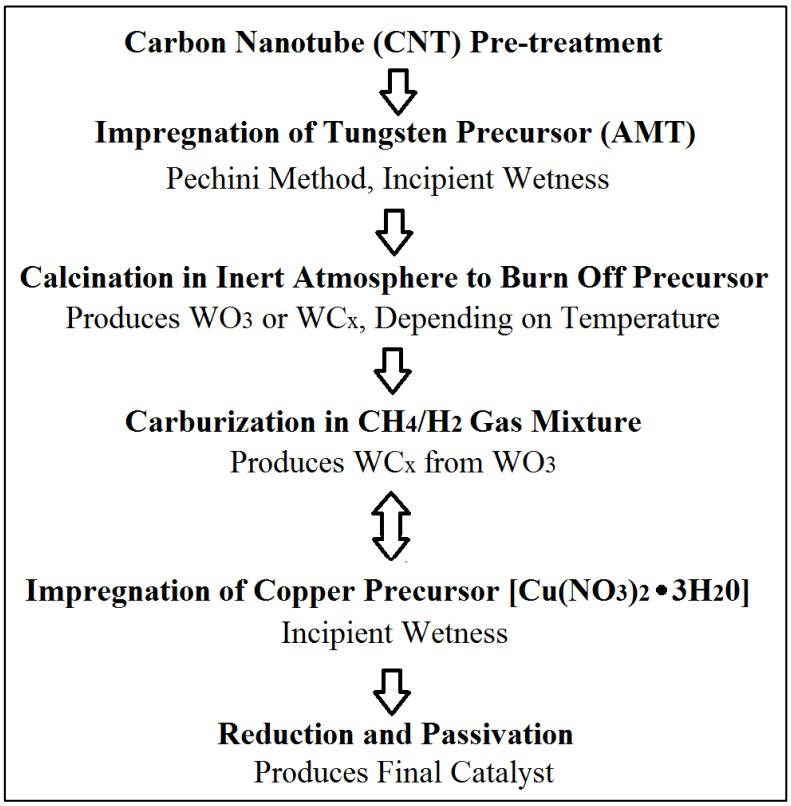

Figure 3.1: Chronological order of catalyst preparation method

3.1.1 Carbon Nanotube (CNT) Pre-treatment

In order to remove the potential remaining grow catalyst from CNT (Chengdu Organic Chemicals Co. Ltd) along with other impurities, pre-treatment of the CNTs is required. The pre-treatment method follows the same procedure reported by Liland [68], involving the use of 65% nitric acid. Approximately 20 g of CNTs were treated with 500 mL 65% nitic acid at 100 °C in a silica oil bath for 1 hour in a round bottom flask with stirring. A water cooled condenser was attached to the top of the flask in order to retain some of the acid vapour forming. The acid mixture containing CNTs was then cooled to room temperature and filtered by vacuum filtration using deionized water to wash the CNTs. This procedure was repeated for a total of three times, and after the final treatment, the CNTs were washed numerous times with large amounts of deionized water until the pH reached 5 or higher. The CNTs were then placed in an oven around 110 °C to dry for at least 12 hours. Finally, the CNTs were ground using a mortar and pestle to obtain a fine powder for even distribution of the metal precursor.

3.1.2 Impregnation of Tungsten Precursor

Before the impregnation of the tungsten (W) precursor, the pore volume of CNT was determined by slowly and carefully dropping water onto a known amount (1g) of CNT until it became fully saturated. It took 3.1 mL of water before the water started to form a wet layer on the outside of the CNT (1g), so this volume was used as the pore volume of CNT and consequently the solution volume for incipient wetness impregnation. In this study, ammonium metatungstate (AMT) hydrate (Sigma-Aldrich, 99%) was used as the W-precursor, which has the molecular formula $(NH_4)_6H_2W_{12}O_{40}\cdot xH_20$. The precursor was loaded using the Pechini method, a modified sol-gel route, involving the in situ polymerization between citric acid (CA) (Sigma-Aldrich, citric acid monohydrate, 99%) and ethylene glycol (EG) (Fluka, 99%), leading to the formation of a W metal citrate complex [61].

Since AMT is a positively charged precursor with a charge of +8, the required molar ratio of AMT and CA can be determined as CA has a charge of -3 [60]. This results in a molar ratio of 3:8:8 for AMT:CA:EG. However, doubling the amount of CA, and consequently EG, will ensure enough of the protective polymer compound to form the metal citrate complex [60]. A molar ratio of 3:16:16 was therefore used in this study. The Pechini solution was then mixed with water to achieve the desired impregnation/pore volume depending on the amount of CNT support used, and dropped onto the CNT by incipient wetness impregnation. The loading was

typically 10 wt% W, but 50 wt% W was also prepared. The calculations for each catalyst along with the amounts of the different compounds are shown in Appendix A and B. The impregnated CNTs were then dried at room temperature for 12 hours and then at 110 °C for another 12 hours.

3.1.3 Calcination in Inert Atmosphere

After impregnation, the tungsten loaded supports were calcined prior to further treatment using a glass quartz reactor. In most cases, calcination was done to transform the tungsten precursor into tungsten oxide, WO_3, which could then be further treated to form tungsten carbide. The calcination was based on the method proposed by Sun et al. [56], which involved calcination at 500 °C in nitrogen flow with a heating rate of 5 °C/min. The temperature was held at 500 °C for 3 hours, resulting in WO_3/CNT.

3.1.4 Carburization in CH_4/H_2 Gas Mixture

Once WO_3/CNT was obtained, it was carburized in a CH_4/H_2 gas mixture at 925 °C for 4 hours with a heating rate of 25 °C/min to form tungsten carbide, based on the methods proposed by Rui [63], with heating and cooling occurring in inert nitrogen flow. Previous work done by Bjørgen only used reduction with hydrogen resulting in the formation of W_2C/CNT [60], but for this study different phases of tungsten carbide were desired. Carburization with a CH_4/H_2 gas mixture was therefore done in order to regulate the amount of carbon introduced by altering the ratio of CH_4/H_2 introduced to WO_3/CNT in order to control the formation of W_2C and WC, due to the sequential formation of W_2C and WC from WO_3. The calibration curves for the CH_4, H_2, and N_2 gas flow controllers are shown in Appendix C.

3.1.5 Impregnation of Copper Precursor

For the copper (Cu) promoted tungsten catalysts, Cu was loaded onto WO_3/CNT or WC_x/CNT by incipient wetness impregnation (non-Pechini) using $Cu(NO_3)_2 \cdot 3H_2O$ (Sigma-Aldrich, 99%) as the precursor. The typical loading was 10 wt% Cu, which was done by dissolving the precursor in water to create a 3.1 mL solution (for 1 g WO_3/CNT or WC_x/CNT), assuming negligible change in pore volume after 10 wt% W loading. The precursor solution was then added dropwise to the desired tungsten catalyst. Copper was also loaded onto CNT by itself for one catalyst, also without using the Pechini method.

3.1.6 Reduction and Passivation

Finally, after Cu loading, the catalyst was reduced in hydrogen flow at 400 °C for 5 hours, with an H_2 flow rate of approximately 60 mL/min and a heating rate of 5 °C /min, based on the method proposed by Morken [69]. The heating and cooling were done in helium (He) flow, which resulted in the precursor being burned off before the target temperature was reached and the gas flow was switched from He to H_2. After cooling, the catalyst was passivated with 1% O_2 in argon for 30 minutes at room temperature.

3.1.7 W_2C-WC/CNT

In an attempt to examine the effect of tungsten carbide phase composition on cellulose conversion, W_2C-WC/CNT was also prepared. The calcination was performed at 925 °C for 4 hours in inert nitrogen, based on the methods proposed by Langfjæran [70], resulting in a mixture of both W_2C and WC. The calcination time was also increased to 8 hours, which also resulted in the same two active phases.

3.1.8 Ru/CNT

Another catalyst that was used in this study was 1 wt% Ru/CNT prepared by Haakon Rui. This catalyst was prepared by incipient wetness without Pechini, and was calcined at 300 °C for 3 hours in nitrogen, followed by reduction in hydrogen at 300 °C for 3 hours, and finally passivated with 1% O_2 in argon for 2 hours at room temperature.

3.2 Catalyst Characterization

The different catalysts produced were characterized by a variety of methods in order to examine the catalyst composition and surface structure. X-ray diffraction (XRD) was used to determine the bulk phase of the catalyst as well as the particle size. N_2 adsorption analysis (BET) was used to determine the specific surface area of the catalyst. Scanning transmission electron microscopy [S(T)EM] was used to image the surface of the catalyst to identify possible layers and particles of the metal compounds on the support.

3.2.1 X-Ray Diffraction (XRD)

X-ray diffraction (XRD) is commonly used to identify crystallographic phases for the different compounds present in the catalyst, and can also indicate the respective particle sizes.

XRD analysis involves placing the catalyst in x-ray radiation, which passes through a number of openings that are placed in a regular lattice [71]. The phases are identified by the structural parameters of the lattices, which are used to identify the shape and size of a subdivision of the crystal (catalyst), referred to as a unit cell. Different compounds have related lattice spacings, so by measuring the angle of diffraction twice, known as the 2-theta (2θ) angle, when chosen x-rays leave the crystal sample, it is possible to derive the corresponding spacings using the Bragg relationship, thereby identifying the different compounds [71]. The crystal size can also be calculated by the Sherrer equation [71]. XRD is therefore a very useful tool for determining the structure and size of the bulk phase components of the catalyst, but a drawback is that it cannot detect small or amorphous phases, meaning some phases may not be detected. For example, especially active phases on the catalyst surface are not visible in standard XRD analysis [71].

In this study, a Bruker D8 Advanca Davinci X-ray Diffractometer was used for XRD analysis to investigate the catalyst composition and the crystal size of the particles. This instrument uses monochromatized Cu Kα radiation (λ–1.54 Å) and a LynxEye SuperSpeed detector. XRD diffractograms were obtained in the 2θ range of 20-80° with a step time of 1 second and a step size of 0.015°.

3.2.2 Thermogravimetric Analysis (TGA)

Thermogravimetric analysis (TGA) is a characterization method that heats a sample in a controlled atmosphere, measuring the weight of the sample versus time and temperature. It can be used to study catalyst behaviour at high temperature, as dehydration, degradation, and phase changes may occur as the temperature changes [72]. In this study, thermogravimetric analysis (TGA) was used to estimate the actual metal loading on CNT by determining the amount of metallic catalytic residue left after burning off the CNT.

The analysis was performed using a Netzsch STA 449C Jupiter TGA/DSC, heating from 300-900 °C in air, with a heating rate of 10 °C/min. For analysis, a sample crucible was filled with approximately 20 mg sample, and was weighed before and after the sample had been added to determine the exact sample mass. The TGA analysis was then started, measuring the sample mass (percentage) as a function of temperature and time. The final mass percentage represents the amount of metallic residue impregnated onto the CNT. It was assumed that all metal species were oxidized during the analysis, resulting in WO_3 as the final

compound for tungsten species. Based on this assumption the tungsten loading was calculated using the following equation:

$$W\ Loading\ (\%) = Final\ TGA\ mass\ \% * \frac{W\ molar\ mass}{WO_3\ molar\ mass} \quad (1)$$

The copper loading was also calculated by subtracting the amount of metallic tungsten residue from the final TGA mass % of the copper promoted tungsten catalysts, as the copper was loaded onto the same initial tungsten catalyst (WO_3 or W_2C). The same oxidation assumption was made for copper species, resulting in CuO as the final compound. The Cu loading was therefore calculated using the following equation:

$$Cu\ Loading\ (\%) = (Final\ TGA\ mass\ \% - W\ Final\ TGA\ mass\ \%) * \frac{Cu\ molar\ mass}{CuO\ molar\ mass} \quad (2)$$

3.2.3 N_2 Adsorption Analysis (BET)

N_2 adsorption analysis can be used to determine the surface area and pore size distribution of a catalyst. Nitrogen is physisorbed onto the catalyst at a constant temperature forming a monolayer on the surface, as well as potentially forming multilayers and condensing inside the catalyst pores. The amount of nitrogen molecules required to form the monolayer is measured, and the surface characteristics can be determined using the Brunauer Emmet and Teller (BET) isotherm [71].

In this study, N_2 adsorption analysis was done using a Micrometrics Tri Star 3020 Area and Porosity Analyser to obtain nitrogen adsorption-desorption isotherms. Sampling was done at 77K using liquid nitrogen to maintain a constant temperature. Approximately 50-100 mg of a sample was added to the sample tube, and the sample tube was weighed before and after the sample was added to determine the exact amount of sample to be analysed. Before running the analysis, the samples were degassed under vacuum at room temperature for 1 hour and then at 200 °C overnight until the pressure dropped to 100m Torr or less. After degassing, the sample holders were attached to the instrument and submerged in liquid nitrogen, and analysis was started.

3.2.4 Scanning (Transmission) Electron Microscopy [S(T)EM]

S(T)EM imaging may be used to evaluate the morphology of the different catalysts, as well as examining the surface coating of the support. S(T)EM functions by exposing the sample

to an electron beam, and when the electrons interact with the surface of the sample a number of effects occur, such as backscattering, secondary electron creation, x-rays, and transmitted electrons, which are detected to create an image of the sample [71]. The difference between SEM and TEM is mainly the method of detection. SEM uses a raster electron beam to detect backscattering or secondary electrons as a function of the position of the primary raster electron beam. The orientation of different particles in the sample causes contrast, which is used to create a greyscale image [71]. TEM, on the other hand, uses a primary beam of high energy and intensity electrons that pass through a condenser, producing parallel rays that interact with the sample. These rays form a 2D image based on the different transmitted electrons caused by the density and thickness of the sample [71]. A combination of both SEM and TEM can be used, which is referred to as S(T)EM.

In this study SEM and S(T)EM were used. The catalyst samples were dispersed on carbon tape before each analysis. The WO_3- and W_2C-based catalysts with and without copper were analysed with S(T)EM using a Hitachi S-5500 S(T)EM. The S(T)EM imaging was carried out in the NTNU Nanolab by Karthik Raghunatan. The acceleration voltage and beam current used for these analyses are shown on each image. The W_2C-Cu/CNT catalyst was also analysed with an Apreo SEM from FEI, to see if the image could be improved. The SEM imaging was done by Greg Rutkowski in the NTNU Nanolab. The Ru/CNT catalyst was analysed with annular dark-field S(T)EM by SINTEF.

3.3 Catalyst Testing

The catalysts developed in this study were tested for the catalytic conversion of cellulose to EG. The reactions were performed in a 100 mL stainless steel Parr 4561 autoclave reactor. Typically, 0.33 g cellulose (Sigma-Aldrich, microcrystalline), 0.1 g catalyst, and 33 mL distilled water were loaded into the autoclave reactor. The reactor was purged with nitrogen at least 5 times to remove air from the system, and then again with hydrogen another 5 times. The hydrogen pressure was then adjusted to 60 bar, and stirring was initiated at a low stir rate. The reactor was then heated to 245 °C, which took approximately 30 minutes to reach the target temperature, and the stirring speed was increased. The reaction time was typically 90 minutes at 245 °C and 60 bar H_2, but a reaction time of 180 minutes was also tested in order to investigate the effect of residence time. It is important to note that the reactor pressure increased to approximately 120 bar when the target temperature of 245 °C was reached.

One reaction was also run with periodic sampling over time as a sampling tube and valves were installed at a later date, allowing for the collection of kinetic data. The sampling tube consisted of two valves, before and after a tube volume of approximately 1 mL, which allowed for filling and emptying the tube with minimal pressure loss from the reactor. For this experiment, samples were periodically taken at 0, 30, 60, 90, and 180 minutes, with stirring being turned off when each sample was taken. Before each sample, the sample tube was filled and emptied twice in order to purge the valve of any remaining solution from the previous sample.

Some adjustments were made to the reactor loading when the tungsten catalysts (without Cu) were tested with Cu_xO/CNT and Ru/CNT separately, mixing both catalysts in the reactor. It is important to note that when the copper precursor was impregnated onto CNT by itself, reduction resulted in CuO-Cu_2O/CNT, denoted as Cu_xO/CNT. For these experiments a Cu/W = 1 and a Ru/W = 0.1 were used base on the results from Wang et al [13]. For the Cu_xO/CNT reactions the tungsten catalyst loading was maintained at 0.1 g, resulting in a Cu_xO/CNT loading of 0.0346 g for the 10 wt% tungsten catalysts. For the Ru/CNT catalyst, a loading of 0.1333 g Ru/CNT was used based on the cellulose/Ru ratio used by Wang et al. [13], resulting in a tungsten catalyst loading of 0.2425 g for the 10 wt% tungsten catalysts and 0.0485 g for the 50 wt% tungsten catalysts. These reactions had a higher catalyst loading than the first reactions using tungsten catalysts and copper promoted tungsten catalysts (0.1g). However, the reaction conditions remained unchanged (245 °C, 60 bar H_2, 90 min). The exact amounts of cellulose and catalyst used for each reaction are shown in Appendix A.

3.4 Product Analysis

In this study, high performance liquid chromatography (HPLC) was used to analyze the product solution after each reaction. HPLC functions by pumping a pressurized liquid solvent (mobile phase) containing the sample mixture through a column filled with an adsorbed solid phase (stationary phase). The different compounds in the reaction solution have different bonding strengths with the stationary phase in the column, which results in separation of the products due to the different retention times of each compound [71]. The HPLC was connected to either a refractive index detector (RID) or a mass spectrometer (MS) to gather quantitative and qualitative data for each compound. The RID measures the refractive index of a compound relative to the solvent. The different compounds in the product solution have different refractive indexes, allowing for identification of each compound [73]. The mass

spectrometer (MS) functions by ionizing the chemical compounds in the sample, creating ions that can be manipulated by external magnetic and electric fields. These ions are separated by their mass-to-charge ratio and detected to display a chart that shows the mass of different compounds within the sample [71].

The HPLC was first calibrated by running standard solutions of known compounds with known concentrations. This enabled the retention time for each compound to be obtained as well as calibration curves based on the response factor of the RID to determine the corresponding concentration. Calibration curves were initially prepared of each compound with concentrations of 0.02, 0.2, and 2.0 g/L, which showed good linearity from 0-2 g/L ($R \geq 0.95$). Later standards were therefore prepared with a concentration of 1.0 g/L as the linearity was the same as between 0-2 g/L, requiring only one response factor for the calibration curve as long as the concentration was below 2 g/L, which was always the case for each reaction.

The HPLC used in this experiment was an Agilent 1260 Infinity HPLC with a Hi-Plex Ca (Duo) 300 x 6.5mm column coupled to an Agilent 1260 Infinity RID or an Agilent 6120 Quadrupole LC/MS. The HPLC column temperature was set to 80 °C with an injection volume of 5.0 µL and a flow rate of 0.3 mL/min with distilled water as the mobile phase. The RID was set to a temperature of 35 °C with a 4-second response time at 2.31 Hz. The MS spray chamber was set to a gas temperature of 350 °C, a drying gas flow rate of 12 L/min, and a nebulizer pressure of 35 psig. The fragmentor voltage of the MS was set to 70 V and the capillary voltage was set to 3000 V. It is important to note that the MS did not detect the exact molar mass of the compound, but rather the molar mass +23. This is due to the presence of Na in the column, which apparently binds to the compounds as they pass through the column, thereby altering the molar mass detected. The retention times and response factors of the RID and the molar masses detected by the MS are shown in Table 3.1.

Table 3.1: HPLC retention time, response factor, and molar mass for each compound

Product	Retention Time (min)	Response Factor	M_m in MS (u)
Glucose	16.23	$6.64 \cdot 10^{-6}$	203
Fructose	19.35	$6.82 \cdot 10^{-6}$	203
Erythritol	21.12	$7.93 \cdot 10^{-6}$	145
Glycerol	22.22	$6.99 \cdot 10^{-6}$	115
Mannitol	22.38	$6.62 \cdot 10^{-6}$	205
Sorbitol	26.27	$6.92 \cdot 10^{-6}$	205
EG	23.48	$9.96 \cdot 10^{-6}$	85
PG	24.27	$8.84 \cdot 10^{-6}$	99
1,2-butanediol	29.75	$4.17 \cdot 10^{-6}$	113
1,2,6-hexanetriol	26.90	$7.32 \cdot 10^{-6}$	157
1,2-hexanediol	58.16	$7.43 \cdot 10^{-6}$	141
1,6-hexanediol	38.68	$7.55 \cdot 10^{-6}$	141
5-HMF	43.94	$5.64 \cdot 10^{-6}$	141
Furfural	57.67	$5.59 \cdot 10^{-6}$	119
THFDM	31.70	$8.50 \cdot 10^{-6}$	119
2,5-DHF	32.41	$8.40 \cdot 10^{-6}$	155
THFA	34.50	$8.07 \cdot 10^{-6}$	125
Void Volume Peak	9-11	-	-

It is important to note that the retention times shifted for some later reactions as the column became damaged and needed to be replaced. The standards were therefore run again after replacing the column, showing a slight shift of approximately two additional minutes for all compounds. In addition, the RID had continuous instability problems resulting in a shifting baseline, which made quantification difficult for compounds detected in small amounts as the baseline was not a straight horizontal line, but exhibited small oscillations at inconsistent times throughout the analysis. The void volume peak detected between 9 and 11 minutes is difficult to analyze as it consists of unidentifiable compounds not retained by the column. Morken suggested that it is mainly the result of HMF polymerization during heating [69], but it is also believed to contain unsaturated byproducts and acids from incomplete hydrogenation, as acids were detected when using a different column (Agilent Zorbax SB-Aq).

In order to quantify the various products, the product yield was calculated on a carbon basis. The concentration obtained from the response factor of the RID was first multiplied by the total product volume to obtain the product weight. The product weight was then multiplied

with the carbon content of the compound and divided by the initial carbon mass of cellulose added to the reactor, as well as the cellulose conversion. The amount of cellulose added was on a dry basis, as it contained 4% humidity, which was determined by weighing a specific amount of cellulose before and after drying at 110 °C for 12 hours. The formula used for the yield calculation is shown below in Equation 3. Cellulose conversion was calculated by weighing the filter paper before and after vacuum filtration to determine the amount of solids left after the reaction. The amount of catalyst added initially was then subtracted from the total solids after reaction to determine the amount of cellulose that was not converted.

$$Yield\ (\%) = A * F_R * V_{sol} * \frac{C*12}{C*12 + O*16 + H} * \frac{1}{C_0*X} \quad (3)$$

Where,

- A = Peak Area
- F_R = Response Factor
- V_{sol} = Volume of Product Solution
- C = Carbon Atoms per Molecule
- O = Oxygen Atoms per Molecule
- H = Hydrogen Atoms per Molecule
- C_0 = Initial Carbon Content (of cellulose)
- X = Cellulose Conversion

4. Results and Discussion

This section discusses the results obtained from catalyst characterization techniques such as XRD, TGA, and BET as well as the reaction products for each catalytic reaction. Various tungsten-based catalysts were tested with and without the addition of copper as well as in combination with Cu_xO/CNT and Ru/CNT.

4.1XRD Results

After each catalyst had been prepared, XRD analysis was performed in order to confirm the correct composition of each catalyst. The first catalyst prepared was WO_3/CNT, as shown in Figure 4.1 (a). Copper was then added to this catalyst to form WO_3-Cu/CNT as shown in Figure 4.1 (b), which had a copper particle size of 25.7 nm. The two broad peaks between the 2θ peaks 42-45° were not labelled, but were identified as iron oxide species due to the presence of some grow catalyst that was not removed during the pre-treatment of CNT. The y-axis of the XRD spectra are not labelled as it becomes arbitrary when the plots are stacked, but it essentially represents the counts.

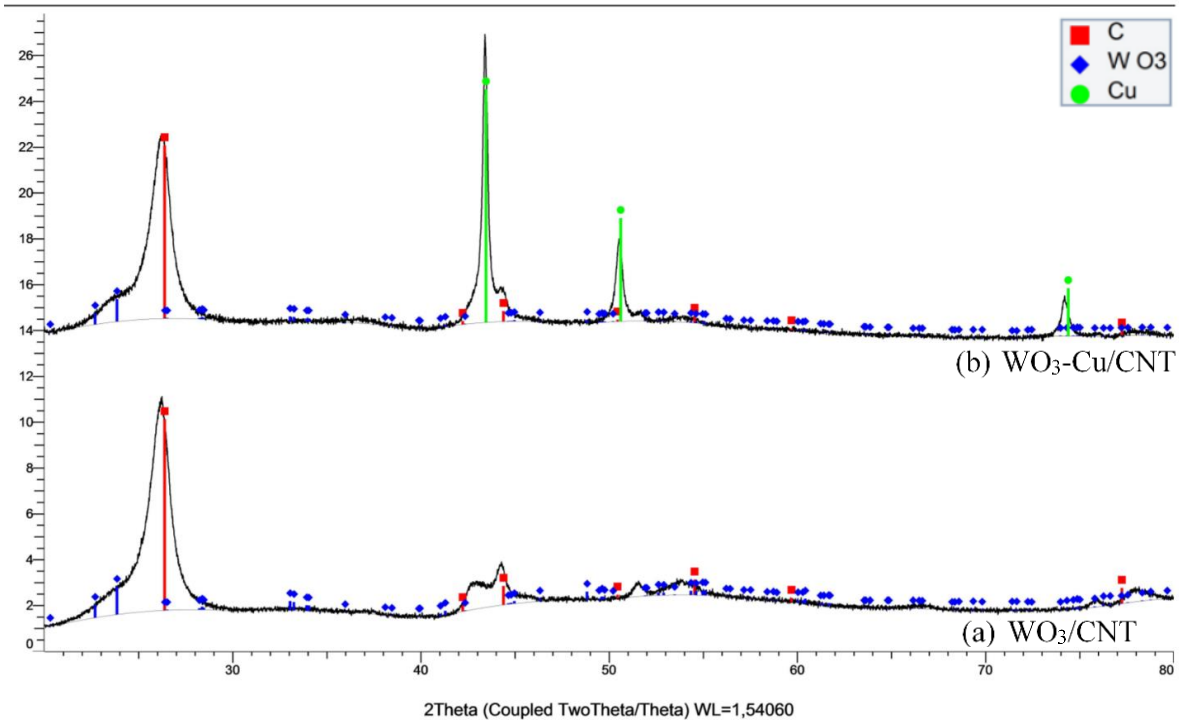

Figure 4.1: XRD spectra for WO_3/CNT and WO_3-Cu/CNT

Then, once WO_3/CNT was created, it was carburized in 2% CH_4/H_2 and 20% CH_4/H_2, where the percentage indicates the amount of CH_4, in attempts to form W_2C/CNT and WC/CNT respectively. The CH_4/H_2 ratios used were based on results from Rui, forming pure W_2C and WC with these ratios respectively when β-SiC was used as the support [63]. However, in this study both ratios resulted in pure W_2C with CNT as the support, as seen in Figure 4.2 (a) and (c). The W_2C/CNT prepared with 2% CH_4/H_2 was therefore carburized again in 60% CH_4/H_2 to see if the introduction of more carbon would form WC, but the composition was unchanged, as seen in Figure 4.2 (b).

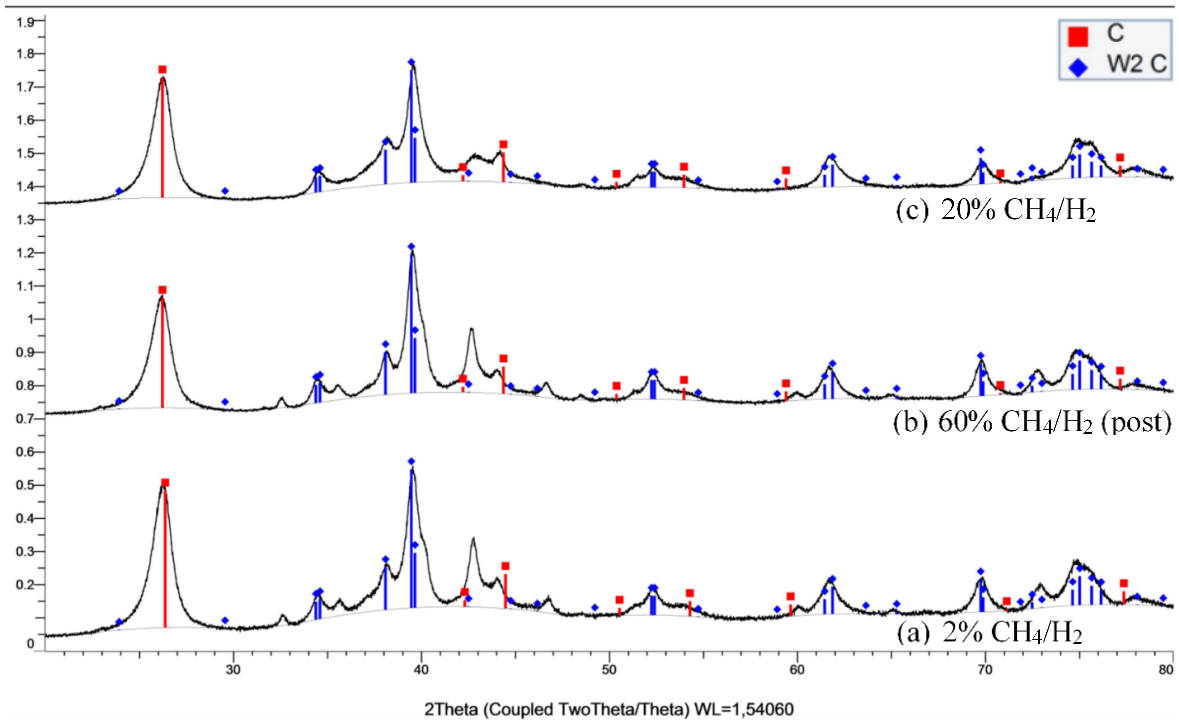

Figure 4.2: XRD spectra of W_2C/CNT for different preparation methods

The W_2C/CNT prepared with 20% CH_4/H_2 was used as the catalyst for catalyst testing as the other two, Figure 4.2 (a) and (b), had 2θ peaks at approximately 32.5° and 46.5° that could not be identified. This W_2C/CNT catalyst is shown again in Figure 4.3 (a), and W_2C-Cu/CNT after copper addition is shown in Figure 4.3 (b), which had a copper particle size of 26.6 nm. These catalysts were all prepared with a nominal 10 wt% W and Cu loading, so the same method was used to prepare 50 wt% WO_3/CNT and W_2C/CNT, resulting in the same tungsten phase composition (Appendix D).

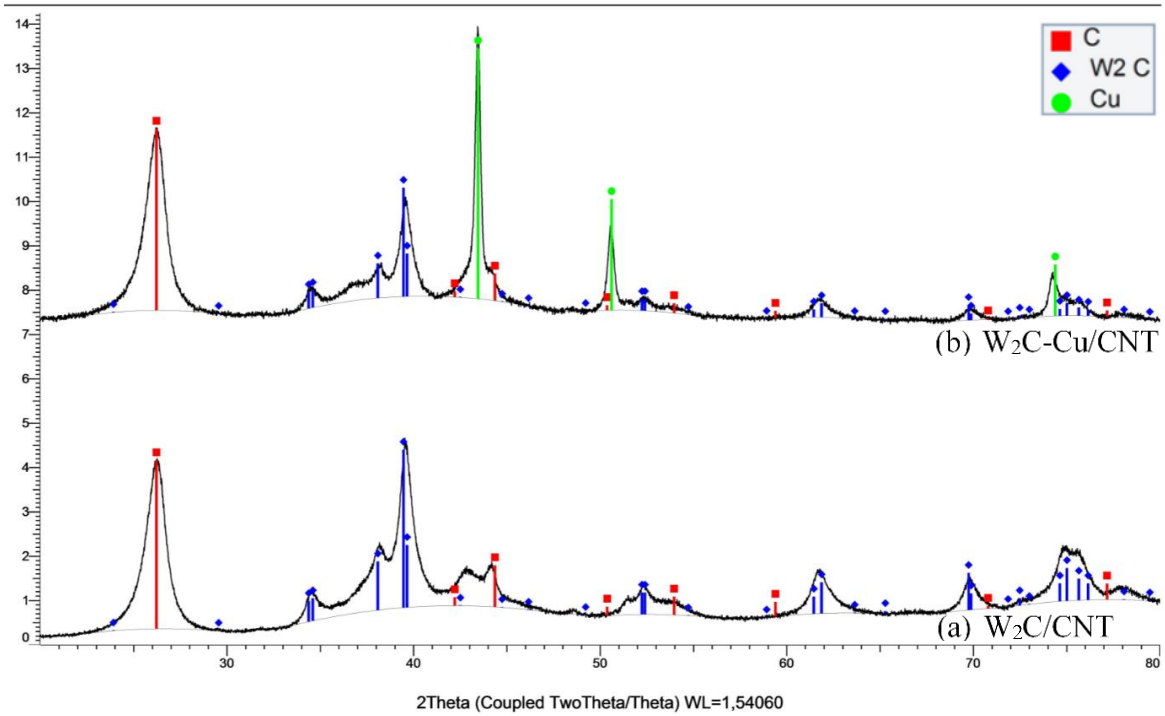

Figure 4.3: XRD spectra of W_2C/CNT and W_2C-Cu/CNT

Since changing the CH_4/H_2 ratio did not seem to affect the formation of W_2C, the initial method used for calcination of the precursor in inert atmosphere was changed as no WC was formed when starting from WO_3. The calcination was performed at 925 °C, rather than 500 °C, for 4 hours in inert nitrogen resulting in a mixture of both W_2C and WC, as shown in Figure 4.4 (a). Further attempts at forming pure WC were done by further carburizing this W_2C-WC/CNT catalyst in 80% CH_4/H_2, which resulted in a higher ratio of WC/W_2C, as seen by the relative peak areas of the two phases, but not pure WC. However, this was not the case when carburizing W_2C/CNT in 60% CH_4/H_2, as no change in composition was seen at all, as shown in Figure 4.2. This suggests that if both W_2C and WC are present, further carburization may change the relative amounts of each, but no change occurs if only W_2C is present. To further examine whether pure WC could be formed, the calcination time of the precursor was increased to 8 hours, but a mixture of W_2C and WC was still seen as shown in Figure 4.4 (c).

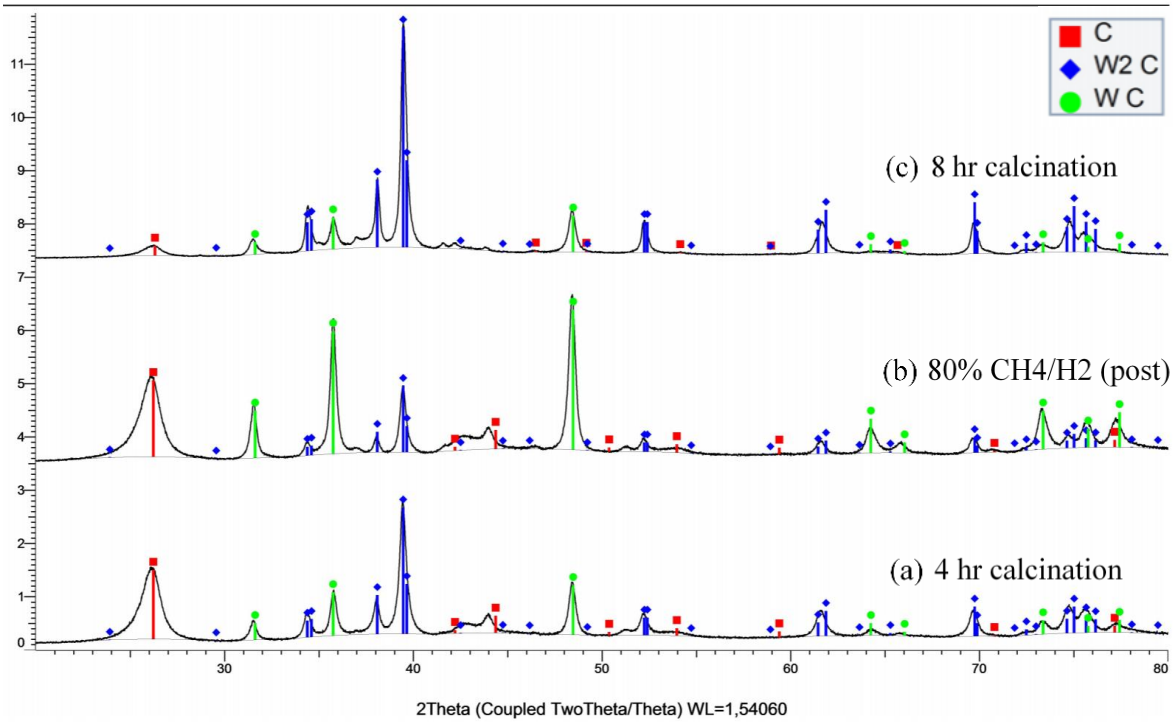

Figure 4.4: XRD spectra of W_2C-WC/CNT for different preparation methods

Calcination at a higher temperature may have resulted in pure WC as suggested by the large effect of calcination temperature on tungsten carbide formation [63]. However, this was not examined because the calcination furnace had a maximum operating temperature of 1000 °C. Further attempts at forming WC were not made as it seems the formation of pure WC is extremely difficult to obtain when CNT is used as the support. The study performed by Rui seemed to draw the same conclusion as pure WC/CNT was never obtained for the numerous methods employed [63]. The W_2C-WC/CNT formed after calcination for 4 hours was therefore used as the catalyst for catalyst testing, which is shown again in Figure 4.5 (a). Copper was then added to this catalyst as well, as shown in Figure 4.5 (b).

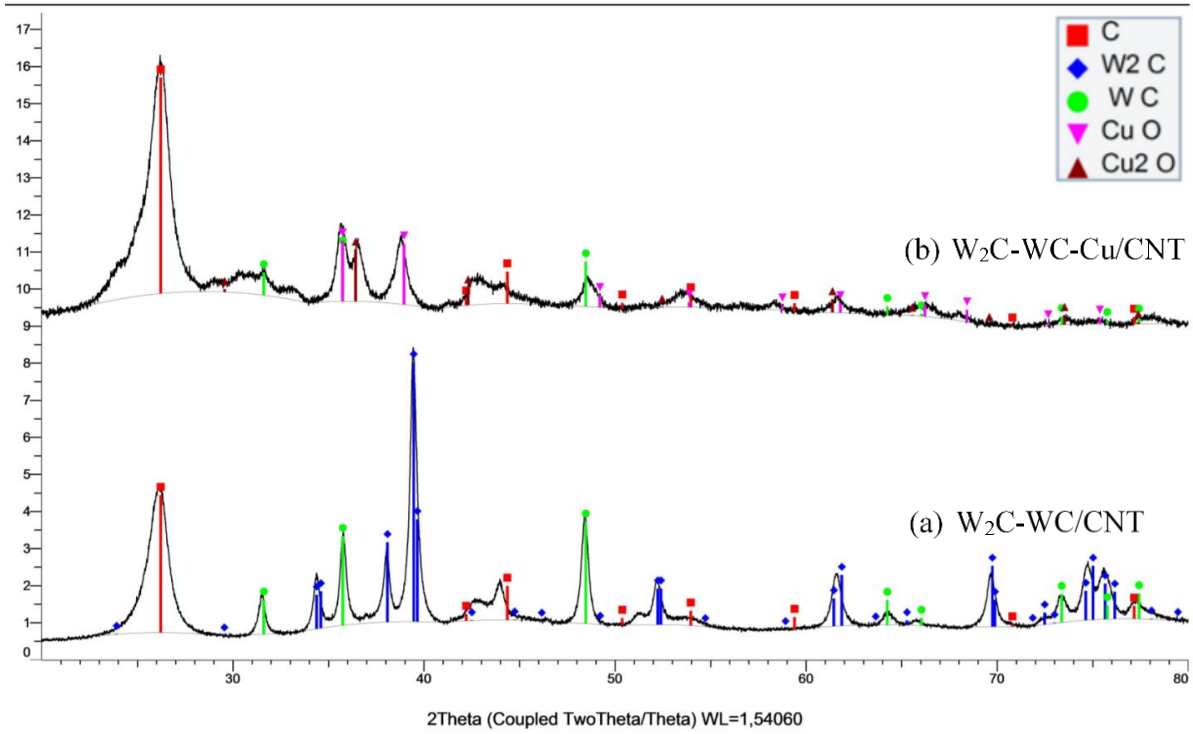

Figure 4.5: XRD spectra for W_2C-WC/CNT and W_2C-WC-Cu/CNT

In this case, however, when copper was added to W_2C-WC/CNT, the composition changed completely, with W_2C disappearing and only WC being present. This was surprising as all other previous attempts at forming pure WC did not succeed. In addition, copper oxide species (CuO and Cu_2O) were formed rather than metallic copper. This did not occur when only WO_3 or W_2C was present, which may suggest that the presence of both species limits the same kind of binding between W and Cu, resulting in copper oxide. As a result, the copper oxide may have entirely covered W_2C and most of the WC, forming a layer of copper oxide on the surface. Another possibility is that Cu promotes the formation of WC from W_2C if WC is already present, which may hinder the formation of metallic copper. However, this was not seen when copper was added to W_2C, as no WC was formed. The cause behind this was not investigated further as it was not the focus of this study.

Copper was also loaded onto CNT by itself, which resulted in the formation of CuO and Cu_2O (denoted as Cu_xO) rather than metallic Cu after reduction, as seen in Figure 4.6 (a). This catalyst was reduced again to ensure no errors occurred during reduction, which resulted in the same XRD spectra, except for a higher ratio of Cu_2O/CuO as seen by the relative areas of both, shown in Figure 4.6 (b). This further suggests that the tungsten species have a

stabilizing effect on Cu, resulting in metallic copper rather than copper oxide. As mentioned earlier, when copper was added to W_2C-WC/CNT, the same oxides were formed further suggesting that the copper covered the majority of the tungsten species allowing for copper oxidation. Another catalyst of 1wt% Ru/CNT was also prepared, as shown in Figure 4.6 (c). The particle size may have been too small to be detected as the only peaks that appear to be ruthenium (43° and 78°) are also present in the other XRD spectra.

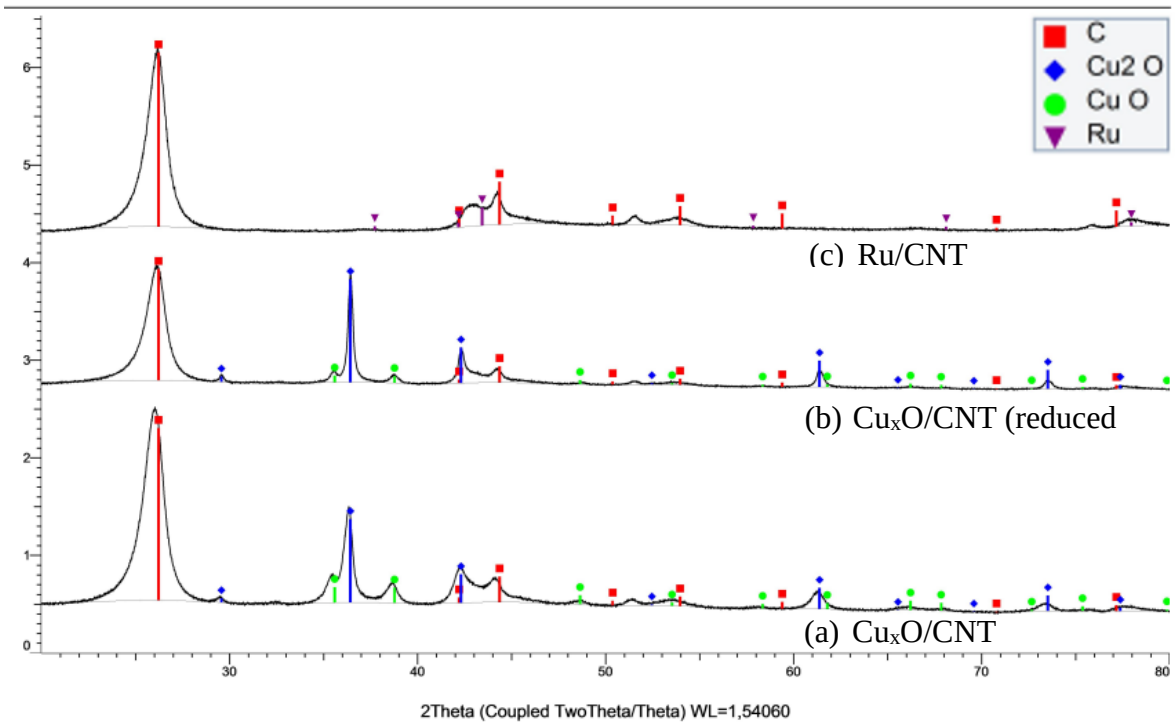

Figure 4.6: XRD spectra of CuxO/CNT and Ru/CNT

4.2 TGA Results

The W and Cu loading of each catalyst from TGA analysis is shown in Table 4.1. The W loading is slightly higher than the nominal loading for the 10 wt% catalysts, but slightly lower for the 50 wt% catalysts. However, the Cu loading is lower than the nominal 10 wt% loading when added to tungsten-based catalysts. This may be due to small inaccuracies during incipient wetness impregnation due to incorrect pore volume measurements. In the case of lower copper loading, it was assumed the pore volume did not change after W loading, which may have resulted in a lower Cu loading as excess precursor solution wetted the outside of the CNT, with some Cu remaining in the excess impregnation solution.

Table 4.1: TGA metal loadings

Catalyst	TGA mass % end	W loading (wt%)	Cu/Ru loading (wt%)
WO_3/CNT	15	11.9	-
W_2C/CNT	17	13.5	-
W_2C-WC/CNT	18	14.3	-
WO_3-Cu/CNT	26	11.9	8.8
W_2C-Cu/CNT	24	13.5	5.6
W_2C-WC-Cu/CNT	27	14.3	7.2
50 wt% WO_3/CNT	52	41.2	-
50 wt% W_2C/CNT	55	43.6	-
Cu_xO/CNT	16	-	12.8
Ru/CNT	7	-	5.3

When copper was loaded onto CNT without the presence of tungsten species, the actual loading was 12.8 wt%. In this case, the actual loading was slightly higher than the nominal loading, just as with the tungsten catalysts, so the same assumptions are made. However, the actual loading of the Ru/CNT catalyst was 5.3%, assuming RuO_2 was the final solid residue, which was much higher than the nominal 1 wt% loading. This may be inaccurate as a higher oxidation state of Ru may have formed when burned in air, such as RuO_3, which would result in a lower actual loading of 4.7wt% based on TGA analysis. However, this is still significantly higher than the nominal loading

4.3 BET Results

The BET surface area of each catalyst obtained from N_2-adsorption analysis are shown in Table 4.2. From this data it is clear that the surface area decreased when WO_3 was formed on the CNT. However, when W_2C was formed from WO_3/CNT, the surface area increased again, but still remained lower than the original CNT. This may be due to methanation occurring during the carburization/reduction at higher temperatures. During methanation, hydrogen reacts with the carbon of the support, producing methane. This results in the removal of carbon from the support, which may lead to additional porous structures, increasing the surface area [60]. Another possibility is that WO_3 results in a coating over the surface, while carburization/reduction to W_2C creates rough edges which increases the surface area.

Table 4.2: BET surface area, pore volume, and pore size

Catalyst	BET Surface Area (m^2/g)
CNT	101.8[a]
WO_3/CNT	78.4
W_2C/CNT	80.2
W_2C-WC/CNT	105.5
WO_3-Cu/CNT	86.1
W_2C-Cu/CNT	65.4
W_2C-WC-Cu/CNT	68.0
50% WO_3/CNT	31.5
50% W_2C/CNT	86.7
Cu_xO/CNT	114.8
Ru/CNT	82.7

[a]Data obtained from Morken [69], as same CNTs were used

The same trend can be seen with the 50 wt% WO_3/CNT and W_2C/CNT. However, in this case the surface area decreased drastically for 50 wt% WO_3/CNT, due to a higher loading. However, the surface area increased to an even higher surface area than 10 wt% W_2C/CNT after carburization/reduction. This suggests that the formation of more rough edges is a possibility, as a higher loading may result in even more edges on the surface, increasing the surface area further. Methanation may also be the cause of the increase in surface area when Cu is added to WO_3/CNT and reduced. However, reduction was conducted at only 100 °C above calcination, which suggests that the Cu may also have broken up some of the WO_3 layer as well due to redistribution of WO_3, creating more rough edges. On the other hand, when Cu is added to W_2C/CNT, the surface area decreases. This is most likely due to the large particle sizes of Cu (~25 nm) as detected by XRD, reducing the surface area.

When W_2C-WC/CNT was formed, the surface area increased beyond the original CNT, which can only be explained by methanation at higher temperatures as original calcination for this catalyst was much higher than the calcination for WO_3/CNT. The surface area then decreased for W_2C-WC-Cu/CNT, which was also seen when copper was added to W_2C/CNT. When Cu was added to CNT by itself, the surface area was also higher than the original CNT. However, this catalyst was not prepared with the Pechini method, which may have some effect on the surface area as the metal citrate complex is not present. In addition, the presence of copper may accelerate methanation, in the same way that nickel does [10], resulting in the higher surface area. This same trend was not seen with Ru/CNT, which was also not prepared with the Pechini method, as surface area decreased from the original CNT.

4.4 S(T)EM Results

Some of the catalysts were examined using S(T)EM in order to examine the distribution of different compounds formed on CNT. The WO_3/CNT catalyst was examined first, which showed CNT clusters of varying sizes, despite being crushed, as shown in Figure 4.7 (a). However, these clusters may separate when added to water in the reactor. It was difficult to identify the WO_3 species on CNT, but some brighter areas may indicate that it coated parts of the CNT, as seen in Figure 4.7 (b), as the tubular structure of CNT was disrupted in these areas. Figure 4.7 (b) also shows a CNT diameter of approximately 45 nm, but this diameter varies within a range of ± 5 nm. The WO_3-Cu/CNT was also examined, which showed clear white spots of various sizes in some areas that were not seen for WO_3/CNT. This suggests that these distinct white areas indicated the presence of copper. The presence of larger copper agglomerates were seen, as shown in Figure 4.8 (a), which shows a particle size of approximately 145 nm. When zooming in, the smaller copper particles were also seen, one being 27.8 nm as shown in Figure 4.8 (b), which was consistent with the particle size determined by XRD.

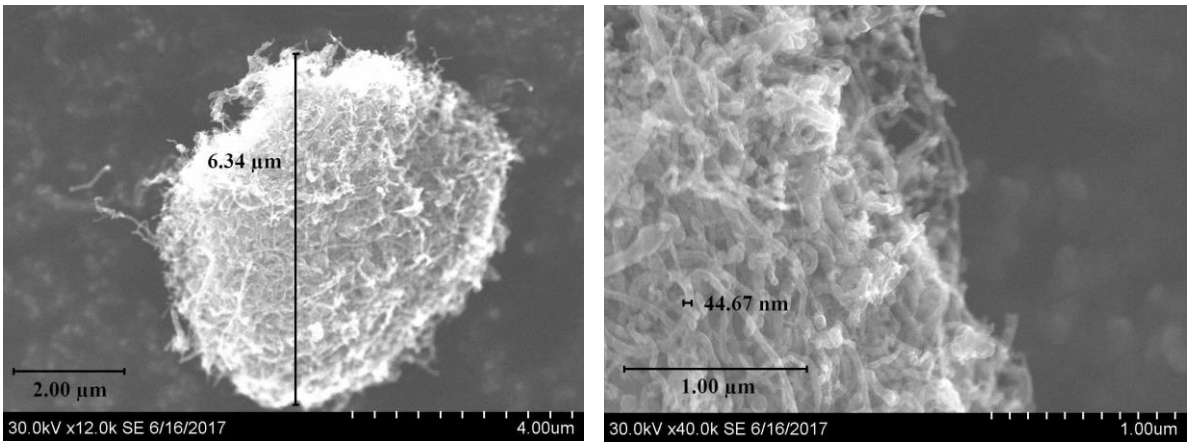

(a) (b)

Figure 4.7: S(T)EM images for WO_3/CNT

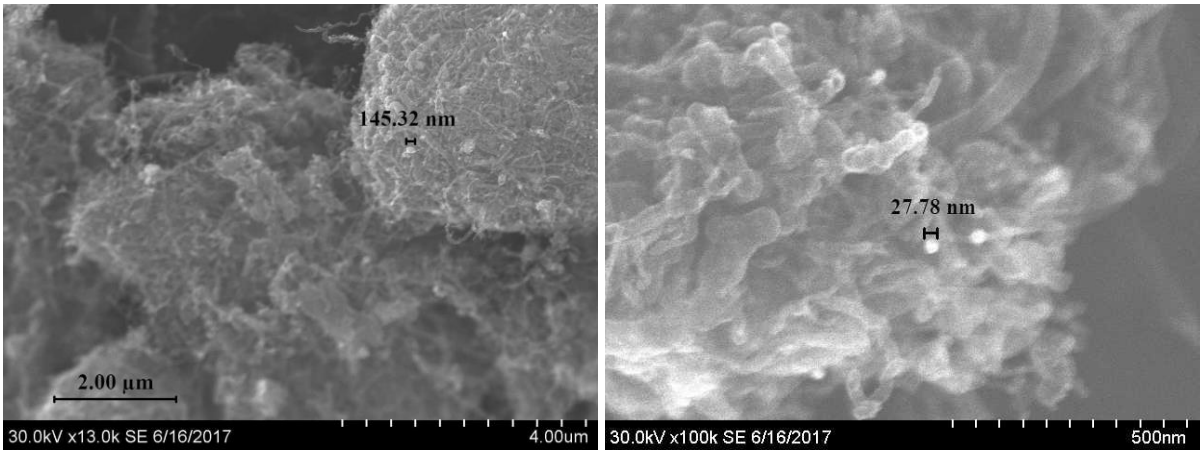

(a) (b)

Figure 4.8: S(T)EM images for WO_3-Cu/CNT

The W_2C/CNT catalyst was also examined, which showed clusters of W_2C on the CNT surface, as indicated by the red circle in Figure 4.9 (a). This may explain the increase in surface area from WO_3/CNT to W_2C/CNT, as seen by BET analysis, as uneven W_2C clusters formed on the surface of CNT, increasing the surface area. In addition, it seems that W_2C particle agglomerates formed, as shown in Figure 4.9 (b). However, EDX was not used to identify certain compounds, so this particle may be contamination. The W_2C-Cu/CNT catalyst was also examined, which showed large areas of CNT covered in copper in some areas, as seen in Figure 4.10 (a). This may affect the activity of W_2C-Cu/CNT as large areas are covered by Cu, inhibiting access to W_2C active sites. However, when examining a different area of the sample, more zoomed in, copper particles of 26.13 nm were also seen, as shown in Figure 4.10 (b). This was also in agreeance with the particle size determined by XRD.

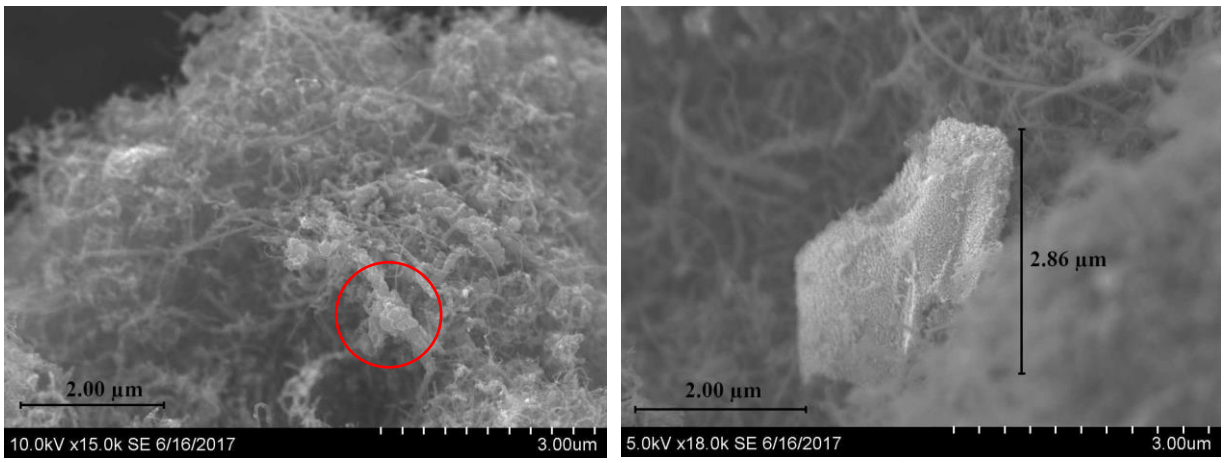

(a) (b)

Figure 4.9: S(T)EM images for W_2C/CNT

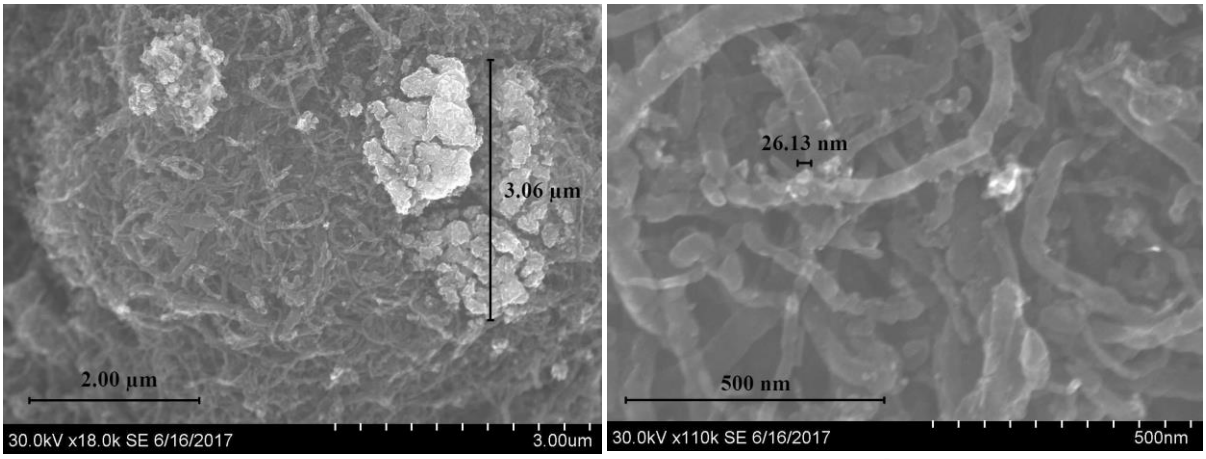

(a) (b)

Figure 4.10: S(T)EM images for W_2C-Cu/CNT

The W_2C-Cu/CNT catalyst was also examined with SEM as W_2C and copper were much easier to identify with S(T)EM compared to WO_3. When using S(T)EM, there was a large issue with the image drifting during analysis, making clear images difficult to obtain. This was most likely due to the use of carbon tape, as the electrons interacting with the carbon tape and CNT produced similar backscattering as both consisted of carbon. W_2C is seen coating parts of the CNT surface, which creates a slightly brighter area compared to CNT, as shown in Figure 4.11 (a). In addition, the copper particles can be seen more clearly with SEM, with a relatively good dispersion, as shown in Figure 4.11 (b). Additional S(T)EM and SEM images are shown in Appendix F.

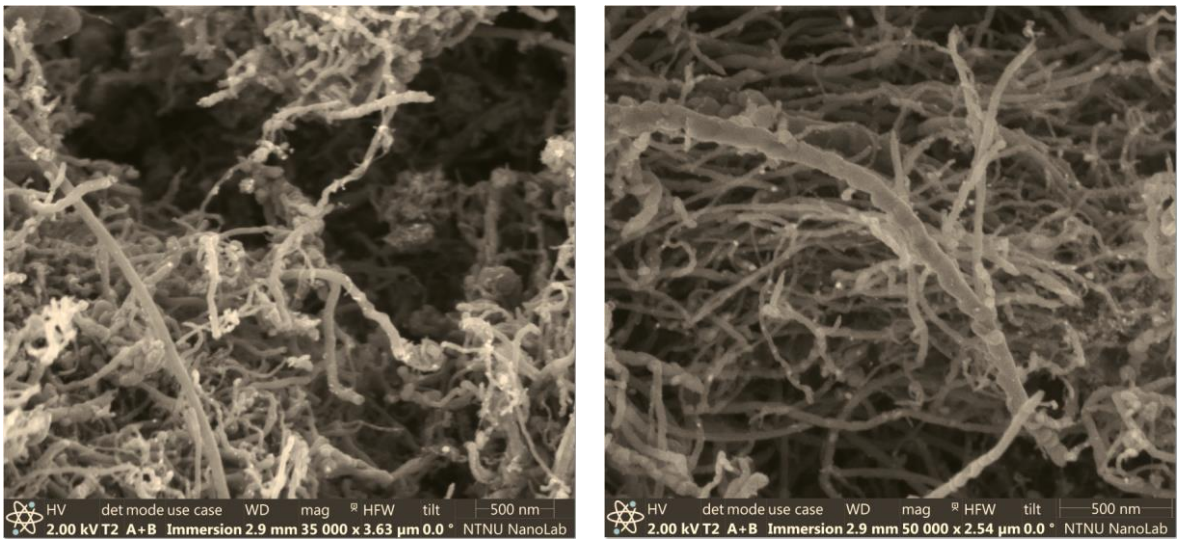

(a) (b)

Figure 4.11: SEM images for W2C-Cu/CNT

The 1 wt% Ru/CNT catalyst was examined by SINTEF using annular dark-field S(T)EM, as seen in Figure 4.12. In contrast, the previous catalysts were all examined with bright-field S(T)EM or SEM. The distribution of Ru on CNT was much better than that of WO_3, W_2C, and Cu, most likely due to a significantly lower loading. In addition, the particle size of Ru was much smaller, measuring 1.9 nm in this figure. The presence of much larger Fe-Ni particles was also seen, as shown in Figure 4.13 (a), with a particle size of approximately 15 nm, compared to a Ru particle size of 1.14 nm shown in Figure 4.13 (b). The presence of these particles is due to remaining grow catalyst (Fe and Ni) after CNT pre-treatment. As mentioned earlier Fe species were seen with XRD as well, but Ni was not screened for in those cases. Since Ru/CNT was prepared from the same CNT, the presence of Fe-Ni particles most likely exists on all catalyst tested for this study. However, it seems that these particles become covered when tungsten and/or copper is impregnated onto CNT.

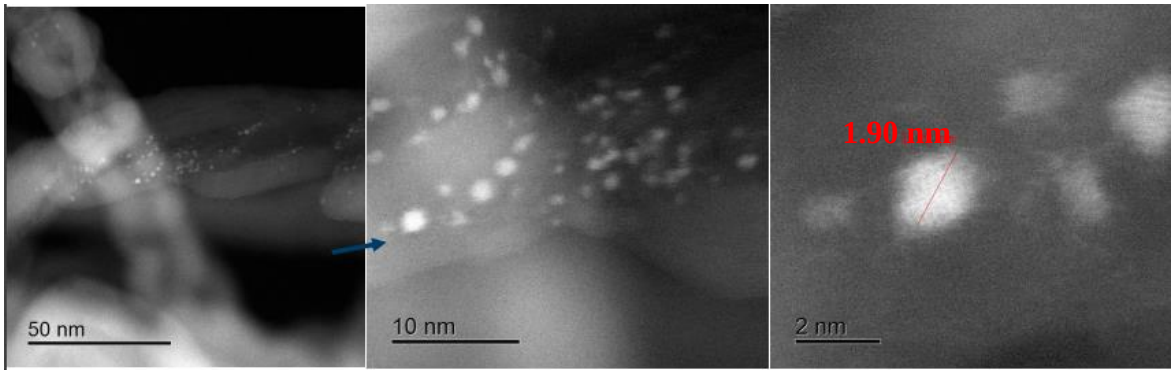

Figure 4.12: Annular dark-field S(T)EM images of Ru/CNT

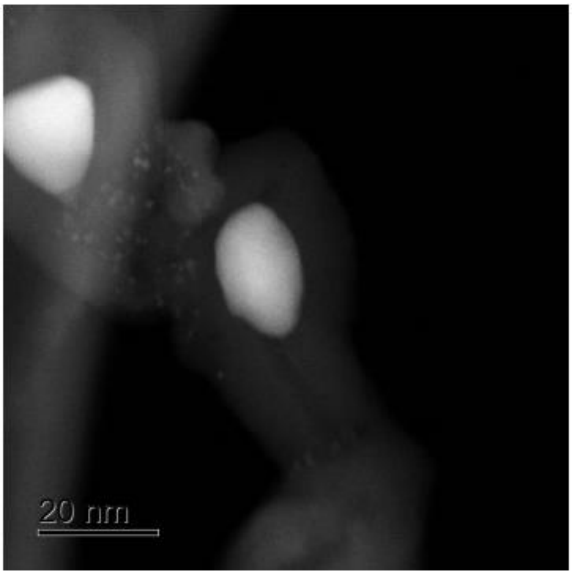

Figure 4.13: Large Fe-Ni particles on Ru/CNT

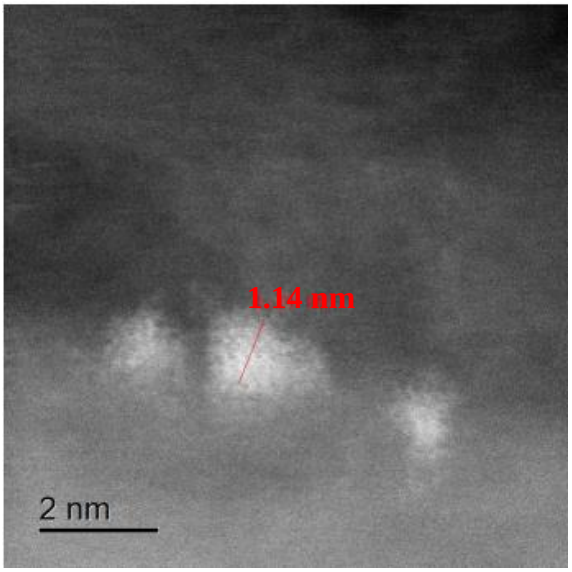

Figure 4.14: Small Ru particles on Ru/CNT

4.5 Reaction Results

In this study, numerous reactions were examined with the use of tungsten-based catalysts. The tungsten-based catalysts (WO_3, W_2C, and W_2C-WC) were tested alone and with the addition of copper to examine the promotion effect of copper (Cu). WO_3 and W_2C were also tested in combination with Cu_xO/CNT and Ru/CNT in order to assess the hydrogenation ability of copper and ruthenium. The effect of tungsten loading was also examined by using 10 and 50 wt% WO_3 and W_2C in combination with Ru/CNT while maintaining a constant Ru/W molar ratio. A very dilute amount of sulfuric acid (H_2SO_4) was also used to examine if the EG yield could be further increased with the addition H_2SO_4.

4.5.1 Examining the promotion effect of copper on tungsten-based catalysts

The first catalysts tested in this study were WO_3/CNT, W_2C/CNT, and W_2C-WC/CNT with a nominal loading of 10 wt% W. Copper was then added to these catalysts, with a nominal loading of 10 wt% Cu. These catalysts were tested at 245 °C and 60 bar H_2 for 90 minutes, with 0.1 g catalyst, 0.33 g cellulose, and 33 mL water. The exact amount of cellulose and catalyst added to each reaction is shown in Appendix A. The product yields for each reaction are shown in Table 4.3, and all achieved 100% conversion.

Table 4.3: Yields for various tungsten and copper promoted tungsten catalysts

Catalyst	Yield (%)							Unidentified Peaks (% of total area)	
	Total	EG	1,2-PG	1,2-BD	THFDM	THFA	1,2,6-HT	Peak 28	Void Volume
WO_3/CNT	12.5	1.6	1.3	-	3.7	3.4	2.5	13.2	62.8
W_2C/CNT	10.1	3.1	1.3	-	0.4	2.2	3.1	13.4	41.9
W_2C-WC/CNT	21.6	6.5	3.4	0.6	1.4	3.6	2.4	8.3	48.6
WO_3-Cu/CNT	15.3	4.0	1.4	-	2.4	5.2	2.3	13.3	53.8
W_2C-Cu/CNT	15.6	6.7	2.1	-	1.1	3.6	2.1	11.2	53.7
W_2C-WC-Cu/CNT	12.6	2.6	1.9	0.7	1.1	3.0	2.4	9.9	55.9

When comparing the tungsten-based catalysts without the addition of copper, it is clear that the EG and 1,2-PG yields increases in the following order WO_3/CNT < W_2C/CNT < W_2C-WC/CNT, as seen in Figure 4.15. The WO_3/CNT catalyst exhibits the poorest EG and 1,2-PG yields as tungsten oxide does not exhibit the same multifunctional retro-aldol condensation and hydrogenation activity as tungsten carbide. This catalyst therefore has the poorest hydrogenation activity, resulting in low EG and 1,2-PG yields. When comparing W_2C-WC/CNT and W_2C/CNT, it was surprising that W_2C-WC/CNT had a higher EG and 1,2-PG

yield compared to W_2C/CNT, which contradicts the study performed by Ji et al., which stated that the EG yield and selectivity is poorer when two tungsten carbide active species are present [10]. This suggests that either the retro/aldol condensation or hydrogenation activity may be enhanced with two active phases.

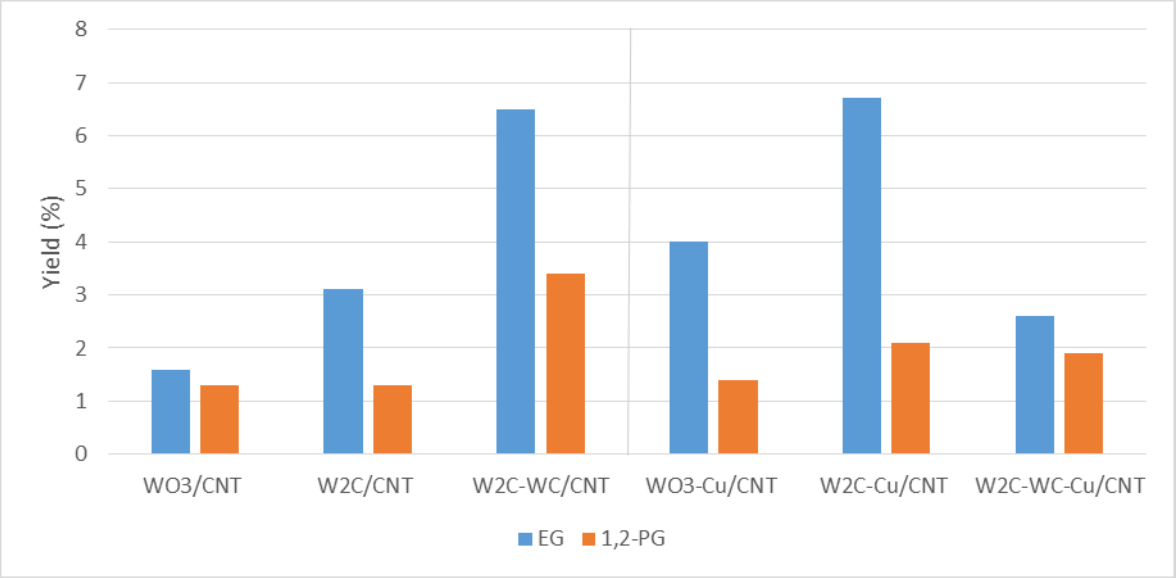

Figure 4.15: EG and 1,2-PG yield for various tungsten and copper promoted tungsten catalysts

The addition of copper had a clear promotional effect on EG and 1,2-PG yield for WO_3/CNT and W_2C/CNT, as seen in Figure 4.15. The promotion effect of copper was expected as transition metals have been shown to enhance the hydrogenation activity of tungsten-based catalysts, as shown by Zheng et al. [26]. However, their study only examined M(8,9,10) transition metals, while Cu is a M(11) transition metal, which may account for the lower activity and yields in this case. The addition of copper had a negative effect on W_2C-WC/CNT, which is explained by the complete change in composition after the addition of copper, as determined by XRD analysis. The W_2C phase disappeared entirely, and only some WC was present, which may have reduced both the retro-aldol condensation and hydrogenation activity of tungsten carbide, as WC may be less active than W_2C. In addition, copper oxides were formed rather than metallic copper, which may have lower hydrogenation activity than Cu.

Although a trend can be seen for EG yield in the increasing order WO_3/CNT < W_2C/CNT < WO_3-Cu/CNT < W_2C-Cu/CNT based on hydrogenation activity, the yields for EG and 1,2-PG are very low. The maximum yield obtain was 6.7% EG with W_2C-Cu/CNT. This is due to other cellulose degradation pathways also occurring during the reaction. A large

cause of the low yields is the large void volume peak that is seen for each catalyst, which contains compounds that are not retained by the column, and therefore cannot be identified. For all these catalysts, the void volume accounts for over 40% of the total peak areas identified by the RID. This indicates that the hydrogenation activity is low, as many unsaturated by-products may be present in the void volume. In addition, the reaction product solutions of these catalysts were very yellow in color, which further indicates the presence of unsaturated by-products and HMF derivatives, as all HMF derivative standards used were initially yellow in color and many synthetic and natural unsaturated polymers also produce a yellow color.

Another unidentifiable peak was seen at a retention time of approximately 28 minutes. The MS showed that this peak consisted of an ion of 137.1 g/mol, meaning the molar mass of the compound was 114.1 g/mol (after subtracting Na). This molar mass is consistent with many furanones, so this peak may be an intermediate furanone in the HMF degradation pathway. Unfortunately, this peak was also the largest peak for all reactions with these catalysts, which further suggests that another pathway occurs, as standards of all compounds in the EG and 1,2-PG pathway were examined. However, it may also be an unidentified intermediate in the studied pathways.

Numerous products from the HMF degradation pathway were also seen with these catalysts, such as tetrahydro-2,5-furandimethanol (THFDM), tetrahydrofurfuryl alcohol (THFA), and 1,2,6-hexanetriol (1,2,6-HT). However, 2,5-dihydroxymethylfuran (2,5-DHF) was not detected, which is the precursor for THFDM and 1,2,6-HT, as shown earlier.. THFA is normally produced from the hydrogenation of furfural, but may possibly be produced from the hydrogenation and C-C cleavage of HMF or 2,5-DHF. The latter is more likely in this study as furfural is typically produced from C_5 sugars, such as xylose present in hemicellulose [7]. In this study cellulose was used as the feedstock, so only C_6 sugars (glucose and fructose) are obtained from cellulose hydrolysis. Since only hydrogenated compounds in the HMF degradation pathway are present, it may be inferred that the catalysts have sufficient hydrogenation of unsaturated C=C bonds, but not C=O bonds.

Concerning the HMF degradation pathway, it is clear that the WO_3/CNT and WO_3-Cu/CNT catalysts produce more HMF degradation products than the other four tungsten carbide based catalysts. This further indicates the lower hydrogenation activity for tungsten oxide compared to tungsten carbide, resulting in more unsaturated by-products. The void volume is also greater with WO_3/CNT and WO_3-Cu/CNT, which may be due to HMF

polymerization products caused by insufficient hydrogenation. The HMF pathway is therefore greater amongst tungsten oxide catalysts compared to tungsten carbide catalysts. In addition, WO_3-Cu/CNT had a higher THFA yield, and lower THFDM and 1,2,6-HT yield, compared to WO_3/CNT. This suggests that the addition of copper to WO_3/CNT resulted in a higher selectivity towards the THFA pathway from HMF. The THFA yield also increased with W_2C-Cu/CNT compared to W_2C/CNT, but in this case the THFDM yield also increased. Despite this difference, it is still reasonable to conclude that the addition of copper results in a higher selectivity towards the production of THFA from HMF.

Another pathway that occurred for the W_2C-WC/CNT and W_2C-WC-Cu/CNT catalysts was the butanediol pathway. Trace amounts of 1,2-butanediol (1,2-BD) were seen with these two catalysts, but not with the other four. Although the yield is extremely low, the presence of two active tungsten species may play a role in this pathway. However, as mentioned earlier, the W_2C phase was not present when copper was added, so the presence of 1,2-butanediol may be due to earlier issues with the HPLC. The products from these two catalysts were examined after the column was replaced, so the small amount detected may just be due to better resolution with the new HPLC column compared to the previous column that was deteriorating over time. These trace amounts may therefore not have been seen with the previous HPLC.

4.5.2 Examining the effect of reaction time on product yield

In order to examine the effect of reaction time, the WO_3/CNT, W_2C/CNT, WO_3-Cu/CNT, and W_2C-Cu/CNT catalysts were tested again at 245 °C and 60 bar H_2 for 180 minutes with the same reactor loading. The W_2C-WC/CNT and W_2C-WC-Cu/CNT were not further tested, as the composition of W_2C-WC-Cu/CNT was not correct, and therefore could not be directly compared to the other catalysts. The product yield for the four catalysts tested for 180 minutes are shown in Table 4.4, along with the product yield for 90 minutes and the change in yield. Cellulose conversion was still 100% when the reaction time was increased.

Table 4.4: Yields for various tungsten and copper promoted tungsten catalysts after 180 and 90 min

Reaction Time	Catalyst	Yield (%)						Unidentified Peaks (% of total area)	
		Total	EG	1,2-PG	THFDM	THFA	1,2,6-HT	Peak 28	Void Volume
180 min	WO_3/CNT	11.1	2.2	1.9	1.4	3.2	2.4	9.2	66.5
	W_2C/CNT	14.4	4.2	3.0	1.2	2.9	3.1	13.7	49.2
	WO_3-Cu/CNT	15.1	4.2	2.7	1.8	3.5	2.9	9.0	54.1
	W_2C-Cu/CNT	17.1	7.7	3.5	0.7	2.5	2.7	9.6	54.1
90 min	WO_3/CNT	12.5	1.6	1.3	3.7	3.4	2.5	13.2	62.8
	W_2C/CNT	10.1	3.1	1.3	0.4	2.2	3.1	13.4	41.9
	WO_3-Cu/CNT	15.3	4.0	1.4	2.4	5.2	2.3	13.3	53.8
	W_2C-Cu/CNT	15.6	6.7	2.1	1.1	3.6	2.1	11.2	53.7
Δ Yield (90-180 min)	WO_3/CNT	-1.4	0.6	0.6	-2.3	-0.2	-0.1	-4.0	3.7
	W_2C/CNT	4.3	1.1	1.7	0.8	0.7	0.0	0.3	7.3
	WO_3-Cu/CNT	-0.2	0.2	1.3	-0.6	-1.7	0.6	-4.3	0.3
	W_2C-Cu/CNT	1.5	1.0	1.4	-0.4	-1.1	0.6	-1.6	0.4

From these results it is evident that the EG and 1,2-PG yields both increased when doubling the reaction time, as shown in Figures 4.16 and 4.17, suggesting that the kinetics are slow. A reaction time of 180 minutes may therefore still be too short with these catalysts. In addition the HMF degradation product yields decreased, except for in the case of W_2C/CNT, which may be due to potential polymerization of HMF derivatives. In addition, the total yield decreases for the WO_3 catalysts, but increases for the W_2C catalysts. This can also be explained by the lower hydrogenation activity of WO_3, resulting in more unsaturated HMF degradation products as the reaction time is increased.

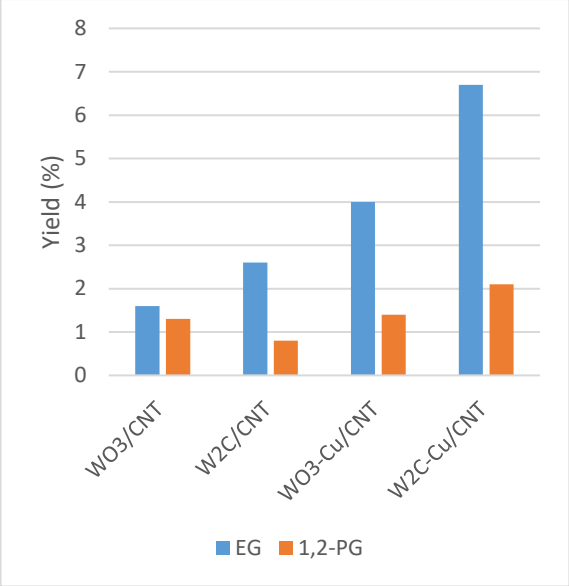

Figure 4.16: EG and 1,2-PG yields after 90 min

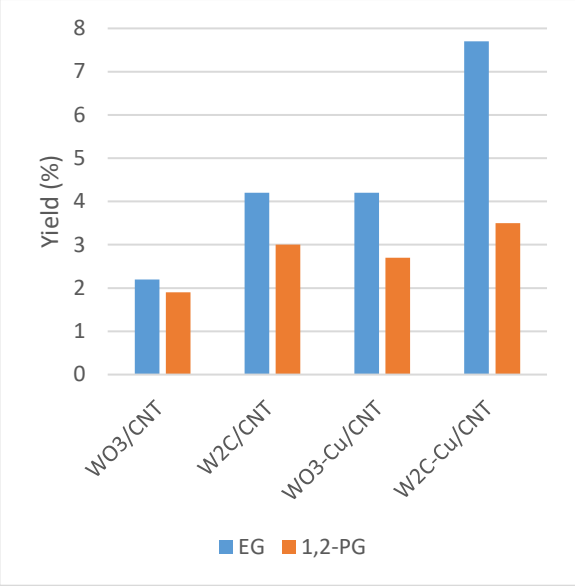

Figure 4.17: EG and 1,2-PG yields after 180 minutes

Another trend that can be seen when comparing Figures 4.16 and 4.17 is that the EG/1,2-PG selectivity decreases when the reaction time is increased, except in the case of WO_3/CNT, which has the lowest hydrogenation activity. This suggests that 1,2-PG is slower to form compared to EG due to a lower reaction rate. In order to examine the change in EG and 1,2-PG over time, the change in EG and 1,2-PG yield from 90 to 180 minutes was also plotted, as shown in Figures 4.18 and 4.19 respectively. From these results it is evident that the EG and 1,2-PG yields are mostly affected with the W_2C catalysts due to the higher hydrogenation activity compared to WO_3. The WO_3/CNT had the lowest change in yield, as it had the lowest hydrogenation activity, while the WO_3-Cu/CNT had a slightly higher increase in yield due to the promotion effect of copper for hydrogenation. However, the change is very small, further suggesting that copper has low hydrogenation activity compared to M(8,9,10) transition metals. The copper may therefore promote hydrogenation by W_2C, but its hydrogenation activity alone with WO_3 is very low.

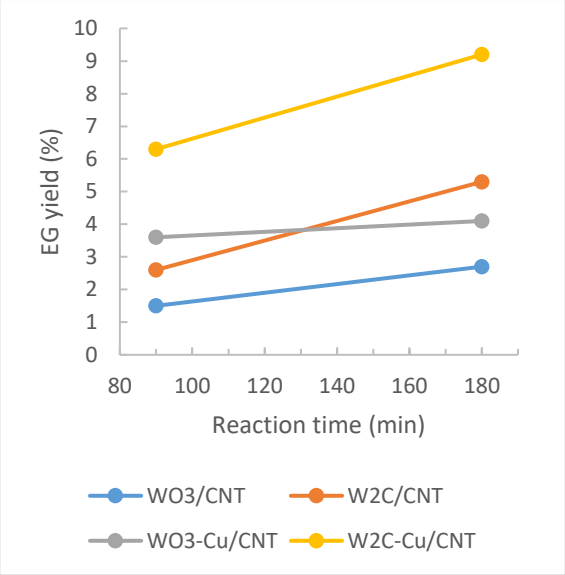

Figure 4.18: Change in EG yield with time

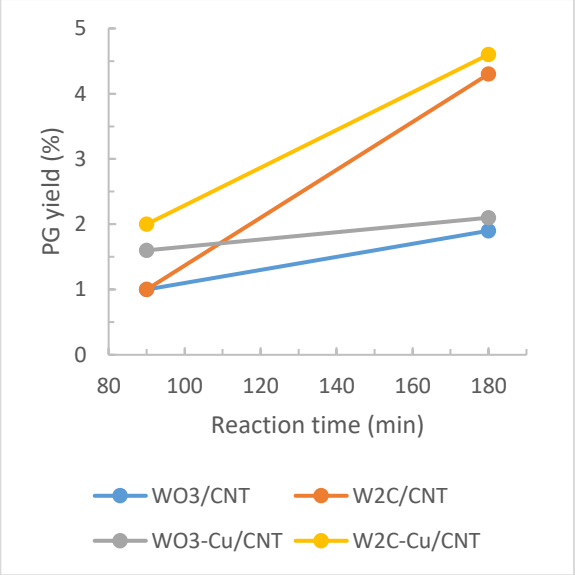

Figure 4.19: Change in PG yield with time

4.5.3 WO_3/CNT and W_2C/CNT in combination with Cu_xO/CNT

After various copper promoted tungsten-based catalysts were tested, WO_3/CNT and W_2C/CNT were also tested in combination with Cu_xO/CNT in order to examine if copper has similar hydrogenation activity to nickel. Wang et al. determined that a molar ratio of Ni/W = 1.0 was the optimal ratio for EG production [13]. Cu_xO/CNT was first tested alone with the same loading as the previous catalyst tests (0.1 g) to examine its activity on cellulose conversion. WO_3/CNT and W_2C/CNT were then tested in combination with Cu_xO/CNT with a molar ratio of Cu/W = 1.0 based on the nominal 10 wt% loading of both the tungsten and copper catalysts. The loading of the tungsten catalysts was maintained at 0.1 g, resulting in a Cu_xO/CNT loading of 0.0346 g. The product yield for these reactions is shown in Table 4.5, along with the previous results with a 90 minute reaction time. The cellulose conversion was also complete with these catalysts. The actual loading was later determined later by TGA analysis, so the actual Cu/W molar ratio based on TGA was 1.08 and 0.95 for WO_3/CNT and W_2C/CNT with Cu_xO/CNT, respectively. These ratios are both very close to the theoretical ratio of 1.0 so the two catalytic systems can be compared directly.

Table 4.5: Yields for WO_3/CNT and W_2C/CNT in combination with Cu_xO/CNT

Catalyst	Yield (%)											Void Volume
	Total	EG	1,2-PG	Sor	1,2-BD	2,5-DHF	THFDM	THFA	1,2,6-HT	1,6-HD	1,2-HD	(% total area)
Cu_xO/CNT	16.6	2.4	4.5	2.3	1.3	1.1	1.0	-	2.1	0.9	0.8	26.6
WO_3/CNT Cu_xO/CNT	11.7	1.9	1.3	0.9	-	-	2.1	3.3	2.2	-	-	61.0
W_2C/CNT Cu_xO/CNT	24.4	5.2	3.6	7.9	1.0	3.8	-	-	0.3	1.9	0.1	30.6
WO_3/CNT	12.5	1.6	1.3	-	-	-	3.7	3.4	2.5	-	-	62.8
W_2C/CNT	10.1	3.1	1.3	-	-	-	0.4	2.2	3.1	-	-	41.9
WO_3-Cu/CNT	15.3	4.0	1.4	-	-	-	2.4	5.2	2.3	-	-	53.8
W_2C-Cu/CNT	15.6	6.7	2.1	-	-	-	1.1	3.6	2.1	-	-	53.7

The first noticeable difference of these reactions is that the unidentified peak at a retention time of 28 minutes disappears, which may mean the possible furanone intermediate is no longer present. After examining the yields from Cu_xO/CNT, it is evident that both retro-aldol condensation and hydrogenation occur, as EG and 1,2-PG are formed. However, the EG/1,2-PG selectivity is in favor of 1,2-PG in contrast to when tungsten is present, as seen in Figure 4.2. This is most likely due to the basic properties of Cu_xO/CNT compared to the acidic properties of tungsten. Acidic sites lead to an intramolecular hydride shift during cellulose hydrolysis, while solid bases can catalyze a proton transfer, which leads to the formation of fructose [74]. The formation of more fructose with Cu_xO/CNT will therefore result in a higher 1,2-PG yield. When Cu_xO/CNT is used in combination with WO_3/CNT and W_2C/CNT, the EG/1,2-PG selectivity favors EG, which suggests that the basic sites from Cu_xO/CNT are neutralized by the acidic sites of the tungsten catalysts. This neutralization process may also be the cause for lower EG and 1,2-PG yields compared to WO_3-Cu/CNT and W_2C-Cu/CNT, as the retro-aldol activity of tungsten species may be partially inhibited.

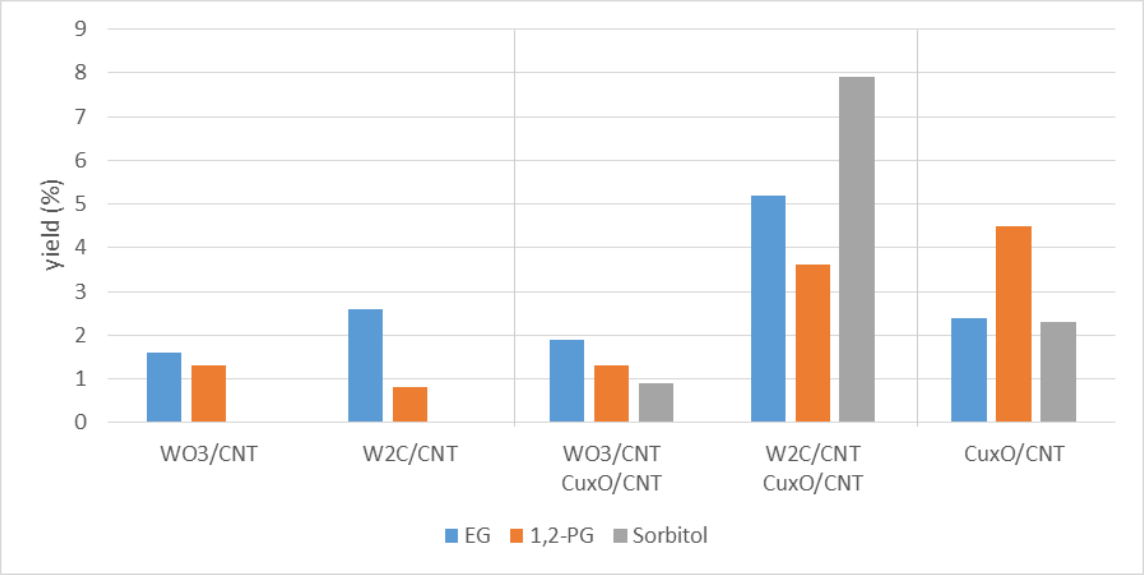

Figure 4.20: EG, 1,2-PG and Sorbitol yields for WO_3/CNT and W_2C/CNT with Cu_xO/CNT

It is also evident that numerous other products were obtained using Cu_xO/CNT compared to the previous catalysts. In these three reactions sorbitol (Sor) was present, indicating that the hydrogenation activity was improved, as some glucose was hydrogenated to sorbitol before retro-aldol condensation occurred. The sorbitol yield was much greater than both the EG and 1,2-PG yields with W_2C/CNT + Cu_xO/CNT. This is due to the combined hydrogenation activity of W_2C and Cu_xO, which in this case occurs much faster than retro-aldol condensation. The sorbitol yield was significantly lower than the EG yield in the study performed by Wang et al. when using a ratio of Ni/W =1.0 [13], which suggests that a Cu/W = 1.0 is too high for this catalytic system. When WO_3/CNT + Cu_xO/CNT was used, the sorbitol yield was much lower due to absent hydrogenation activity of WO_3.

Although the presence of sorbitol indicated higher hydrogenation activity, the EG and 1,2-PG yield was lower than WO_3-Cu/CNT and W_2C-Cu/CNT, but higher than WO_3/CNT and W_2C/CNT. This may be due to the different properties of Cu_xO compared to metallic Cu, as neutralization of the basic sites of Cu_xO/CNT may result in lower hydrogenation activity compared to metallic Cu. However, there is also less Cu present in these reactions compared to the tungsten-copper catalysts, which may result in less hydrogenation activity. In this case it seems that the retro-aldol activity is inhibited by Cu_xO, rather than hydrogenation, as the presence of sorbitol suggests higher hydrogenation activity and the lower EG and 1,2-PG yields suggests that the hydrogenation occurs faster than retro-aldol condensation. Regardless, it is clear that the EG and 1,2-PG yield is lower when the tungsten catalysts are used in combination

with Cu_xO/CNT compared to the tungsten-copper catalysts. This may be due to the combination of neutralization of retro-aldol active sites on WO_3/CNT and W_2C/CNT and neutralization of hydrogenation active sites on Cu_xO/CNT when used in combination.

Another product that was only previously seen with W2C-WC/CNT and W_2C-WC-Cu/CNT was 1,2-butanediol (1,2-BD) when Cu_xO/CNT was used as the catalyst alone and in combination with W_2C/CNT, suggesting that the Cu_xO species may have a higher selectivity towards the butanediol pathway compared to Cu. This may further explain the presence of 1,2-BD for the W_2C-WC-Cu/CNT catalyst as copper oxide was formed rather than metallic copper. However, 1,2-BD was not seen with WO_3/CNT + Cu_xO/CNT, which may be the result of the absent hydrogenation activity of WO_3. However, erythrose and erythritol were not seen either, which are precursors for 1,2-butanediol, suggesting that the pathway may be inhibited. In addition, 1,2-hexanediol (1,2-HD) and 1,6-hexanediol (1,6-HD) are seen with Cu_xO/CNT alone and in combination with W_2C/CNT, but not with WO_3/CNT. All three reactions produced 1,2,6-hexanetriol (1,2,6-HT), but WO_3/CNT with Cu_xO/CNT did not result in the further decomposition to 1,2-HD and 1,6-HD due to its inability to remove a hydroxyl group from 1,2,6-HT. This suggests that a larger synergistic effect occurs between Cu_xO/CNT and W_2C/CNT compared to Cu_xO/CNT and WO_3/CNT due to the combined hydrogenation activities.

In addition to the hexane polyols, other HMF degradation products were also seen with these catalyst systems, similar to that of the previous catalysts. In this case, THFA was only seen with WO_3/CNT + Cu_xO/CNT in contrast to being present in all previous reactions. However, the THFA yield was always higher than other HMF degradation products for any WO_3-based catalyst system. This further suggests that WO_3 has a higher selectivity towards THFA compared to THFDM. Additionally, 2,5-DHF was seen for Cu_xO/CNT alone and in combination with W_2C/CNT, which was not present earlier. This suggests that the hydrogenation to THFDM is much slower with Cu_xO/CNT. In addition, since no 2,5-DHF was present with WO_3/CNT + Cu_xO/CNT, the reaction pathway towards THFA appears to occur faster than the reaction pathway towards THFDM.

4.5.4 WO_3/CNT and W_2C/CNT in combination with Ru/CNT

After analysing the previous results it became clear that copper does not possess sufficient hydrogenation activity as the void volume peak remained large and the product solution was always yellow in color. A new catalyst system using Ru/CNT in combination with WO_3/CNT and W_2C/CNT was therefore tested as Ru has been shown to be the most active metal for the hydrogenation of non-furanic carbonyl groups in aqueous phase reactions [19]. Both 10 wt% and 50 wt% WO_3/CNT and W_2C/CNT were tested in combination with 1 wt% Ru/CNT with a constant molar ratio of Ru/W = 0.1, as this was the optimal ratio for the production of EG from cellulose determined by Wang et al. [13].

For these reactions, the amount of tungsten catalyst was not maintained at 0.1 g, but instead the amount of Ru/CNT was kept constant at 0.1333 g based on the Ru/cellulose ratio used by Wang et al [13]. This resulted in a tungsten catalyst loading of 0.2425 g for the 10 wt% tungsten catalysts and 0.0485 g for the 50 wt% tungsten catalysts. The product yield for these catalytic systems are shown in Table 4.6 with 100% conversion. The maximum EG yield obtained was 30.5% with 10 wt% WO_3/CNT + Ru/CNT. This catalyst system was therefore examined again with extremely dilute sulfuric acid (H_2SO_4) with an H_2SO_4/W ratio of 0.03 to see if the EG yield could be improved even further, as proposed by Xu et al. [38]. However, it is important to note that Xu et al. used tungsten acid with a H_2SO_4/H_2WO_4 ratio of 0.03 rather than solid tungsten catalysts.

Table 4.6: Yields for varying loadings of WO_3/CNT and W_2C/CNT in combination with Ru/CNT

Catalyst	Yield (%)										Void Volume
	Total	EG	1,2-PG	Sor	Man	Gly	Ery	1,2-BD	2,5-DHF	1,6-HD	(% total area)
10% WO_3/CNT Ru/CNT + H_2SO_4	43.8	20	7.4	9.4	-	0.9	-	6.1	-	-	22.5
10% WO_3/CNT Ru/CNT	50.1	30.5	12.3	1.7	-	-	-	5.6	-	-	9.1
50% WO_3/CNT Ru/CNT	39.5	25.3	7.0	2.0	-	-	0.8	4.4	-	-	6.6
10% W_2C/CNT Ru/CNT	49.5	11.9	11.4	2.3	-	10.8	1.9	5.6	2.7	2.9	4.3
50% W_2C/CNT Ru/CNT	58.1	3.9	14	14.1	4.5	7.2	2.9	3.2	6.8	1.5	0.9

The first immediate result that could be seen was the improved hydrogenation when using Ru rather than Cu, based on the color of the product solution, as shown in Figure 4.21. It is clear that going from right to left the yellow color gets lighter from WO_3/CNT to W_2C-Cu/CNT, and then becomes even lighter when using Cu_xO/CNT both alone and in combination with W_2C/CNT. The yellow color then completely disappears for the 10 and 50 wt% WO_3/CNT and W_2C/CNT in combination with Ru/CNT. This suggests that the hydrogenation activity of hydrogenation catalysts increases in the order Cu < Cu_xO < Ru if hydrogenation activity is based solely on the color of the product solution. In addition, the void volume area was significantly reduced, attributing to less than 10% of the total area, except for when H_2SO_4 was added. This also suggests much greater hydrogenation activity with less unsaturated by-products being formed.

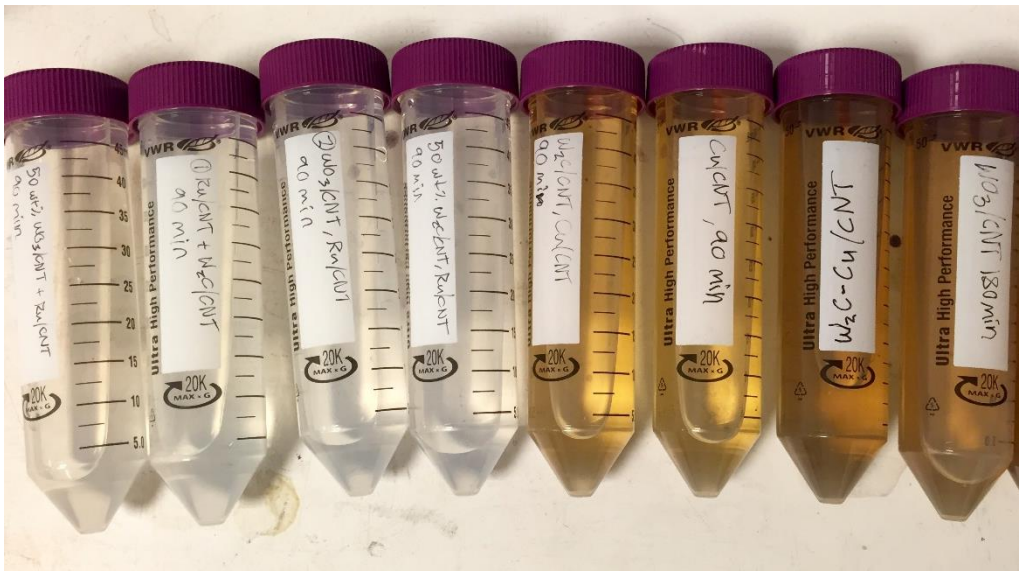

Figure 4.21: Product solution from various reactions using different catalysts

Although the total yield increased significantly for these systems compared to previous results, the total yield was still below 60% in all cases. This is most likely due to the formation of gases such as CH_4 and CO_2 when Ru/CNT is used, as Ru is known to catalyze the further degradation of EG into gases such as CH_4 and CO_2 [27]. For example, Li et al. only detected trace amounts of diols and mono-phenols with the Ru-W_2C/AC catalyst using birchwood as the feedstock, but the gas products attributed to 72.08 wt% of the total carbon in the feedstock [51]. Since the void volume is very low in these systems, and all other compounds are accounted for, the low total yield is due to the larger amounts of gaseous products being formed.

The EG yield is much higher with WO_3/CNT + Ru/CNT compared to W_2C/CNT + Ru/CNT, as shown in Figure 4.22. When comparing the tungsten loading of WO_3/CNT, it is clear that the 10 wt% WO_3/CNT had a higher yield than 50 wt%. This is most likely due to the significantly lower surface area of 50 wt% WO_3/CNT (31.5 m^2/g) compared to 10 wt% (78.4 m^2/g) as determined by BET analysis. When extremely dilute H_2SO_4 (0.12 mM) was used with 10 wt% WO_3/CNT + Ru/CNT, the EG and 1,2-PG yield decreased, rather than increasing. However, the sorbitol yield increased significantly, as seen in Figure 4.23, suggesting that H_2SO_4 inhibited the retro-aldol activity of WO_3/CNT, but did not affect the hydrogenation activity of Ru/CNT. The addition of dilute sulfuric acid may therefore be detrimental to heterogeneous solid tungsten catalysts, but beneficial for homogenous tungsten catalysts.

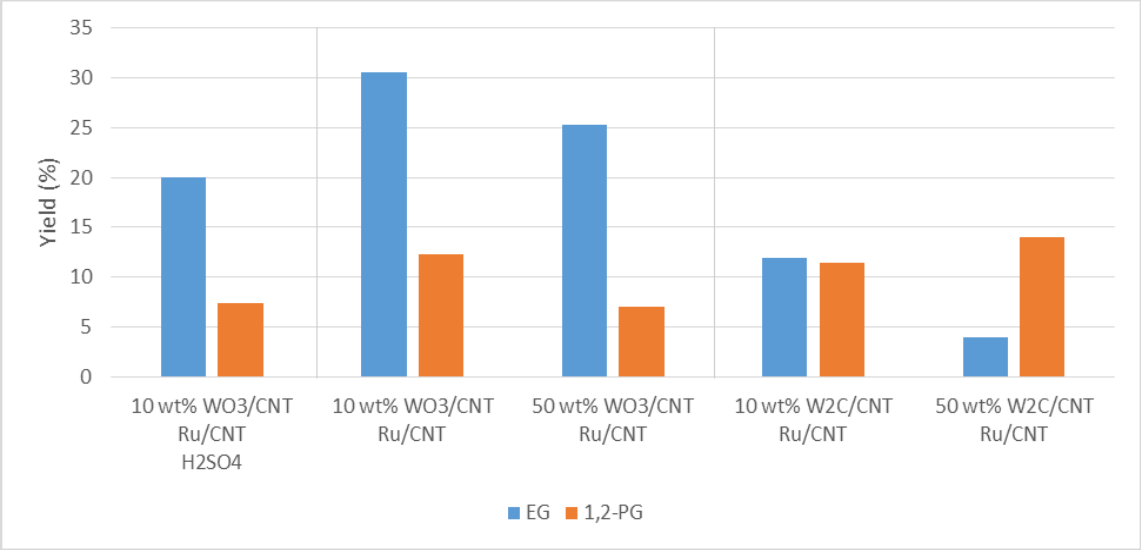

Figure 4.22: EG and 1,2-PG yields for WO_3/CNT and W_2C/CNT with Ru/CNT

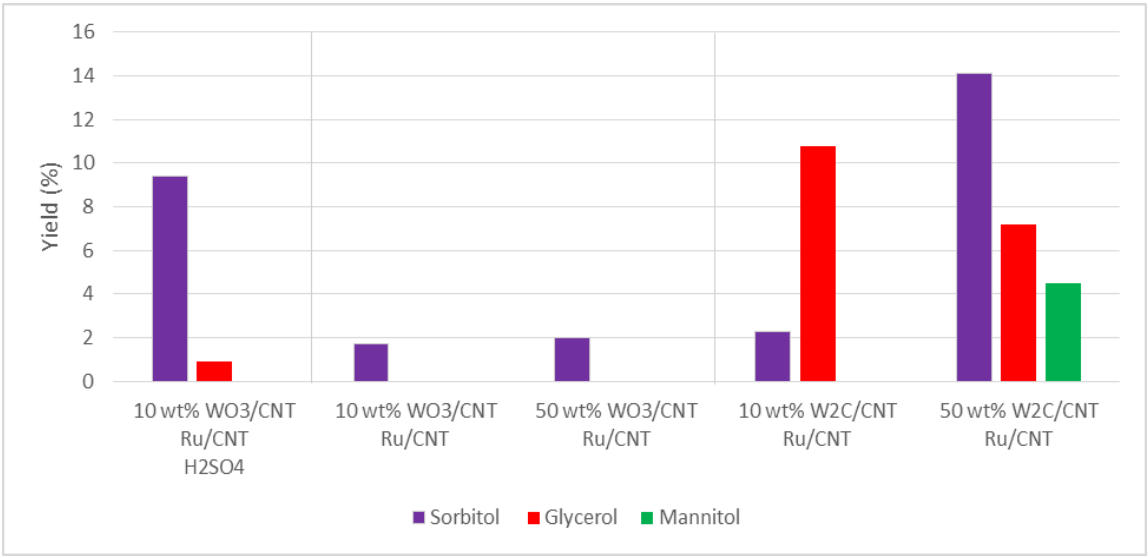

Figure 4.23: Glycerol, Sorbitol, and Mannitol yields for WO_3/CNT and W_2C/CNT with Ru/CNT

When W_2C/CNT was tested in combination with Ru/CNT, the EG yield was significantly lower than WO_3/CNT + Ru/CNT, as seen in Figure 4.22. However, numerous other hydrogenation products were present, such as glycerol (Gly), sorbitol (Sor), and mannitol (Man), as seen in Figure 4.23. Glycerol was previously not detected for the other catalysts, except for in small amounts when dilute H_2SO_4 was used. Glycerol is a product formed from the fructose pathway, which suggests that glucose-fructose isomerization increased compared to WO_3/CNT. This also explains the much lower EG/1,2-PG selectivity, as more 1,2-PG is also formed via the fructose pathway. The glucose-fructose isomerization was greater for 50 wt% W_2C/CNT + Ru/CNT compared to 10 wt% as seen by a higher 1,2-PG yield compared to EG and the presence of mannitol, which is also formed from fructose.

The high yields of sorbitol and mannitol suggest that the hydrogenation activity is too great compared to retro-aldol condensation due to the additional hydrogenation activity of W_2C/CNT. The hydrogenation is even greater with 50 wt% W_2C/CNT + Ru/CNT compared to 10 wt%. This could not be explained by the difference in surface area as 10 wt% W_2C/CNT had a BET surface area of 80.2 m^2/g and 50 wt% W_2C/CNT had a BET surface area of 86.7 m^2/g, which are not significantly different. The molar ratio of Ru/W = 0.1 is therefore too high for this catalyst system. However, the amount of each catalyst needed for this ratio was calculated based on the nominal W and Ru loading. The actual loading was determined by TGA analysis later, which showed a Ru/W ratio of 0.39 and 0.61 for 10 wt% and 50 wt% W_2C/CNT in combination with Ru/CNT respectively. This is much higher than the theoretical Ru/W ratio, which explains the higher hydrogenation activity and lower EG and 1,2-PG yields, as Wang et al. reported a consistent decrease in EG yield as the Ru/W ratio was increased above 0.1 [13].

The difference in the Ru/W ratio for the different wt% of W_2C/CNT may also be the cause of the higher mannitol and 1,2-PG yield compared to EG for 50 wt% W_2C/CNT + Ru/CNT. The Ru/W ratio was much higher than the 10 wt% W_2C/CNT + Ru/CNT based on the actual W and Ru loading. Ru/CNT may therefore be the cause of increased glucose-fructose isomerization, as this was not seen with Cu, and only to some degree with Cu_xO. The difference in W loading may therefore not be the cause of the differences in yield as with WO_3/CNT, but rather the different Ru/W ratio.

The actual Ru/W ratio was also calculated for the WO_3/CNT catalysts, resulting in a Ru/W ratio of 0.45 and 0.64 for 10 wt% and 50 wt% WO_3/CNT in combination with Ru/CNT respectively. In this case, it did not matter that the ratio was too high as WO_3 does not possess the same hydrogenation activity as W_2C, so excessive hydrogenation did not occur. The lower EG and 1,2-PG yields for 50 wt% WO_3/CNT compared to 10 wt% may therefore not be caused by the difference in the Ru/W ratio, but rather by the surface area. However, the slightly higher sorbitol yield for 50 wt% WO_3/CNT compared to 10 wt% may be a result of the higher Ru/W ratio, so both surface area and the Ru/W ratio play a role. The Ru/W ratio could therefore possibly be increased even further with the WO_3/CNT + Ru/CNT catalyst systems, but should be lowered significantly for the W_2C/CNT + Ru/CNT catalyst systems.

The yield of 1,2-butanediol (1,2-BD) was significantly higher for these catalytic systems compared to previous ones, which suggests Ru may play a role in facilitating this pathway as well. In addition, erythritol (1,2-BD precursor) was also seen for some of the reactions with Ru/CNT, which was not seen earlier. Another difference from previous reactions is that when WO_3/CNT was used in combination with Ru/CNT, no products from the HMF degradation pathway were present. The combination of WO_3/CNT and Ru/CNT therefore seems to inhibit this pathway entirely, which is beneficial for increasing the EG selectivity of the reaction. The W_2C/CNT + Ru/CNT catalyst system did produce 2,5-DHF, but no 1,2,6-HT was seen, as it was all converted to 1,6-HD (no 1,2-HD). The removal of a hydroxyl group therefore occurred to a greater extent with Ru compared to Cu or Cu_xO, as only 1,2,6-HT was seen with Cu and only some 1,6-HD and 1,2-HD formed with Cu_xO.

4.5.5 Examining Reaction Kinetics

In order to examine the kinetics of the reaction, samples were taken periodically via a sampling tube that allowed for sample retrieval during the reaction. However, the HPLC column was damaged again so only the 10 wt% WO_3/CNT + Ru/CNT catalyst system was tested. When the samples were examined with the HPLC, the separation of products was extremely poor, with the majority of the peaks tailing and overlapping with others, so reasonable quantitative data could not be obtained. Despite poor resolution, some trends could still be seen over time, as shown in Figure 4.24. This figure is an overlay of the HPLC diagrams for samples taken from 0-180 minutes for 10 wt% WO_3/CNT + Ru/CNT. The HPLC diagrams for each reaction are shown in Appendix E.

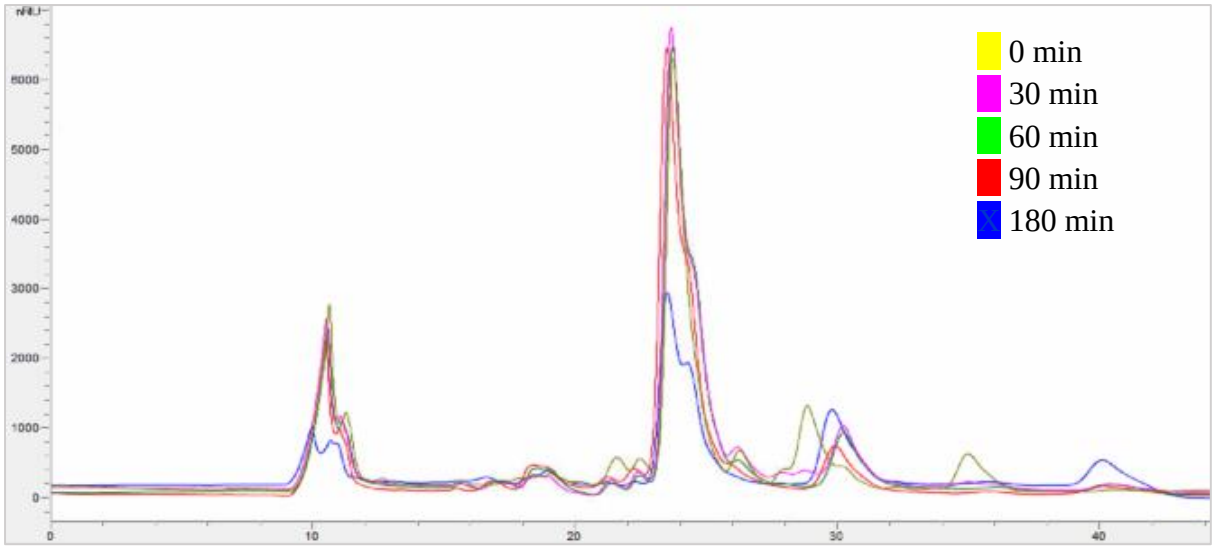

Figure 4.24: Overlay of HPLC diagrams for 10 wt% WO_3/CNT + Ru/CNT from 0-180 min

From this figure, both sorbitol (~29 min) and THFA (~34.5 min) can be seen for the sample taken at 0 minutes, when the reactor hit the target temperature of 245 °C, which diminishes after 30 minutes, and is essentially gone after 60 minutes. This validates the assumption that sorbitol formation is reversible, and can be converted further to the desired products. The disappearance of THFA may suggest that it is converted further or broken down by the presence of Ru, as THFA was present with all other WO_3-based catalyst systems. However, no other unidentified peaks appear in the samples taken at later times, suggesting that it may also be converted to gases by the presence of Ru. In addition the 1,2-BD peak (~30 min), seems to increase with time, then decreases slightly at 90 minutes, and increases again at 180 minutes, suggesting the formation of 1,2-BD is much slower than the formation of EG and 1,2-PG.

The EG and 1,2-PG yield is very hard to quantify due to poor separation, but it is evident that 1,2-PG (~24.2 min) forms later than EG (~23.7 min), as seen by the broadening of the peak in this area, with a slight indication of two defined peaks over time. The peak width remains constant at 30 and 60 minutes, then becomes narrower again at 90 minutes, suggesting 1,2-PG degradation began to occur. When examining the change in EG/1,2-PG yield over time, the EG/1,2-PG peak remains relatively constant in terms of peak height (and area) until 90 minutes, with a slight peak at 30 minutes, suggesting that EG forms quickly and remains relatively constant until 90 minutes. The void volume peak also remains relatively constant from 0-90 min, suggesting that the products in the void volume form quickly and remain constant. This indicates that the void volume in the case of high hydrogenation activity consists

of mostly acids and not unsaturated by-products. This confirms the assumption that the void volume contains both unsaturated by-products and acids.

After 90 minutes, both the void volume and EG/1,2-PG yield decreases sharply, which suggests an increase in gas products at prolonged reaction times, as EG, 1,2-PG, and the acids in the void volume may be converted to gases. However, a new peak also appeared (~40 min) after 180 minutes, which was identified to have a molar mass of 116.1 g/mol using MS. According to this molar mass and retention time, it may be tetrahydropyran-2-methanol (THP2M) as this standard was analysed earlier with HPLC. However, it seems unlikely that this compound would only form at a later time as THP2M is formed directly from cellulose [75], so it cannot form via the HMF degradation pathway. The molar mass is also consistent with trans-1,2-cyclohexane, which could be the result of hexanediol ring formation, but the retention time is not consistent with the standard that was tested. Regardless, it is evident that a reaction time of 180 minutes is too long for this catalyst system, while a reaction time of 90 minutes was not excessive as the desired product yields remained relatively constant from 30-90 min.

The EG and 1,2-PG stability was also tested by adding 0.33 g of EG and 1,2-PG to water with 0.1 g Ru/CNT for 180 minutes prior to this reaction in order to see if degradation products other than gases were formed. The EG and 1,2-PG yields were significantly reduced after 180 minutes, confirming that Ru converts both EG and 1,2-PG to gaseous products under these reaction conditions. It is also evident that 1,2-PG underwent greater degradation, as the EG yield decreased by 23.3%, while the 1,2-PG yield decreased by 64.4%. The larger decrease in 1,2-PG yield can be explained by the appearance of a third peak after 180 minutes, which had a molar mass of 134.1 g/mol determined by MS, which is consistent with dipropylene glycol. This suggests that some of the 1,2-PG polymerized to dipropylene glycol in addition to being converted to gases. There was no standard for this product, so quantification of dipropylene glycol was not possible in order to examine how much 1,2-PG was converted to gases. The instability of EG and 1,2-PG after 180 minutes further confirms that a reaction time of 180 minutes is too long when using Ru/CNT.

5. Conclusion

In this study, the one-pot conversion of cellulose to ethylene glycol (EG) and propylene glycol (1,2-PG) was examined with the use of various tungsten-based catalysts with copper (Cu) and ruthenium (Ru) in a batch reactor at 245 °C and 60 bar H_2 for 90/180 minutes. The results of these different studies indicates that the hydrogenation activity of copper is too low compared to Ni and Ru in the ratios used in this study, resulting in low EG and 1,2-PG yields and a large amount of unsaturated by-products. The maximum EG and 1,2-PG yield obtained using tungsten and copper was 7.7% and 3.5% respectively for W_2C-Cu/CNT after 180 minutes, which increased from a reaction time of 90 minutes. The yield was even lower when tungsten-based catalysts were used in combination with Cu_xO/CNT, with a molar ratio of Cu/W =1.0, due to neutralization of retro-aldol and hydrogenation activity of each catalyst by the respective acidic and basic sites. In all cases, the hydrogenation activity is too low, suggesting that the Cu/W ratio needs to be increased. It is also evident that the HMF degradation pathway occurs with all tungsten/copper-based catalyst systems, but the selectivity towards THFA compared to THFDM is greater amongst WO_3 compared to W_2C, and is even further enhanced by the presence of Cu. The 1,2-butanediol pathway is only significantly seen when Ru is present, suggesting Ru plays a role in this pathway.

The maximum EG and 1,2-PG yield obtained was 30.5% and 12.5% respectively for 10 wt% WO_3/CNT + Ru/CNT after 90 minutes, with a significant reduction of the void volume. The EG and 1,2-PG yield was lower with 50 wt% WO_3/CNT, suggesting that the metal loading affects the product yield. This catalyst system was also tested with the addition of dilute sulfuric acid (H_2SO_4) in a molar ratio of H_2SO_4/W = 0.03, which resulted in a lower EG yield and higher sorbitol yield, indicating that H_2SO_4 inhibited the retro-aldol activity of WO_3/CNT. The W_2C/CNT + Ru/CNT catalyst systems resulted in too high hydrogenation activity as glycerol, sorbitol, and mannitol were produced in high amounts. The Ru/W ratio could therefore possibly be increased even further with the WO_3/CNT + Ru/CNT catalyst systems, but should be lowered significantly for the W_2C/CNT + Ru/CNT catalyst systems. It is also evident that W_2C/CNT plays a role in glucose to fructose isomerization, as seen by the higher 1,2-PG (and in in the latter case mannitol) yield when used in combination with Cu_xO/CNT and Ru/CNT. When examining the reactions over time, it became clear that a reaction time of 180 minutes may be too low for the tungsten-copper catalyst systems, but is too high for the tungsten-ruthenium catalyst systems.

The WO_3/CNT catalyst systems are a promising alternative for tungsten-based catalysts, despite their lack of hydrogenation activity. Most recent studies have mostly focused on the use of tungsten carbide catalysts or homogenous tungsten-based acids. The side-products when using WO_3/CNT are limited compared to W_2C/CNT, especially when used in combination with Ru/CNT, in which the HMF degradation pathway was inhibited entirely. This may be extremely beneficial in terms of limiting the formation of other side products and increasing EG selectivity. In addition, it is evident that THFA is preferred over other HMF degradation products when WO_3 is used, which would increase product selectivity even further. There is also less concern with stability issues when using WO_3, as W_2C suffers from oxidation after each reaction. WO_3/CNT could therefore potentially be used numerous times without suffering deactivation between each reaction. The lack of hydrogenation activity can easily be mitigated by the addition of a hydrogenation catalyst, so by tuning the ratio of hydrogenation and retro-aldol condensation, WO_3 may be a very good tungsten-based catalyst for the conversion of cellulose to EG.

6. Future Work

In this study, the ratio of retro-aldol activity and hydrogenation activity was not optimized, as nominal loadings of 10 wt% W and 10 wt% Cu were used for WO_3-Cu/CNT and W_2C-Cu/CNT. The 10 wt% W loading was much lower than what was typically suggested in literature (30 wt%) so further studies can be done on increasing the tungsten loading to compare with literature. It was evident that these catalysts did not result in significant hydrogenation activity. In addition, when WO_3/CNT and W_2C/CNT were tested in combination with Cu_xO/CNT, the Cu/W ratio was based on literature regarding the use of nickel, with an optimum molar ratio of Ni/W = 0.1. The hydrogenation activity in this case was still too low, so optimization of the Cu/W ratio is necessary.

Further work may also be done on optimizing the Ru/W ratio based on whether WO_3/CNT or W_2C/CNT is used in combination with Ru/CNT. The Ru/W ratio in this study was based on literature, which showed an optimal molar ratio of Ru/W = 0.1 when using tungsten acid with Ru. The actual ratio used in this study was later determined to be much higher, so optimization of the Ru/W ratio with both WO_3/CNT and W_2C/CNT may therefore result in higher EG yields. It was seen that WO_3/CNT may be a very promising tungsten-based catalyst due to limiting side-reactions and mitigating issues with reusability due to oxidation. Further research focusing on the use of WO_3/CNT with a hydrogenation catalyst may provide high EG yield and selectivity.

Kinetic studies for the various catalytic reactions were attempted during this study, but they were hindered due to deterioration of the HPLC column. Further studies may therefore be done on the kinetics of the reactions by taking periodic samples over time in order to gain further insight into the reaction mechanism and potential intermediates. The potential gas products were not analysed for this study, so developing a method to collect and analyse the gas products present in the reactor can be done in order to achieve a better understanding of the carbon balance of the cellulose derived products. In addition, the catalysts may be further tested in a fixed bed reactor or other reactor systems, rather than just in a batch reactor. The use of a fixed bed reactor would make the catalytic conversion of cellulose to EG much more feasible for industrial applications.

References

1. Bentley, R.W., *Global oil & gas depletion: an overview.* Energy Policy, 2002. 30(3): p. 189-205.

2. Verbruggen, A., et al., *Renewable energy costs, potentials, barriers: Conceptual issues.* Energy Policy, 2010. 38(2): p. 850-861.

3. Kamm, B., et al., *Biorefinery Systems – An Overview*, in *Biorefineries-Industrial Processes and Products*. 2008, Wiley-VCH Verlag GmbH. p. 1-40.

4. Dahmen, N., et al., *Biomass Liquefaction and Gasification*, in *Biomass to Biofuels*. 2010, Blackwell Publishing Ltd. p. 89-122.

5. Xiao, Z., et al., *Conversion of highly concentrated cellulose to 1,2-propanediol and ethylene glycol over highly efficient CuCr catalysts.* Green Chemistry, 2013. 15(4): p. 891-895.

6. Huber, G.W., S. Iborra, and A. Corma, *Synthesis of Transportation Fuels from Biomass: Chemistry, Catalysts, and Engineering.* Chemical Reviews, 2006. 106(9): p. 4044-4098.

7. Zhou, P. and Z. Zhang, *One-pot catalytic conversion of carbohydrates into furfural and 5-hydroxymethylfurfural.* Catalysis Science & Technology, 2016. 6(11): p. 3694-3712.

8. Zhou, C.-H., et al., *Catalytic conversion of lignocellulosic biomass to fine chemicals and fuels.* Chemical Society Reviews, 2011. 40(11): p. 5588-5617.

9. Serrano-Ruiz, J.C. and J.A. Dumesic, *Catalytic Production of Liquid Hydrocarbon Transportation Fuels*, in *Catalysis for Alternative Energy Generation*, L. Guczi and A. Erdôhelyi, Editors. 2012, Springer New York: New York, NY. p. 29-56.

10. Ji, N., et al., *Catalytic conversion of cellulose into ethylene glycol over supported carbide catalysts.* Catalysis Today, 2009. 147(2): p. 77-85.

11. Rinaldi, R. and F. Schuth, *Design of solid catalysts for the conversion of biomass.* Energy & Environmental Science, 2009. 2(6): p. 610-626.

12. Corma, A., S. Iborra, and A. Velty, *Chemical Routes for the Transformation of Biomass into Chemicals.* Chemical Reviews, 2007. 107(6): p. 2411-2502.

13. Wang, A. and T. Zhang, *One-Pot Conversion of Cellulose to Ethylene Glycol with Multifunctional Tungsten-Based Catalysts.* Accounts of Chemical Research, 2013. 46(7): p. 1377-1386.

14. Yue, H., et al., *Ethylene glycol: properties, synthesis, and applications.* Chemical Society Reviews, 2012. 41(11): p. 4218-4244.

15. Li., Y., et al., *Advances in hexitol and ethylene glycol production by one-pot hydrolytic hydrogenation and hydrogenolysis of cellulose.* Biomass and Energy, 2015. 74: p. 148-161.

16. Fukuoka, A. and P.L. Dhepe, *Catalytic conversion ofcellulose into sugar alcohols.* Angewandte Chemie, 2006. 118(31): p. 5285-5287.

17. Luo, C., S. Wang, and H. Liu, *Cellulose conversion into polyols catalyzed by reversibly formed acids and supported ruthenium clusters in hot water.* Angewandte Chemie, 2007. 119(40): p. 7780-7783.

18. Besson, M., P. Gallezot, and C. Pinel, *Conversion of Biomass into Chemicals over Metal Catalysts.* Chemical Reviews, 2014. 114(3): p. 1827-1870.

19. Lee, J., Y. Xu, and G.W. Huber, *High-throughput screening of monometallic catalysts for aqueous-phase hydrogenation of biomass-derived oxygenates.* Applied Catalysis B: Environmental, 2013. 140–141: p. 98-107.

20. Michel, C. and P. Gallezot, *Why Is Ruthenium an Efficient Catalyst for the Aqueous-Phase Hydrogenation of Biosourced Carbonyl Compounds?* ACS Catalysis, 2015. 5(7): p. 4130-4132.

21. Wan, H., et al., *Kinetic investigations of unusual solvent effects during Ru/C catalyzed hydrogenation of model oxygenates.* Journal of Catalysis 2014. 309: p. 174-184.

22. Ji, N., et al., *Direct Catalytic Conversion of Cellulose into Ethylene Glycol Using Nickel-Promoted Tungsten Carbide Catalysts.* Angewandte Chemie International Edition, 2008. 47(44): p. 8510-8513.

23. Conradin, F., *Process for the direct hydrogenation splitting of*. 1962, Google Patents.

24. Zhang, T., et al., *Method of preparing ethylene glycol from cellulose*. 2011, Google Patents.

25. Chen, J.G., *Carbide and Nitride Overlayers on Early Transition Metal Surfaces: Preparation, Characterization, and Reactivities.* Chemical Reviews, 1996. 96(4): p. 1477-1498.

26. Zheng, M., et al., *One-pot catalytic conversion of cellulose to ethylene glycol and other chemicals: From fundamental discovery to potential commercialization.* Chinese Journal of Catalysis, 2014. 35(5): p. 602-613.

27. Tai, Z., et al., *Temperature-controlled phase-transfer catalysis for ethylene glycol production from cellulose.* Chemical Communications, 2012. 48(56): p. 7052-7054.

28. Zhang, K., et al., *Catalytic conversion of cellulose for efficient ethylene glycol production and insights into the reaction pathways.* RSC Advances, 2016. 6(81): p. 77499-77506.

29. Ji, N., et al., *Nickel-Promoted Tungsten Carbide Catalysts for Cellulose Conversion: Effect of Preparation Methods.* ChemSusChem, 2012. 5(5): p. 939-944.

30. Ooms, R., et al., *Conversion of sugars to ethylene glycol with nickel tungsten carbide in a fed-batch reactor: high productivity and reaction network elucidation.* Green Chemistry, 2014. 16(2): p. 695-707.

31. Quanli, Z., et al., *The promotion of nickel to Mo2C/Al2O3 catalyst for the partial oxidation of methane to syngas.* New Journal of Chemistry, 2003. 27(11): p. 1633-1638.

32. Zhang, Y., A. Wang, and T. Zhang, *A new 3D mesoporous carbon replicated from commercial silica as a catalyst support for direct conversion of cellulose into ethylene glycol.* Chemical Communications, 2010. 46(6): p. 862-864.

33. Pang, J., et al., *Catalytic conversion of cellulose to hexitols with mesoporous carbon supported Ni-based bimetallic catalysts.* Green Chemistry, 2012. 14(3): p. 614-617.

34. Levy, R.B. and M. Boudart, *Platinum-Like Behavior of Tungsten Carbide in Surface Catalysis.* Science, 1973. 181(4099): p. 547-549.

35. Zheng, M.-Y., et al., *Transition Metal–Tungsten Bimetallic Catalysts for the Conversion of Cellulose into Ethylene Glycol.* ChemSusChem, 2010. 3(1): p. 63-66.

36. Palkovits, R., et al., *Hydrogenolysis of cellulose combining mineral acids and hydrogenation catalysts.* Green Chemistry, 2010. 12(6): p. 972-978.

37. Jensen, J., et al., *Kinetic characterization of biomass dilute sulfuric acid hydrolysis: Mixtures of hardwoods, softwood, and switchgrass.* AIChE Journal, 2008. 54(6): p. 1637-1645.

38. Xu, G., et al., *Remarkable effect of extremely dilute H2SO4 on the cellulose conversion to ethylene glycol.* Applied Catalysis A: General, 2015. 502: p. 65-70.

39. Sasaki, M., et al., *Cellulose hydrolysis in subcritical and supercritical water.* Journal of Supercritical Fluids, 1998. 13: p. 261-268.

40. Kruse, A. and N. Dahmen, *Water – A magic solvent for biomass conversion.* The Journal of Supercritical Fluids, 2015. 96: p. 36-45.

41. Yu, Y. and H. Wu, *Understanding the Primary Liquid Products of Cellulose Hydrolysis in Hot-Compressed Water at Various Reaction Temperatures.* Energy & Fuels, 2010. 24(3): p. 1963-1971.

42. Baek, I.G., S.J. You, and E.D. Park, *Direct conversion of cellulose into polyols over Ni/W/SiO2-Al2O3.* Bioresource Technology, 2012. 114: p. 684-690.

43. Tai, Z., et al., *Catalytic Conversion of Cellulose to Ethylene Glycol over a Low-Cost Binary Catalyst of Raney Ni and Tungstic Acid.* ChemSusChem, 2013. 6(4): p. 652-658.

44. Liu, Y., C. Luo, and H. Liu, *Tungsten Trioxide Promoted Selective Conversion of Cellulose into Propylene Glycol and Ethylene Glycol on a Ruthenium Catalyst.* Angewandte Chemie International Edition, 2012. 51(13): p. 3249-3253.

45. Zhou, L., et al., *Selective Production of 1,2-Propylene Glycol from Jerusalem Artichoke Tuber using Ni–W2C/AC Catalysts.* ChemSusChem, 2012. 5(5): p. 932-938.

46. Kabyemela, B.M., et al., *Kinetics of Glucose Epimerization and Decomposition in Subcritical and Supercritical Water.* Industrial & Engineering Chemistry Research, 1997. 36(5): p. 1552-1558.

47. Kabyemela, B.M., et al., *Glucose and Fructose Decomposition in Subcritical and Supercritical Water: Detailed Reaction Pathway, Mechanisms, and Kinetics.* Industrial & Engineering Chemistry Research, 1999. 38(8): p. 2888-2895.

48. Sasaki, M., et al., *Kinetics and Mechanism of Cellobiose Hydrolysis and Retro-Aldol Condensation in Subcritical and Supercritical Water.* Industrial & Engineering Chemistry Research, 2002. 41(26): p. 6642-6649.

49. van der Wijst, C.G., *Publication Proposal* in *Department of Chemical Engineering*. 2017, Norwegian Institute of Science and Technology.

50. Yao, S., et al., *One-Step Conversion of Biomass-Derived 5-Hydroxymethylfurfural to 1,2,6-Hexanetriol Over Ni–Co–Al Mixed Oxide Catalysts Under Mild Conditions.* ACS Sustainable Chemistry & Engineering, 2014. 2(2): p. 173-180.

51. Li, C.Z., et al., *One-pot catalytic hydrocracking of raw woody biomass into chemicals over supported carbide catalysts: simultaneous conversion of cellulose, hemicellulose and lignin.* Energy and Environmental Science, 2012. 5(4): p. 6383-6390.

52. Bjorkman, A., *Isolation of Lignin from Finely Divided Wood with Neutral Solvents.* Nature, 1954. 174(4440): p. 1057-1058.

53. Bezanehtak, K., et al., *Vapor−Liquid Equilibrium for Binary Systems of Carbon Dioxide + Methanol, Hydrogen + Methanol, and Hydrogen + Carbon Dioxide at High Pressures.* Journal of Chemical & Engineering Data, 2002. 47(2): p. 161-168.

54. Deng, W., et al., *Conversion of Cellulose into Sorbitol over Carbon Nanotube-Supported Ruthenium Catalyst.* Catalysis Letters, 2009. 133(1): p. 167.

55. Van de Vyver, S., et al., *Selective Bifunctional Catalytic Conversion of Cellulose over Reshaped Ni Particles at the Tip of Carbon Nanofibers.* ChemSusChem, 2010. 3(6): p. 698-701.

56. Sun, J., et al., *Catalytic Performance of Activated Carbon Supported Tungsten Carbide for Hydrazine Decomposition.* Catalysis Letters, 2008. 123(1): p. 150-155.

57. Zhu, J., A. Holmen, and D. Chen, *Carbon Nanomaterials in Catalysis: Proton Affinity, Chemical and Electronic Properties, and their Catalytic Consequences.* ChemCatChem, 2013. 5(2): p. 378-401.

58. HU, C.Y., et al., *A study concerning the pretreatment of CNTs and its influence on the performance of NiB/CNTs amorphous catalyst.* Journal of the Serbian Chemical Society, 2006.

59. Haber, J., J.H. Block, and B. Delmon, *Manual of methods and procedures for catalyst characterization (Technical Report)*, in *Pure and Applied Chemistry*. 1995. p. 1257.

60. Bjørgen, C., *One-pot Conversion of Biomass to Ethylene Glycol, Propylene Glycol and other Polyols over Carbon Supported Tungsten Catalysts*, in *Department of Chemical Engineering*. 2013, Norwegian University of Science and Technology. p. 94.

61. Zhao, T., et al., *Synthesis of Supported Catalysts by Impregnation and Calcination of Low-Temperature Polymerizable Metal-Complexes.* Topics in Catalysis, 2011. 54(16): p. 1163.

62. Sakka, S., *Handbook of sol-gel science and technology. Processing, characterization and applications*. Vol. 1. 2005: Kluwer Academic Publishers.

63. Rui, H., *Synthesis and Characterization of Tungsten Carbide*, in *Department of Chemical Engineering*. 2015, Norwegian University of Science and Technology. p. 143.

64. Hunyadi, D., I. Sajó, and I. Szilágyi, *Structure and thermal decomposition of ammonium metatungstate.* Journal of Thermal Analysis & Calorimetry, 2014. 116(1): p. 329-337.

65. Gao, L. and B.H. Kear, *Low temperature carburization of high surface area tungsten powders.* Nanostructured Materials, 1995. 5(5): p. 555-569.

66. Venables, D.S. and M.E. Brown, *Reduction of tungsten oxides with hydrogen and with hydrogen and carbon.* Thermochimica Acta, 1996. 285(2): p. 361-382.

67. Löfberg, A., et al., *Mechanism of WO3 Reduction and Carburization in CH4/H2 Mixtures Leading to Bulk Tungsten Carbide Powder Catalysts.* Journal of Catalysis, 2000. 189(1): p. 170-183.

68. Liland, I.S., *One-pot conversion of cellulose to ethylene glycol and propylene glycol over nickel zinc oxide catalysts with cnt support*, in *Department of Chemical Engineering*. 2013, Norwegian University of Science and Technology.

69. Morken, S.F., *One-pot conversion of biomass to chemicals on Ni-Cu/ZnO based catalysts*, in *Department of Chemical Engineering*. 2015, Norwegian University of Science and Technology. p. 118.

70. Langfjæran, S., *Synthesis and characterization of tungsten carbide*, in *Departmentof Chemical Engineering*. 2016, Norwegian Institute of Science and Technology. p. 71.

71. Niemantsverdriet, J.W., *Spectroscopy in Catalysis: An Introduction*. 2008: Wiley.

72. Che, M., *Characterization of Solid Materials and Heterogeneous Catalysts: From Structure to Surface Reactivity*. 2012: Wiley-VCH.

73. Robinson, J.W., E.M.S. Frame, and G.M. Frame, *Undergraduate Instrumental Analysis, Sixth Edition*. 2004: Taylor & Francis.

74. Román-Leshkov, Y., et al., *Mechanism of Glucose Isomerization Using a Solid Lewis Acid Catalyst in Water.* Angewandte Chemie International Edition, 2010. 49(47): p. 8954-8957.

75. Xia, Q., et al., *Direct hydrodeoxygenation of raw woody biomass into liquid alkanes.* 2016. 7: p. 11162.

Appendix

This appendix contains experimental data, calculations, and analytical results that were mentioned, but not included, throughout the report.

A. Actual Experimental Data

Table A.1: Amount of ammonia metatungstate (AMT), ethylene glycol (EG), and citric acid (CA) in 3:16:16 molar ratio used for tungsten impregnation onto CNT by the Pechini method, as well as the amount of copper nitrate trihydrate precursor used for copper impregnation

	W/Cu precursor (g)	EG (g)	CA (g)
10 wt% W (6g CNT)	0.8898	0.3594	0.1022
50 wt% W (2g CNT)	2.6817	1.0170	0.3001
10 wt% Cu (1g WO_3/CNT)	0.4245	-	-
10 wt% Cu (1g W_2C/CNT)	0.4228	-	-
10 wt% Cu (1g CNT)	0.4226	-	-

Table A.2: Cellulose and catalyst reactor loading for tungsten-copper catalysts at 90 min

Reaction/Catalyst	Cellulose (g)	Catalyst (g)
WO_3/CNT	0.3304	0.1000
W_2C/CNT	0.3298	0.0096
W_2C-WC/CNT	0.3303	0.0998
WO_3-Cu/CNT	0.3299	0.1004
W_2C-Cu/CNT	0.3302	0.1005
W_2C-WC-Cu/CNT	0.3310	0.0999

Table A.3: Cellulose and catalyst reactor loading for tungsten-copper catalysts at 180 min

Reaction/Catalyst	Cellulose (g)	Catalyst (g)
WO_3/CNT	0.3303	0.1003
W_2C/CNT	0.3303	0.1011
WO_3-Cu/CNT	0.3311	0.1002
W_2C-Cu/CNT	0.3305	0.1001

Table A.4: Cellulose and catalyst reactor loading for W + Cu_xO catalyst systems

Reaction/Catalyst	Cellulose (g)	W Catalyst (g)	Cu_xO catalyst (g)
Cu_xO/CNT	0.3307	-	0.1009
WO_3/CNT + Cu_xO/CNT	0.3302	0.1001	0.0348
W_2C/CNT + Cu_xO/CNT	0.3306	0.0998	0.0347

Table A.5: Cellulose and catalyst reactor loading for W + Ru catalyst systems

Reaction/Catalyst	Cellulose (g)	W Catalyst (g)	Ru catalyst (g)
10 wt% WO_3/CNT + Ru/CNT	0.3308	0.2430	0.1331
10 wt% W_2C/CNT + Ru/CNT	0.3305	0.2423	0.1335
50 wt% WO_3/CNT + Ru/CNT	0.3302	0.0488	0.1334
50 wt% W_2C/CNT + Ru/CNT	0.3304	0.0484	0.1334
10 wt% WO_3/CNT + Ru/CNT + H_2SO_4	0.3304	0.2427	0.1334

B. Sample Calculations

The amount of ammonia metatungstate (AMT) precursor to be added according to the desired wt% was calculated by Equation B.1. The calculation for 10 wt% W loading onto 6g CNT is used as an example.

$$L = \frac{X * \frac{W_{mwt} * 12}{AMT_{mwt}}}{S + X * \frac{W_{mwt} * 12}{AMT_{mwt}}} \quad \xrightarrow{rearrange} \quad X = \frac{L * S}{\frac{W_{mwt} * 12}{AMT_{mwt}} * (1 - L)} \tag{B.1}$$

$$X = \frac{0.1 * 6}{\frac{183.84 * 12}{2956.3} * (1 - 0.1)} = 0.8934\ g\ AMT$$

Where,

L = desired wt% loading (as decimal)
X = amount of AMT (g)
S = amount of support (g)
W_{mwt} = molecular weight of tungsten (183.84 g/mol)
AMT_{mwt} = molecular weight of AMT (2956.3 g/mol)

The amount of citric acid (CA) and ethylene glycol (EG) to be added for the Pechini method in a 3:16:16 molar ratio of AMT:CA:EG was calculated by the following two equations:

$$CA = X * \frac{CA_{mwt}}{AMT_{mwt}} * \frac{16}{3} \tag{B.2}$$

$$EG = X * \frac{EG_{mwt}}{AMT_{mwt}} * \frac{16}{3} \tag{B.3}$$

$$CA = 0.8934 * \frac{210.14}{2956.3} * \frac{16}{3} = 0.3387\ g\ CA$$

$$EG = 0.8934 * \frac{62.07}{2956.3} * \frac{16}{3} = 0.1000\ g\ EG$$

Where,

CA = amount of CA (g)
EG = amount of EG (g)
X = amount of AMT (g)
CA_{mwt} = molecular weight of CA (210.14 g/mol)
EG_{mwt} = molecular weight of EG (62.07 g/mol)

The amount of copper precursor to be added was calculated in a similar manner by Equation B.4. The addition of 10 wt% Cu to 1 g CNT is used as an example.

$$X = \frac{L*S}{\frac{Cu_{mwt}}{Cu\ precursor_{mwt}}*(1-L)} \tag{B.4}$$

$$X = \frac{0.1*1}{\frac{63.546}{241.6}*(1-0.1)} = 0.4224\ g\ Cu$$

Where,

X = amount of copper precursor, $Cu(NO_3)_2 \cdot 3H_2O$ (g)
L = desired wt% loading (as decimal)
S = amount of support (g)
Cu_{mwt} = molecular weight of copper (63.546 g/mol)
Cu $precursor_{mwt}$ = molecular weight of $Cu(NO_3)_2 \cdot 3H_2O$ (241.6 g/mol)

The amount of Cu_xO/CNT to be added in combination with a tungsten catalyst for a molar ratio of Cu/W = 1.0 was calculated using Equation B.5. The addition of Cu_xO/CNT to 0.1 g 10 wt% WO3/CNT is used as an example.

$$Cu_xO = \frac{W_{wt\%}*W_{cat}}{W_{mwt}} * 1.0 * \frac{Cu_{mwt}}{Cu_{wt\%}} \tag{B.5}$$

$$Cu_xO = \frac{0.1*0.1}{183.84} * 1.0 * \frac{63.546}{0.1} = 0.0346\ g\ Cu_xO$$

Where,

Cu_xO = amount of Cu_xO/CNT required (g)
$W_{wt\%}$ = nominal wt% of tungsten catalyst (as decimal)
W_{cat} = amount of tungsten catalyst (g)
W_{mwt} = molecular weight of tungsten (183.84 g/mol)
Cu_{mwt} = molecular weight of copper (63.546 g/mol)
$Cu_{wt\%}$ = nominal wt% of Cu_xO/CNT (as decimal)

The amount of Ru/CNT to be added in combination with a tungsten catalyst for a molar ratio of Ru/W = 0.1 was calculated in a similar manner using Equation B.6. The addition of 10 wt% WO_3/CNT with 0.1333 g Ru/CNT is used as an example.

$$W_{cat} = \frac{Ru_{wt\%}*Ru_{cat}}{Ru_{mwt}} * \frac{1.0}{0.1} * \frac{W_{mwt}}{W_{wt\%}} \tag{B.6}$$

$$W_{cat} = \frac{0.01*0.1333}{101.07} * \frac{1.0}{0.1} * \frac{183.84}{0.1} = 0.2425\ g\ W_{cat}$$

Where,

W_{cat} = amount of tungsten catalyst (g)
$Ru_{wt\%}$ = nominal wt% of ruthenium catalyst (as decimal)
Ru_{cat} = amount of ruthenium catalyst (g)
Ru_{mwt} = molecular weight of ruthenium (101.07 g/mol)
W_{mwt} = molecular weight of tungsten (183.84 g/mol)
$W_{wt\%}$ = nominal wt% of tungsten catalyst (as decimal)

The amount of dilute sulfuric acid (H_2SO_4) required to achieve a molar ratio of H_2SO_4/W = 0.03 was calculated using Equation B.7. The calculation using 10 wt% WO3/CNT will be used as an example.

$$SA = \frac{W_{cat} * W_{wt\%}}{W_{mwt}} * 0.03 * \frac{SA_{mwt}}{\rho_{SA}} \quad \text{(B.7)}$$

$$SA = \frac{0.2425 * 0.1}{183.84} * 0.03 * \frac{98.079}{1.84} = 2.11 * 10^{-4}\ cm^3 = 0.211\ \mu L$$

Where,

SA = amount of sulfuric acid required (cm^3)
W_{cat} = amount of tungsten catalyst (g)
$W_{wt\%}$ = nominal wt% of tungsten catalyst (as decimal)
W_{mwt} = molecular weight of tungsten (183.84 g/mol)
SA_{mwt} = molecular weight of sulfuric acid (98.079 g/mol)
ρ_{SA} = density of sulfuric acid (1.84 g/cm^3)

Since a volume of 21 µL is very small, a series of dilutions was used to achieve a similar sulfuric acid molarity in a reactor solution volume of 33 mL. The pipette had a maximum of 20 µL, so this volume was used as the effect of 1 µL was assumed to be negligible. The sulfuric acid used had a purity of 95%, which meant 20 µL corresponded to 0.03496 g H_2SO_4. The first dilution was done using 20 µL H_2SO_4 and water to create a 100 mL solution, which resulted in 3.564 mM H_2SO_4 solution. The amount of this solution to be added to the reactor was then calculated using Equation B.8 to achieve the desired molarity of 0.12 mM H_2SO_4 based on a reactor volume of 33 mL and a molar ratio of H_2SO_4/W = 0.03.

$$C1 * V1 = C2 * V2 \quad \xrightarrow{rearrange} \quad V1 = \frac{C2 * V2}{C1} \quad \text{(B.8)}$$

$$V1 = \frac{0.12\ mM * 33\ mL}{3.564\ mM} = 1.11\ mL$$

C. Calibration Curves for Carburization Gas Flow Controllers

The calibration curves for the N_2, H_2, and CH_4 flow controllers are shown in Figuures C.1-C.3 respectively. The exponential curve fit was used to determine the flow, as the linear regression lines that are also shown did not fit the calibration data well.

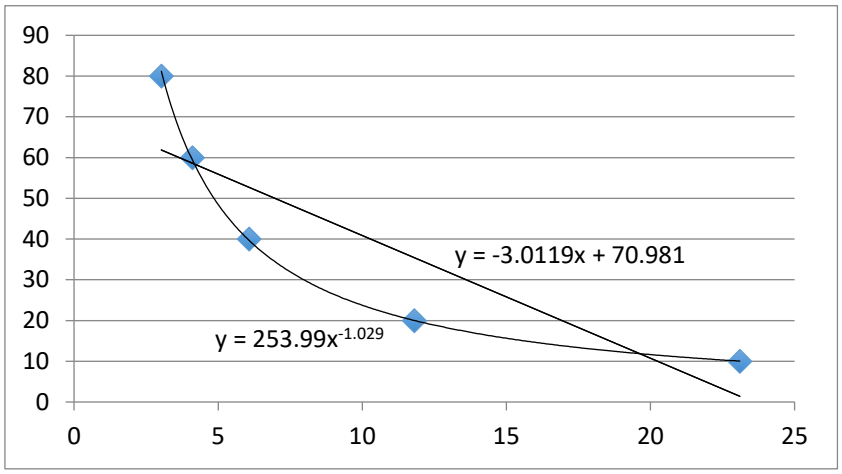

Figure C.1: Calibration curve for N_2 flow controller

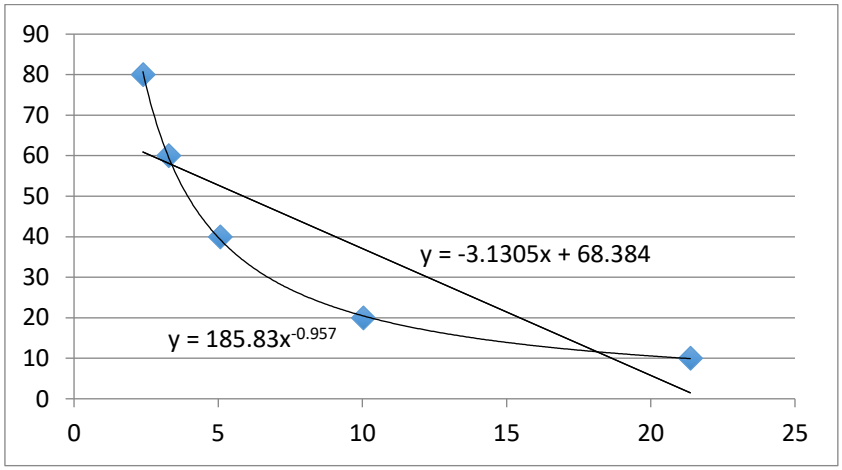

Figure C.2: Calibration curve for H_2 flow controller

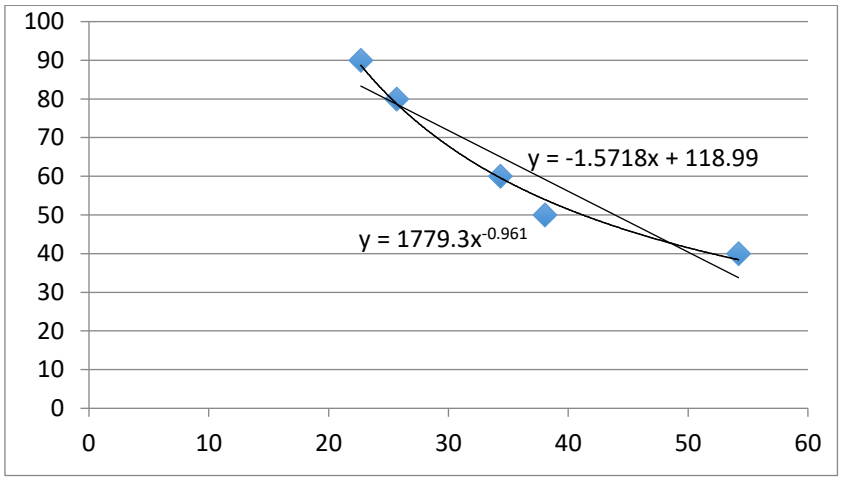

Figure C.3: Calibration curve for CH_4 flow controller

D. Additional XRD Diagrams

The additional XRD spectra for 50 wt% WO3/CNT and 50 wt% W2C/CNT are shown in Figures D.1 and D.2 respectively.

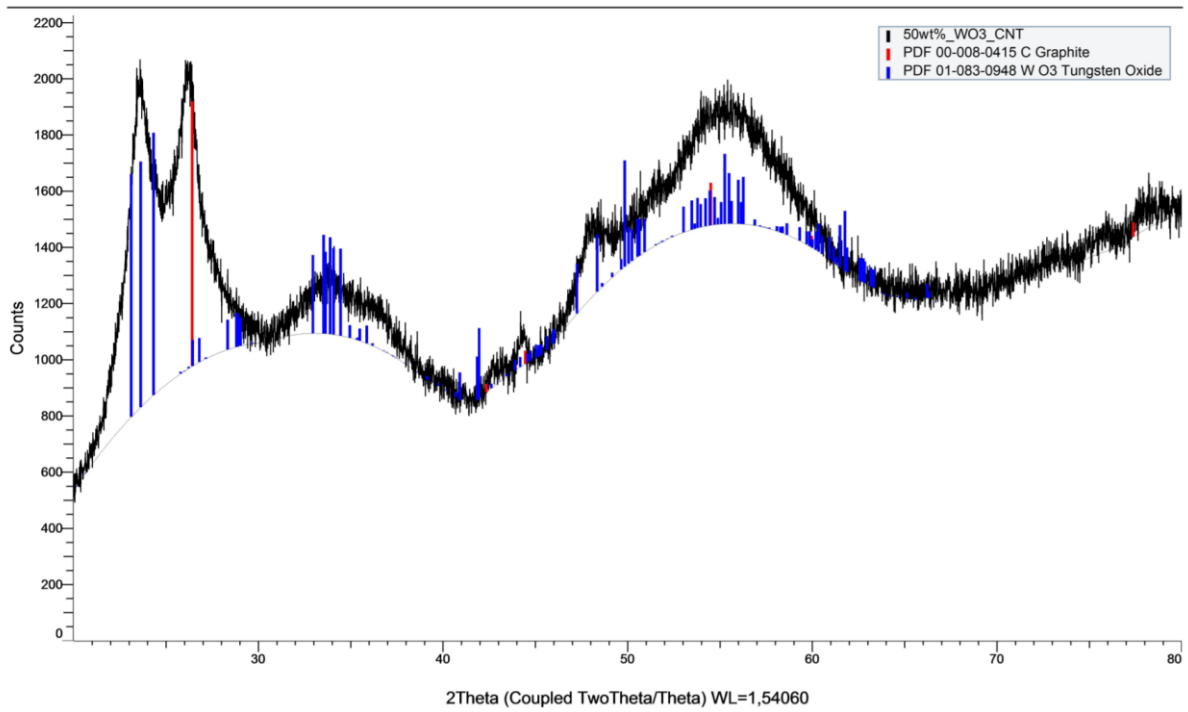

Figure D.1: XRD spectra for 50 wt% WO3/CNT

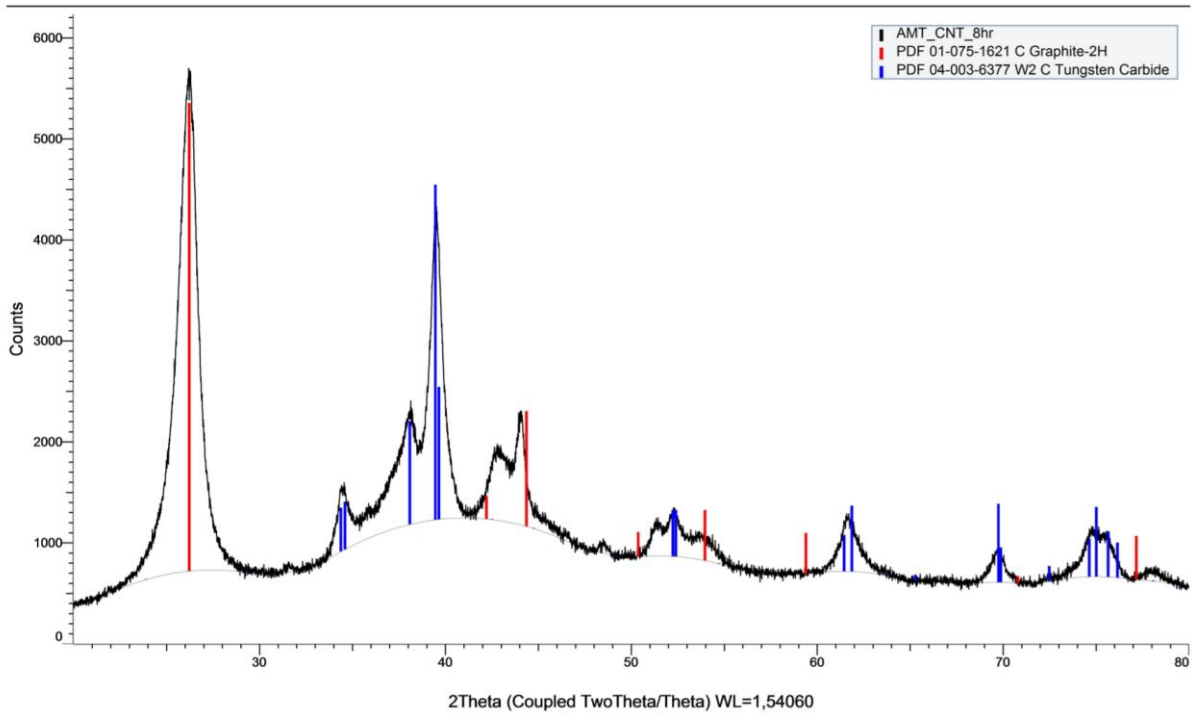

Figure D.2: XRD spectra for 50 wt% W2C/CNT

E. HPLC Diagrams

All HPLC diagrams used in this study are shown in Figures C.1-C.24.

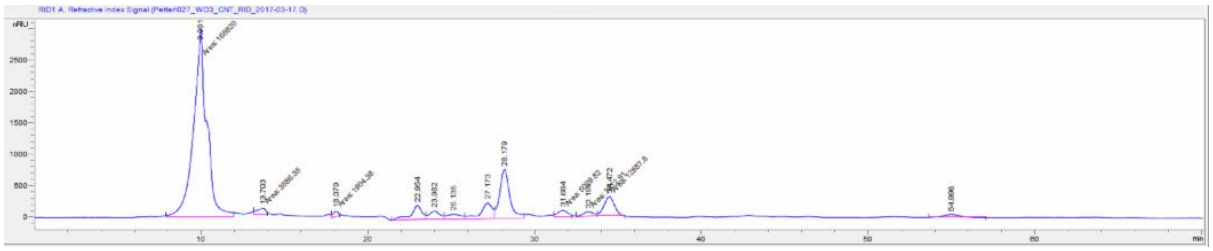

Figure E.1: WO_3/CNT, 90 min

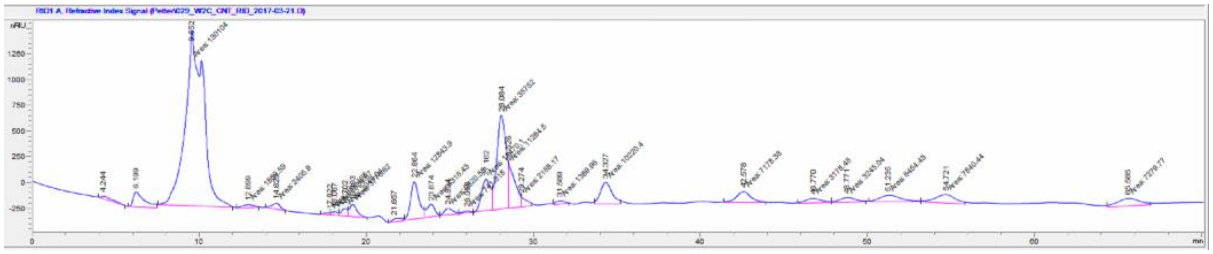

Figure E.2: W_2C/CNT, 90 min

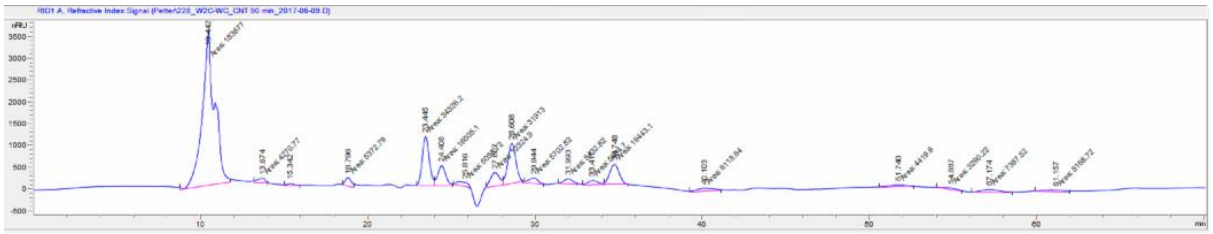

Figure E.3: W_2C-WC/CNT, 90 min

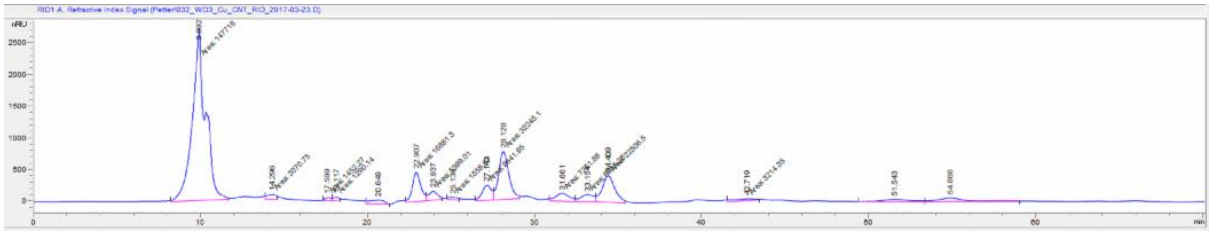

Figure E.4: WO_3-Cu/CNT, 90 min

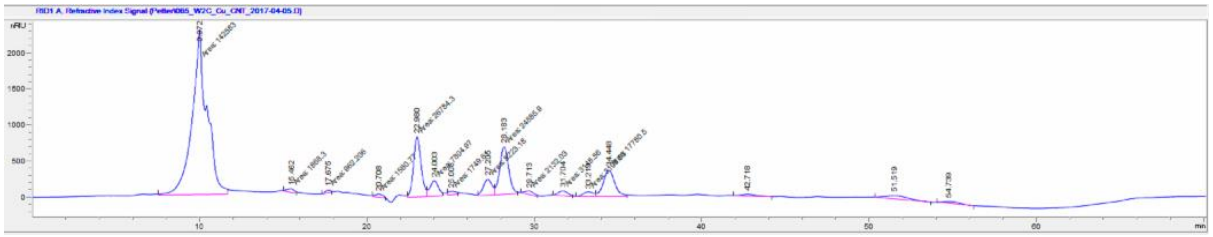

Figure E.5: W_2C-Cu/CNT, 90 min

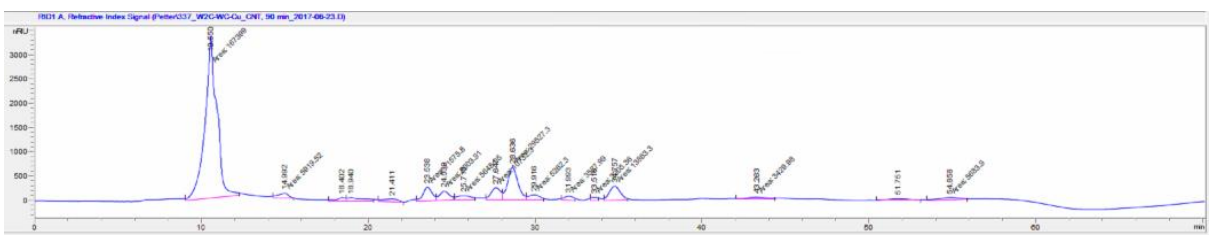

Figure E.6: W_2C-WC-Cu/CNT, 90 min

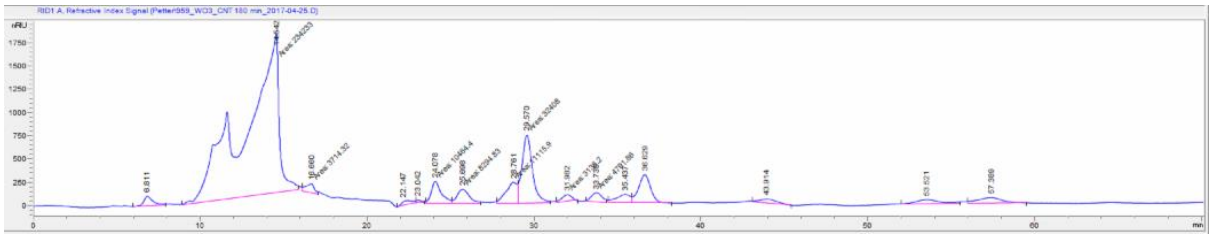

Figure E.7: WO_3/CNT, 180 min

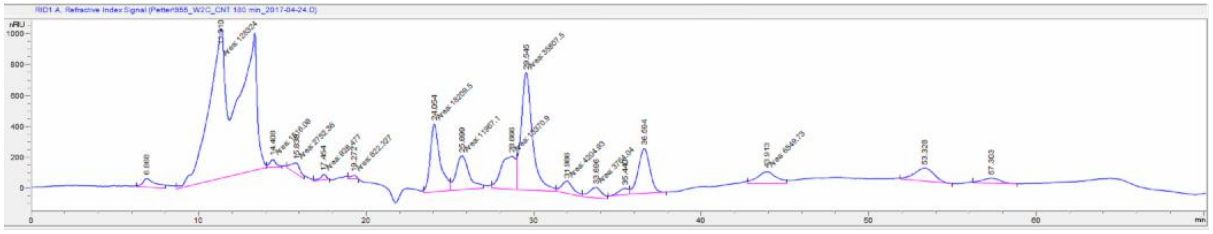

Figure E.8: W_2C/CNT, 180 min

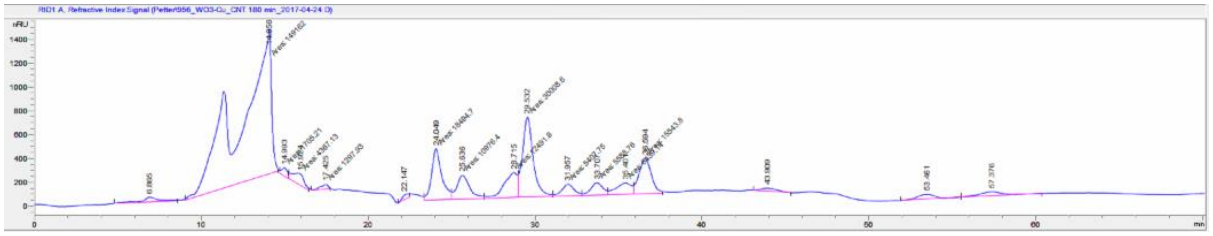

Figure E.9: WO_3-Cu/CNT, 180 min

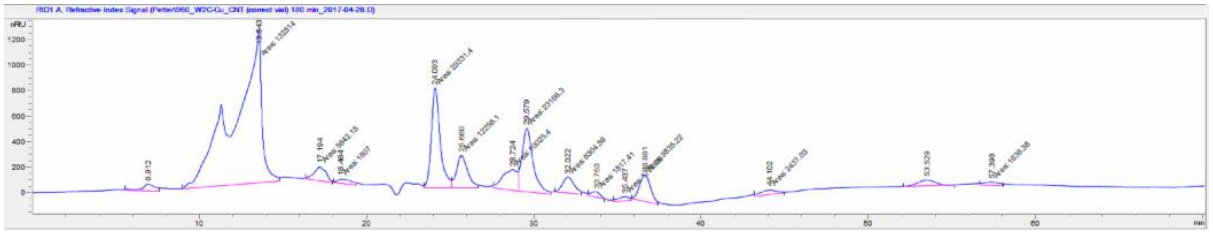

Figure E.10: W_2C-Cu/CNT, 180 min

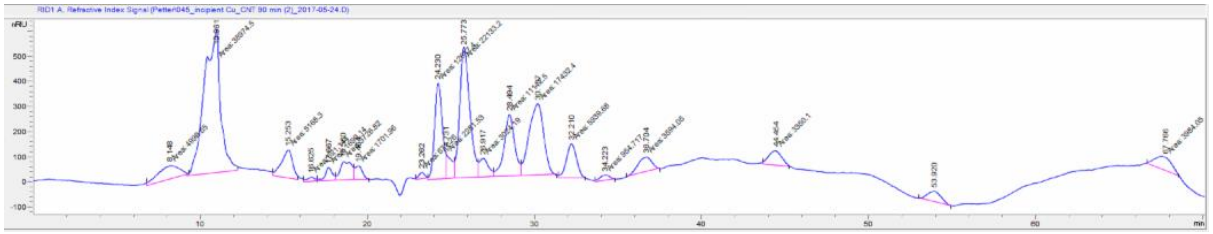

Figure E.11: Cu_xO/CNT

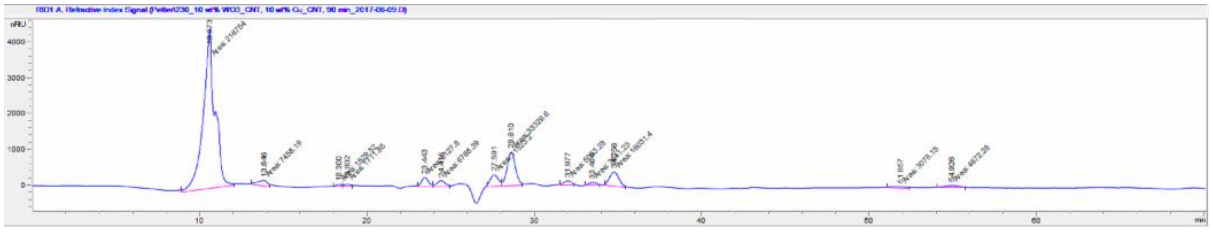

Figure E.12: WO_3/CNT + Cu_xO/CNT

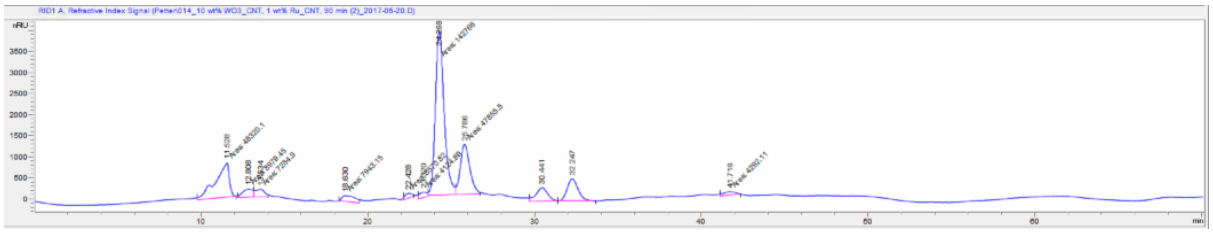

Figure E.13: 10 wt% WO_3/CNT + Ru/CNT

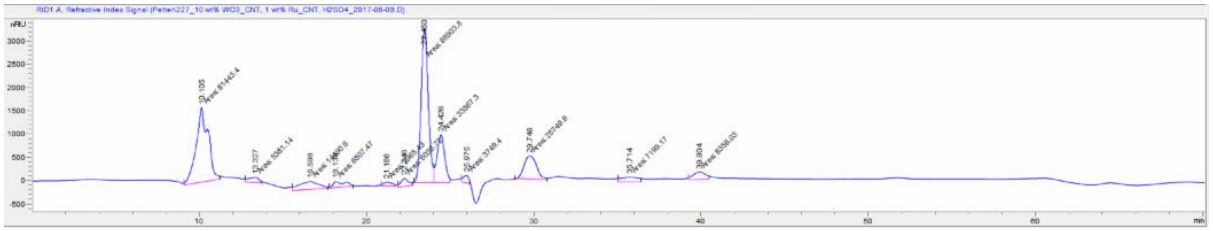

Figure E.14: 10 wt% WO_3/CNT + Ru/CNT + H_2SO_4

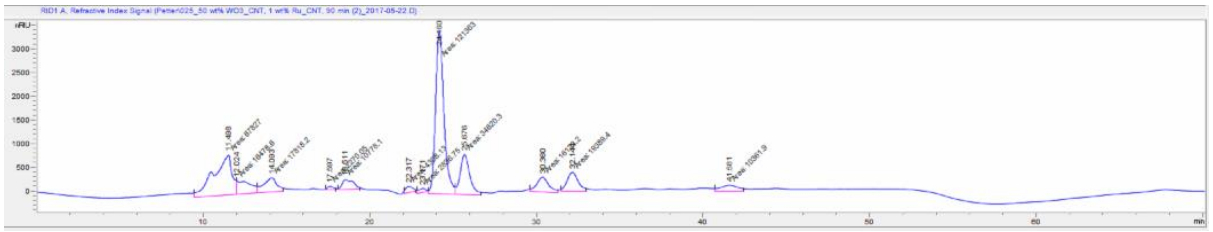

Figure E.15: 50 wt% WO_3/CNT + Ru/CNT

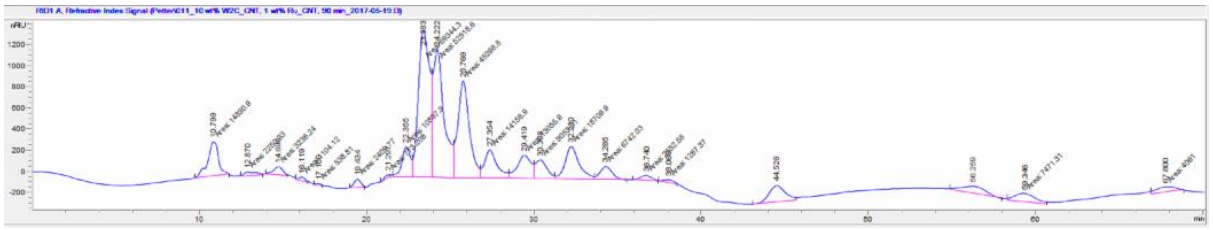

Figure E.16: 10 wt% W_2C/CNT + Ru/CNT

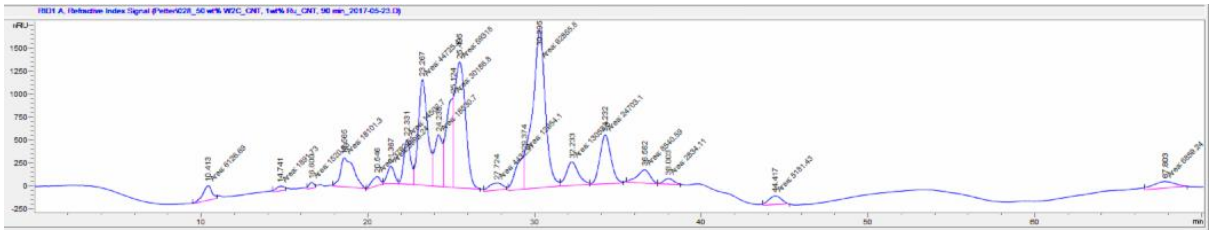

Figure E.17: 50 wt% W_2C/CNT + Ru/CNT

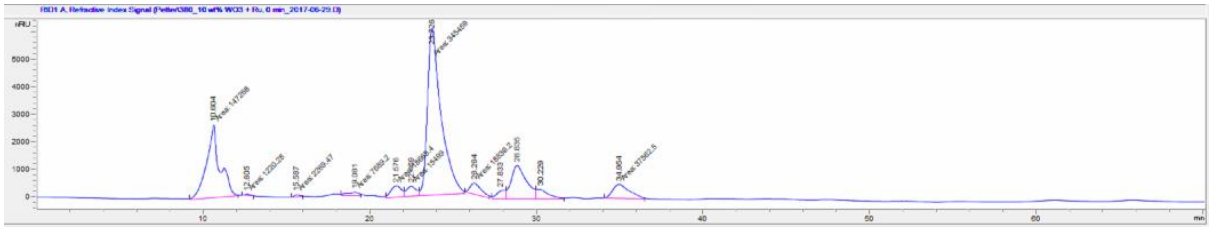

Figure E.18: 10 wt% WO_3/CNT + Ru/CNT, t = 0 min

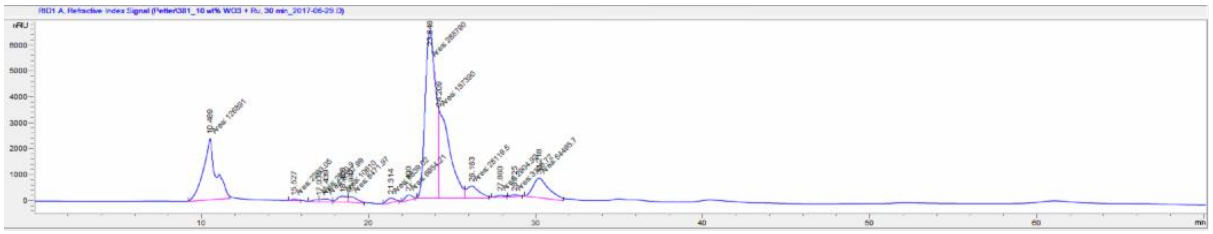

Figure E.19: 10 wt% WO_3/CNT + Ru/CNT, t = 30 min

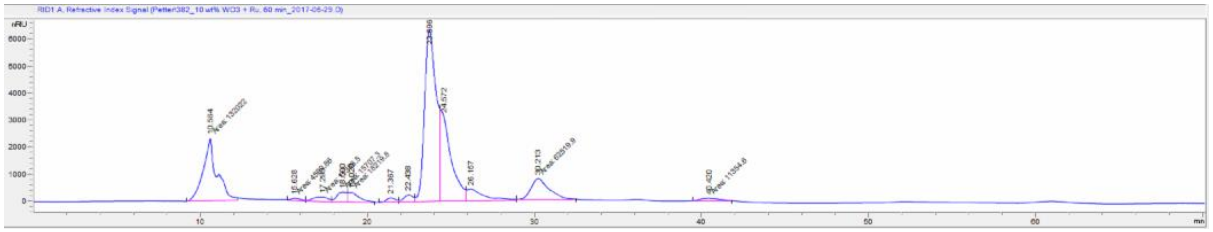

Figure E.20: 10 wt% WO_3/CNT + Ru/CNT, t = 60 min

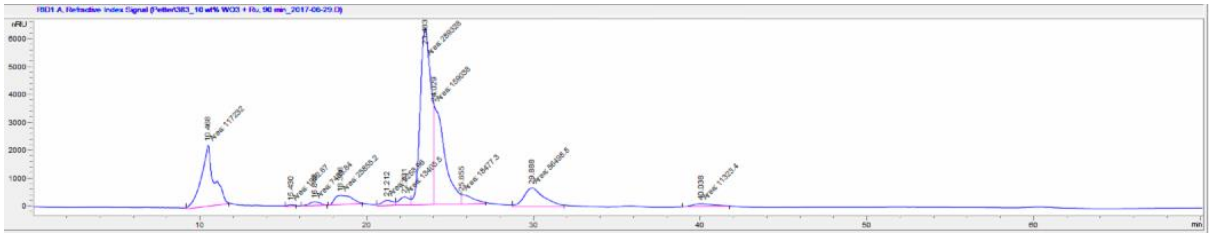

Figure E.21: 10 wt% WO_3/CNT + Ru/CNT, t = 90 min

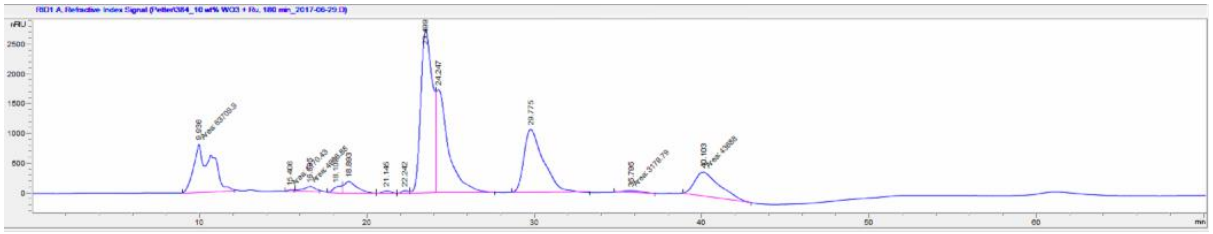

Figure E.22: 10 wt% WO_3/CNT + Ru/CNT, t = 180 min

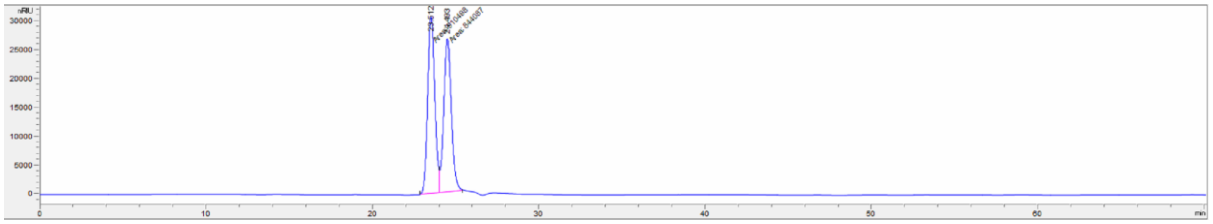

Figure E.23: EG and 1,2-PG with Ru/CNT, pre-reaction

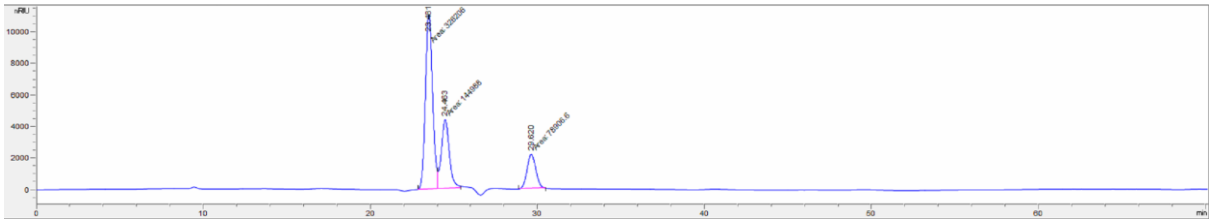

Figure E.24: EG and 1,2-PG with Ru/CNT, pre-reaction

F. Additional S(T)EM and SEM Images

Numerous S(T)EM and SEM images were taken, so a few additional images are shown here in Figures F.1-F.10.

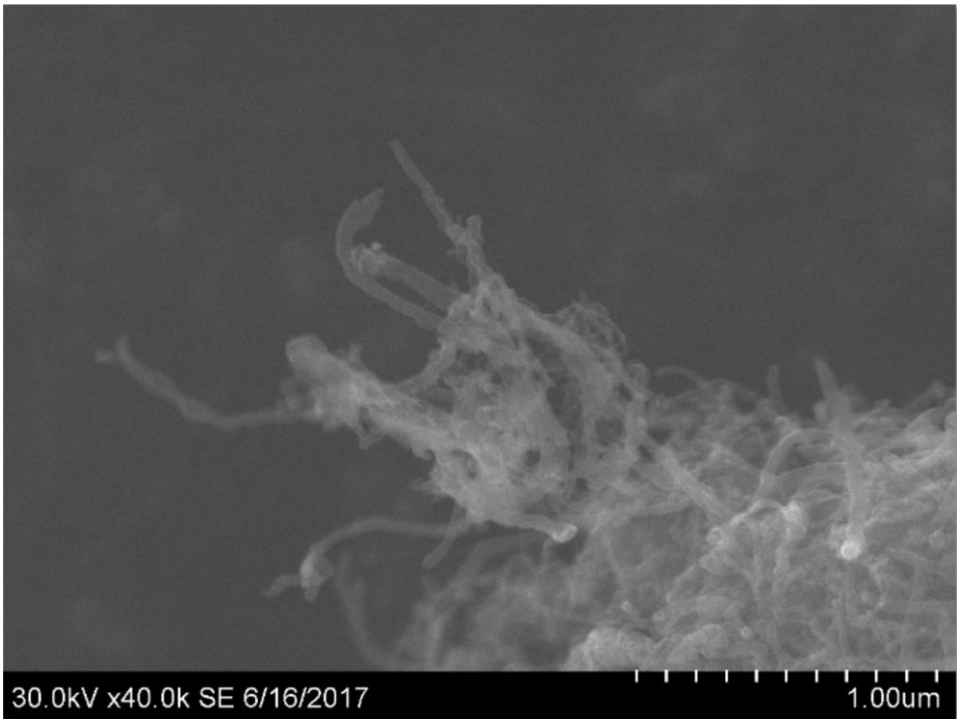

Figure F.1: S(T)EM image of WO_3/CNT, 1 μm scale

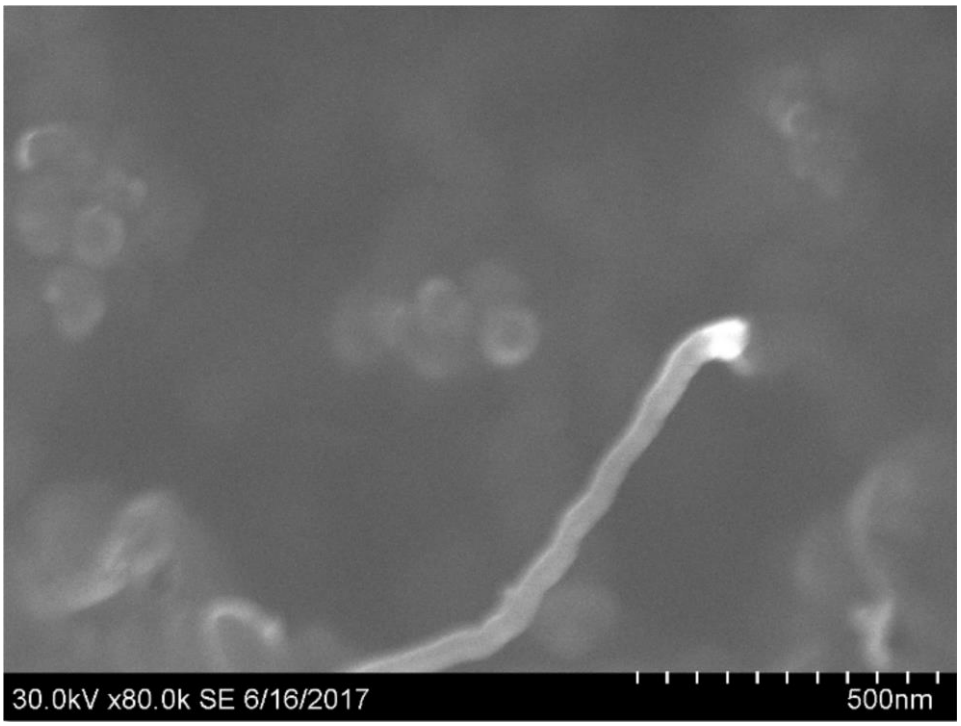

Figure F.1: S(T)EM image of WO_3/CNT, 500 nm scale

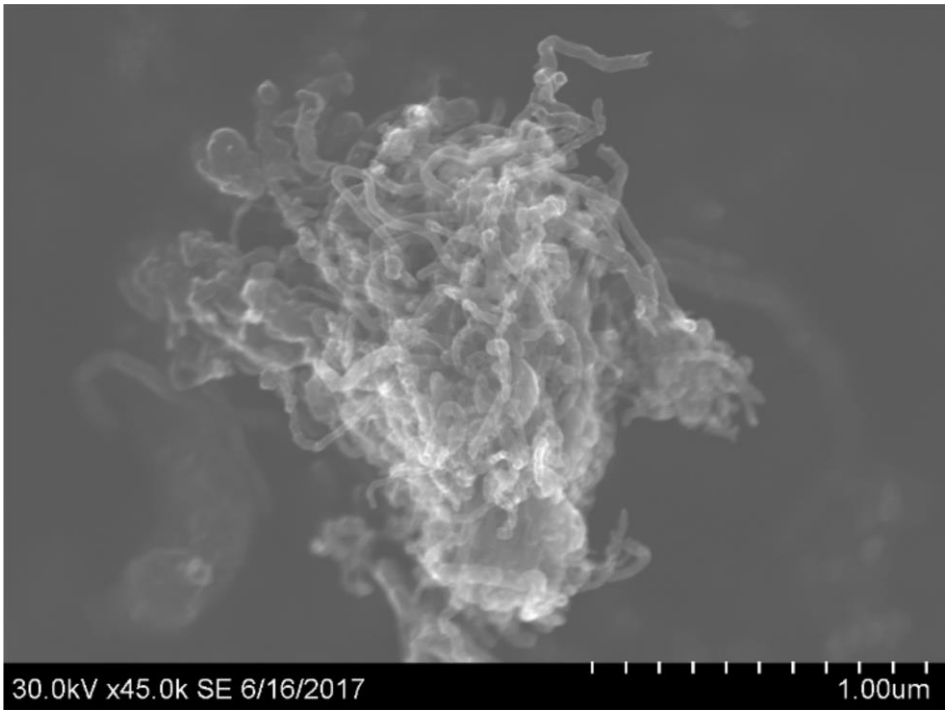

Figure F.3: S(T)EM image of WO_3-Cu/CNT, 1 μm scale

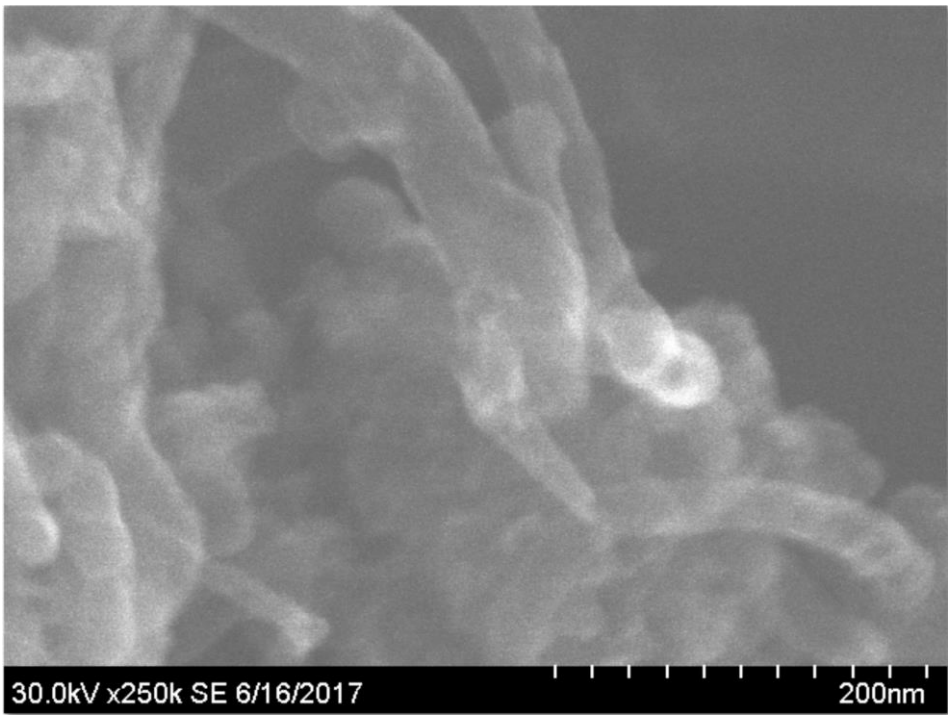

Figure F.4: S(T)EM image of WO_3-Cu/CNT, 200 nm scale

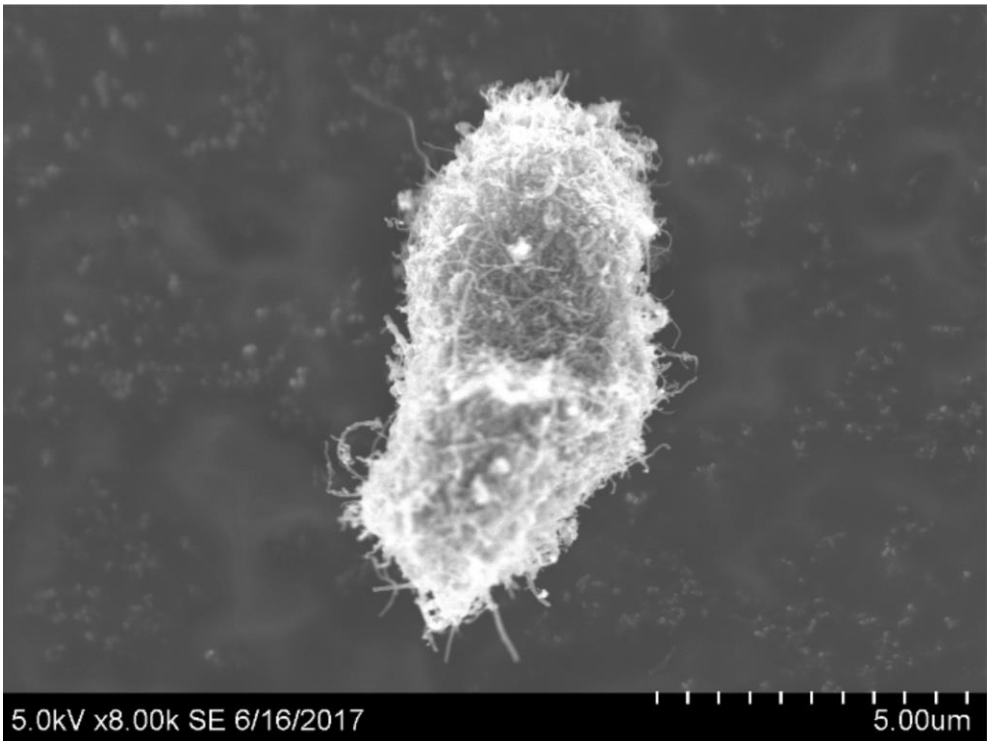

Figure F.5: S(T)EM image of W_2C/CNT, 5 μm scale

Figure F.6: S(T)EM image of W_2C/CNT, 200 nm scale

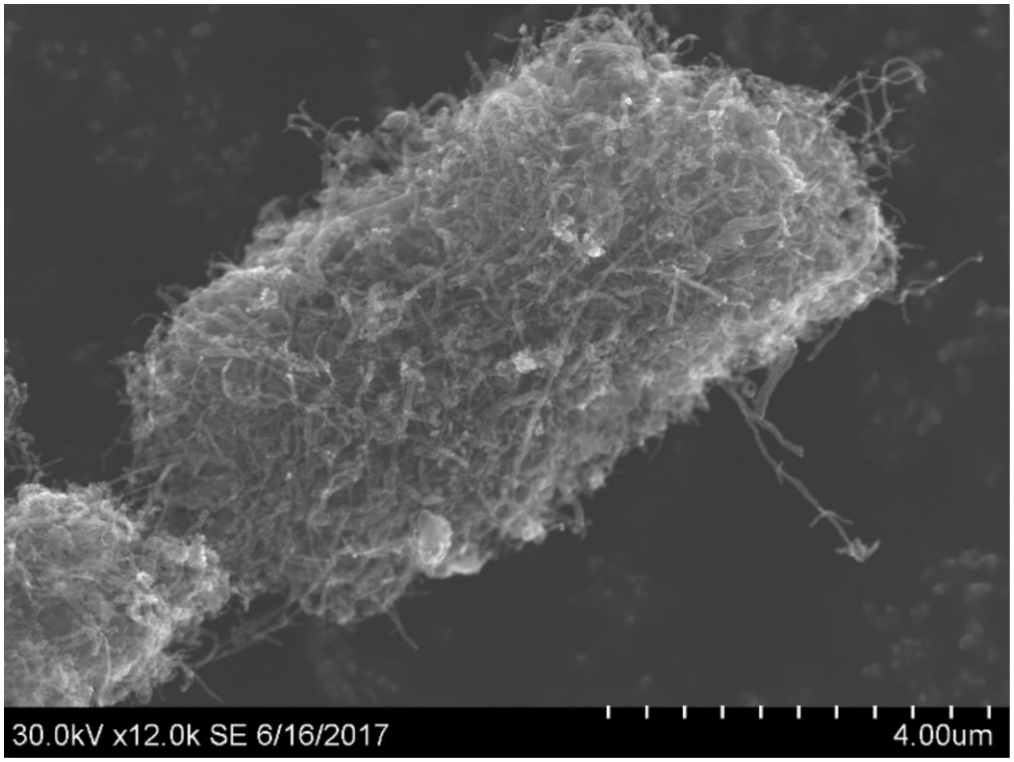

Figure F.7: S(T)EM image of W_2C-Cu/CNT, 4 μm scale

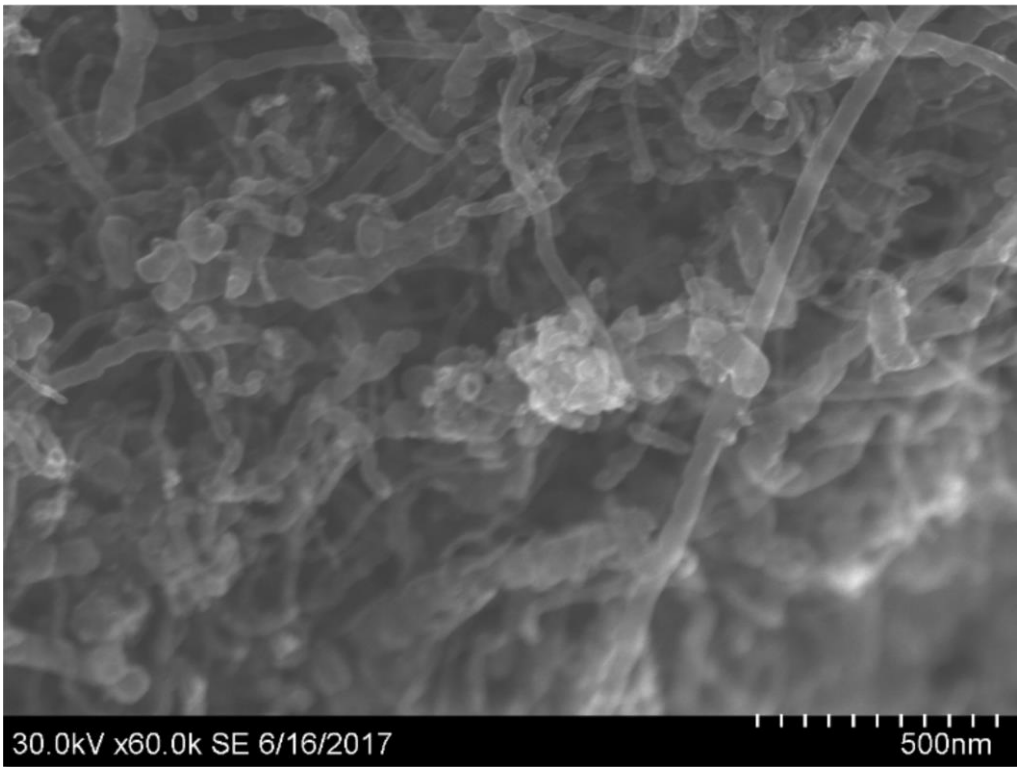

Figure F.8: S(T)EM image of W_2C-Cu/CNT, 500 nm scale

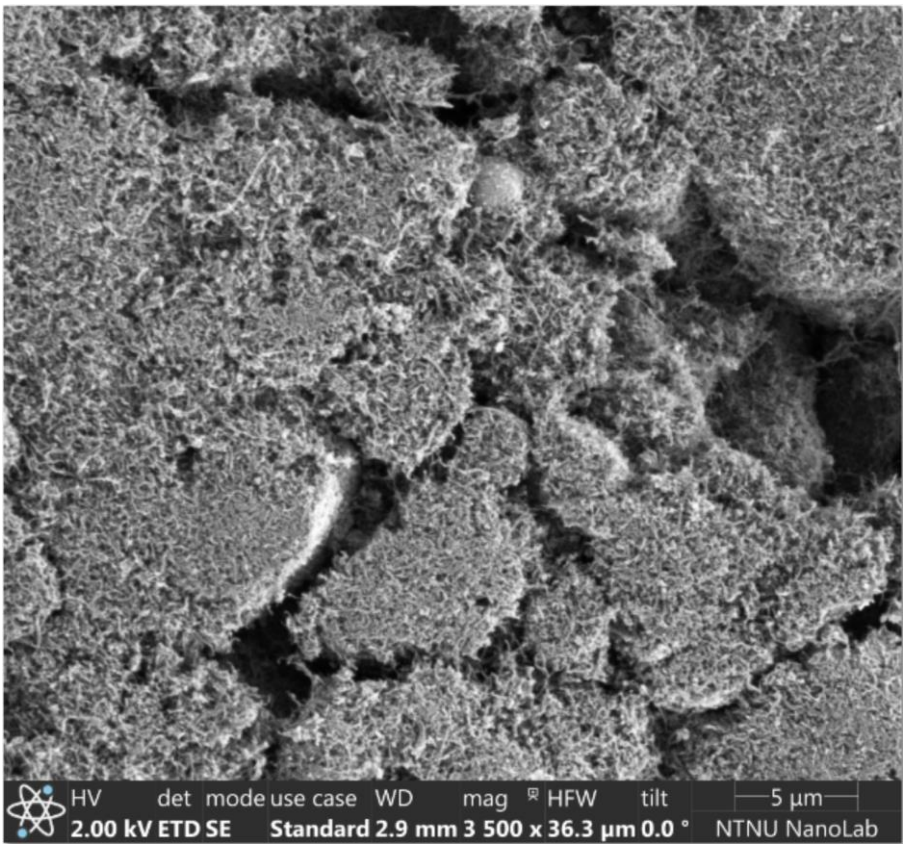

Figure F.9: SEM image of W_2C-Cu/CNT, 5 µm scale

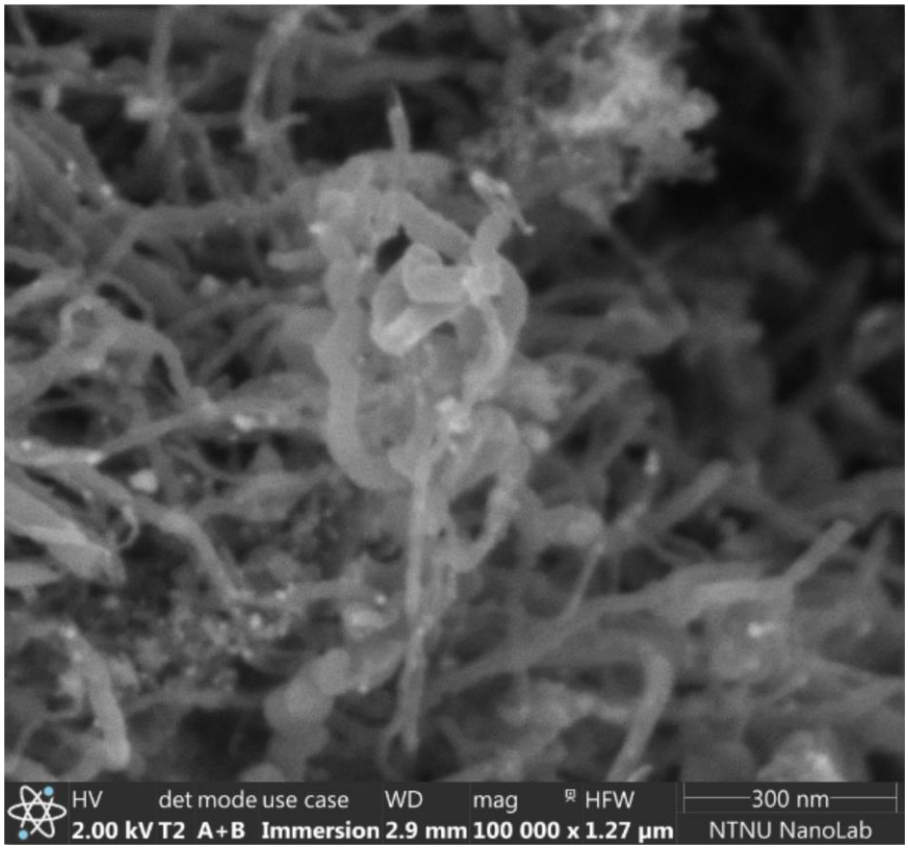

Figure F.10: SEM image of W_2C-Cu/CNT, 300 nm scale